Antioxidant defense in

Trypanosoma brucei brucei

Von der Gemeinsamen Naturwissenschaftlichen Fakultät

der Technischen Universität Carolo-Wilhelmina

zu Braunschweig

zur Erlangung des Grades einer
Doktorin der Naturwissenschaften

(Dr. rer. nat.)

genehmigte

D i s s e r t a t i o n

von

Heike Budde

aus Salzburg / Österreich

1. Referent:	Prof. Dr. Leopold Flohé
2. Referent:	Prof. Dr. Jürgen Bode
Eingereicht am:	30. Juni 2003
Mündliche Prüfung am:	04. September 2003

Druckjahr:	2003

Vorveröffentlichungen

Teilergebnisse aus dieser Arbeit wurden mit Genehmigung der Gemeinsamen Naturwissenschaftlichen Fakultät, vertreten durch den Mentor der Arbeit, in folgenden Beiträgen vorab veröffentlicht:

Publikationen

Budde H. and Flohé L. (2003). Enzymes of the thiol-dependent hydroperoxide metabolism in pathogens as potential drug targets. BioFactors *17*, 83-92.

Budde H., Flohé L., Hecht H.-J., Hofmann B., Stehr M., Wissing J. and Lünsdorf H. (2003). Kinetics and redox-sensitive oligomerization reveal negative cooperativity in tryparedoxin peroxidase of *T. brucei brucei*. Biol. Chem. *384*, 619-633.

Budde H., Flohé L., Hofmann B. and Nimtz M. (2003). Verification of the interaction of a tryparedoxin peroxidase with tryparedoxin by ESI-MS/MS. Biol. Chem. *384*, 1305-1309.

Budde H. and Flohé L. (2002). Enzymes of the thiol-dependent hydroperoxide metabolism in pathogens as potential drug targets. In thiol metabolism and redox regulation of cellular functions, A. Pompella, G. Bánhegyi, M. Wellman-Rousseau, eds. (IOS Press, Ohmsha NATO Science Series Vol. 347), pp 85-95.

Hofmann B., **Budde H.**, Bruns K., Guerrero S., Kalisz H., Menge U., Montemartini M., Nogoceke E., Steinert P., Wissing J., Flohé L. and Hecht H.-J. (2001). Structures of tryparedoxin revealing interaction with trypanothione. Biol. Chem. *382*, 459-471.

Flohé L., **Budde H.**, Bruns K., Castro H., Clos J., Hofmann B., Kansal-Kalavar S., Krumme D., Menge U., Plank-Schumacher K., Sztajer H., Wissing J., Wylegalla C. and Hecht H.-J. (2002). Tryparedoxin peroxidase of *Leishmania donovani*: Molecular cloning, heterologous expression, specificity and catalytic mechanism. Arch. Biochem. Biophys. *397*, 324-335.

Castro, H., **Budde, H.**, Flohé, L., Hofmann, B., Lünsdorf, H., Wissing, J. and Tomás, A. M. (2002). Specificity and kinetics of a mitochondrial peroxiredoxin of *Leishmania infantum*. Free Radic. Biol. Med. *33*, 1563-1574.

Flohé L., **Budde H.** and Hofmann B. (2003). Peroxiredoxins in antioxidant defense and redoxregulation. Biofactors, in press.

Krumme D., **Budde H.**, Hecht H.-J., Menge U., Ohlenschläger O., Roß A., Wissing J., Wray V. and Flohé L. (2003). NMR studies of the interaction of tryparedoxin with redox-inactive substrate homologs. Biochemistry, submitted.

Tagungsbeiträge

Budde H., Hofmann B., Stehr M., Wissing J. and Flohé L. (2002). Reconstitution of the trypanothione-mediated hydroperoxide metabolism of *Trypanosoma brucei*. 2nd International Symposium on antioxidants in nutrition and therapy. 02.-04.10. 2002, Kuta, Indonesia.

Budde H., Hecht H.-J., Hofmann B., Lünsdorf H. and Flohé L. (2002). Tryparedoxin peroxidase of *Trypanosoma brucei*: a decameric ring with ten reaction centers. 2nd International Symposium on antioxidants in nutrition and therapy. 02.-04.10. 2002, Kuta, Indonesia.

Krumme D., **Budde H.**, Hecht H.-J., Hofmann B., Menge U., Reichelt J., Ross A. and Flohé L. (2002). Trypanothione/tryparedoxin interaction. 2nd International Symposium on antioxidants in nutrition and therapy. 02.-04.10. 2002, Kuta, Indonesia.

Castro H., Sousa C., Santos M., **Budde H.**, Lünsdorf H., da Silva A.C., Flohé L. and Tomás A.M. (2002). Compartmented antioxidant defense by peroxiredoxins in *Leishmania infantum*. 2nd International Symposium on antioxidants in nutrition and therapy. 02.-04.10. 2002, Kuta, Indonesia.

Budde H., Hecht H.-J., Hofmann B. and Flohé L. (2002). Molecular target for trypanocidal drugs. 53. Mosbacher Kolloquium: Impact of molecular medicine on drug development. 04.-07.04. 2002, Mosbach, Germany

Krumme D., **Budde H.**, Hecht H.-J., Hofmann B., Lünsdorf H. and Flohé L. (2002). Molecular tools to design trypanocidal drugs. Joint Annual Fall Meeting of GBM and DGPT. 07.-10. 09. 2002, Halle, Germany

Antioxidant defense in *Trypanosoma brucei brucei*

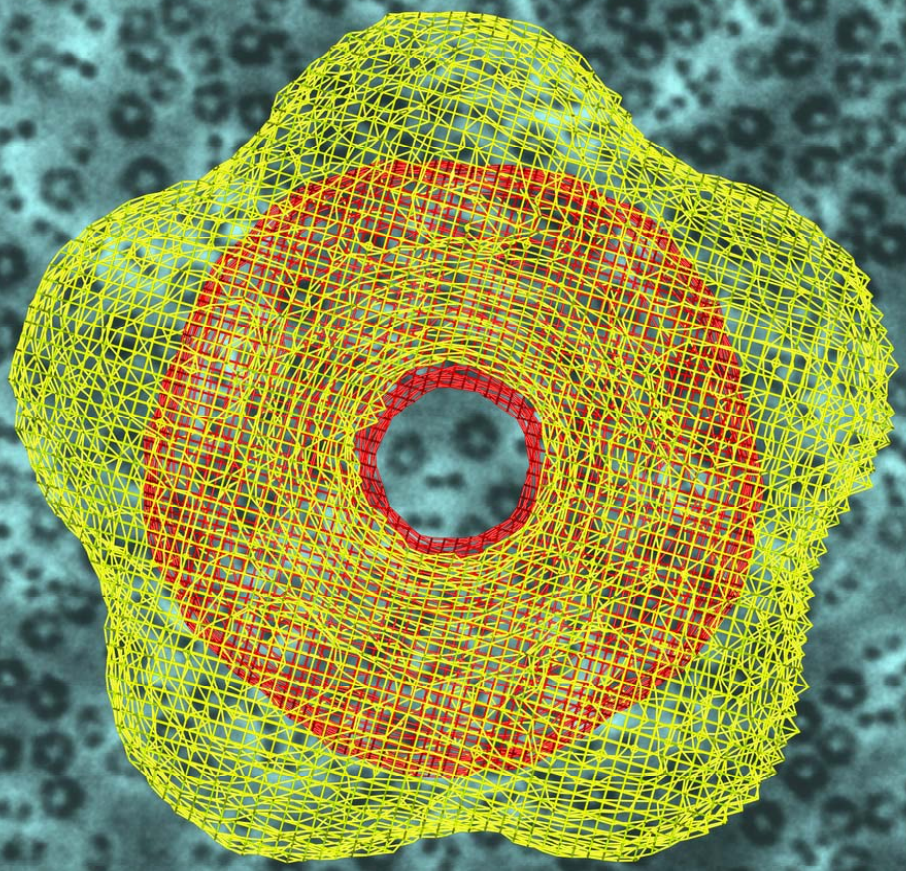

Illustration:

Shape of tryparedoxin peroxidase of *Trypanosoma brucei* in different functional states. The oxidized peroxidase of *T. brucei* forms an almost regular ring (red) consisting of ten subunits, as inferred from averaged electron microscopic images. In reaction with a pseudosubstrate, *i. e.* a tryparedoxin with Cys43 mutated to Ser, a dead-end intermediate with pentangular appearance (superimposed yellow net) is formed that mimics the catalytic intermediate proposed for the reduction of the peroxidase by tryparedoxin. Original electron micrographs (blue) of reduced tryparedoxin peroxidase are seen in the background.

Contents

1 Introduction

Today´s Kinetoplastida form a diverse order of flagellated protozoans that have evolved from an ancient lineage, rooted near the base of the eukaryotic tree, at least 500 million years ago. They have adopted a lifestyle that has fascinated generations of biochemists and parasitologists. Kinetoplastida are a group of protozoa characterized by the presence of a specific organelle, the kinetoplast (Vickermann, 1976). This structure was observed by early researchers in light microscopy as basophilic granules near the basal body of the flagellum. It represents a mitochondrium containing a large mass of circular mitochondrial DNA.

Diseases caused by some species of the order Kinetoplastida have always plagued mankind, and today most of them are at least as prevalent as they have been. The parasites cause diseases in animals, plants, are severely affecting human health and are retarding agriculture development in less developed countries. Pathogenic trypanosomatids have digenic life-cycles that alternate between their mammalian and insect host (see chapter 1.2). At least about 21 of 30 different *Leishmania* species have been identified as causative agents of the cutaneous, mucocutaneous and visceral forms (kala-azar) of leishmaniasis. These include the *L. donovani* complex with 3 species (*L. donovani*, *L. infantum* and *L. chagasi*), the *L. mexicana* complex with 3 main species (*L. mexicana*, *L. amazonensis* and *L. venezuelensis*), the subgenus *Viannia* and the species *L. tropica*, *L. major* and *L. aethiopica*. The different species are morphologically indistinguishable, but they can be differentiated by isoenzyme analysis, molecular methods or monoclonal antibodies.

The most intensively studied members of the genus *Trypanosoma* are *Trypanosoma brucei brucei*, the causative agent of nagana in cattle and the human pathogen subspecies *Trypanosoma brucei gambiense*, that causes west African sleeping sickness and *Trypanosoma brucei rhodesiense*, the causative agent of east African sleeping sickness. The two human pathogen subspecies are morphologically indistinguishable.

The protozoan parasite *Trypanosoma cruzi* causes Chagas disease, a zoonotic disease that can be transmitted to humans and is also called American trypanosomiasis.

1.1 Epidemiology of Kinetoplastida

1.1.1 Leishmaniasis

Leishmaniasis is found in parts of about 88 countries, where approximately 350 million people live. Most of the affected countries are in the tropics and subtropics. The disease is spread in some parts of Mexico, central America, south America, Asia, the middle east, and Africa. More than 90 % of cutaneous leishmaniasis cases occur in Iran, Afghanistan, Syria, Saudi Arabia, Brazil and Peru. More than 90 % of visceral leishmaniasis cases occur in Bangladesh, Brazil, India and Sudan (see Figure 1.1)(CDC, 2003; WHO, 2003c).

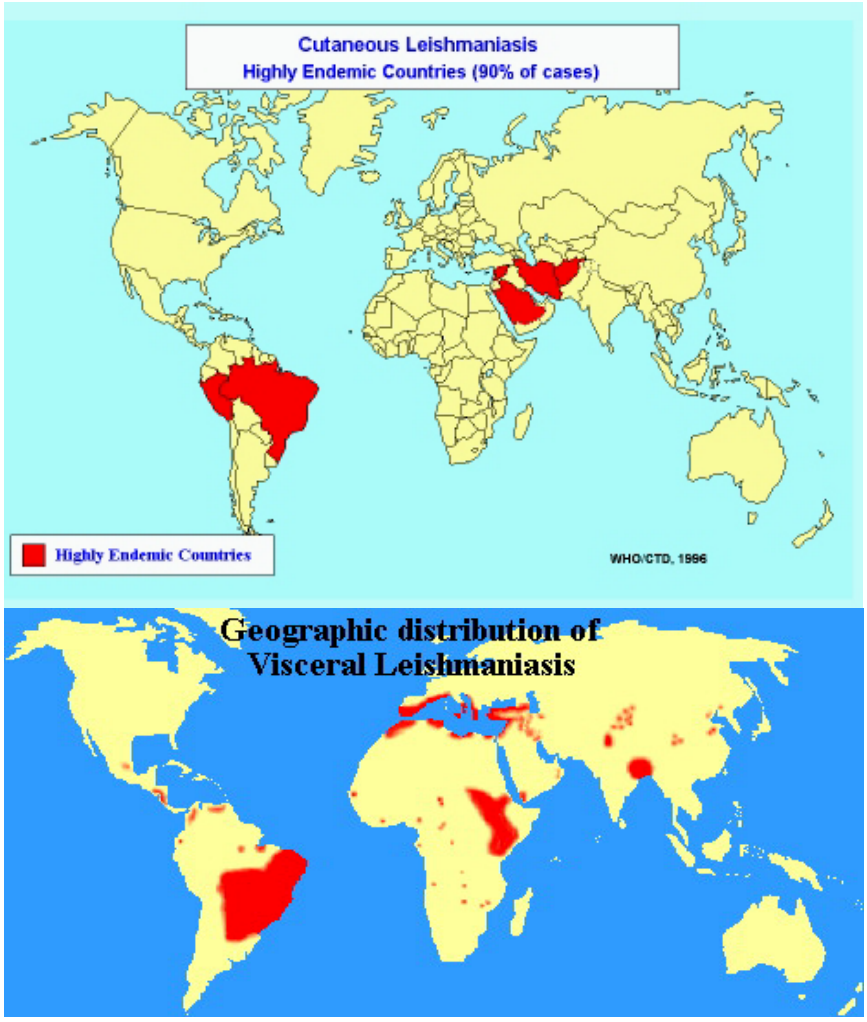

Figure 1.1: Distribution of cutaneous and visceral leishmaniasis. Highly endemic countries are shown in red. (C.D. Foundation, 2003; WHO, 2003c)

For cutaneous leishmaniasis 1 – 1.5 million new cases and for visceral leishmaniasis 500,000 new cases per year are estimated. The overall prevalence is 12 million people.

1.1.2 Sleeping sickness

There have been three severe epidemics in Africa over the last century: one between 1896 and 1906, mostly in Uganda and the Congo Basin, one in 1920 in several African countries, and one that began in 1970 and is still in progress. The disease had practically disappeared between 1960 and 1965. After that success, screening and effective surveillance were relaxed, and the disease has reappeared in endemic form in several foci over the last 30 years.

Trypanosoma brucei gambiense (*T. b. gambiense*) is found in central and west Africa and causes chronic infection. A person can be infected for months or even years without developing obvious symptoms. *Trypanosoma brucei rhodesiense* (*T. b. rhodesiense*) is found in southern and east Africa. It causes acute infection that emerges after a few weeks. It is more virulent than the other strain and develops more rapidly, which means that it is more quickly detected clinically. Almost 45,000 cases were reported in 1999, but the World Health Organization (WHO) estimates that the number of people affected is higher between 300,000 and 500,000 (WHO, 2003c).

Countries are divided in four categories in terms of prevalence. In each country the spatial distribution of the disease is very diverse; it is found in foci and micro-foci. (i) Countries where there is an epidemic of the disease, in terms of very high cumulated prevalence and high transmission: Angola, Democratic Republic of Congo and Sudan; (ii) highly endemic countries, where prevalence is moderate but increase is certain: Cameroon, Central African Republic, Chad, Congo, Côte d´Ivoire, Guinea, Mozambique, Uganda and United Republic of Tanzania; (iii) countries where the endemic level is low; (iv) countries whose present status is not clear (see Figure 1.2) (WHO, 2003a).

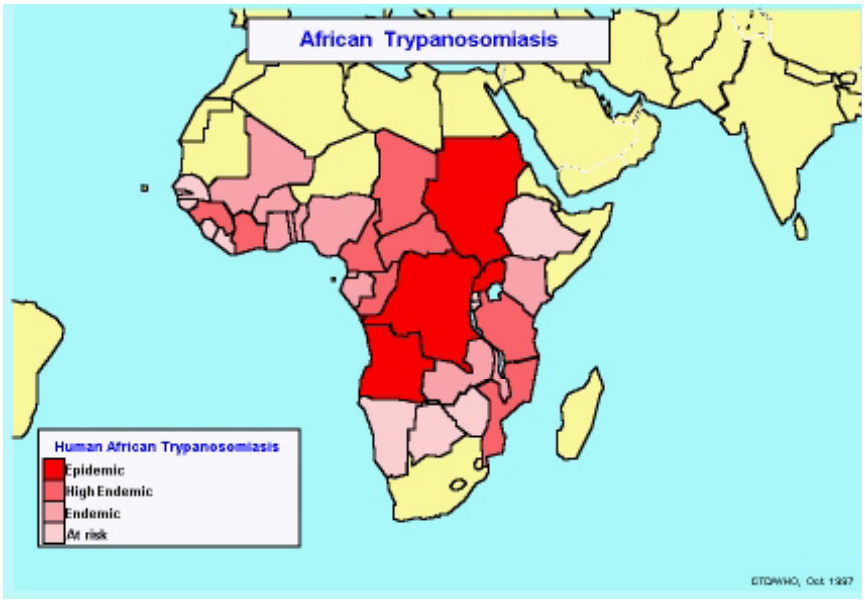

Figure 1.2: Depending on their level of disease prevalence, endemic countries can be classified in four major levels of endemicity (WHO, 2003a): epidemic countries (red); high endemic countries (deep purple); endemic countries (purple); countries at risk (light purple).

1.1.3 Chagas disease

Detected in Andean mummies dating back to 4000 BC (Guhl *et al.*, 1999), Chagas disease started to expand at the end of the 19th century and reached a peak in the first half of the 20th century. Chagas disease occurs throughout Mexico and central and southern America, and continues to pose a serious threat to health in many countries of that region (see Figure 1.3).

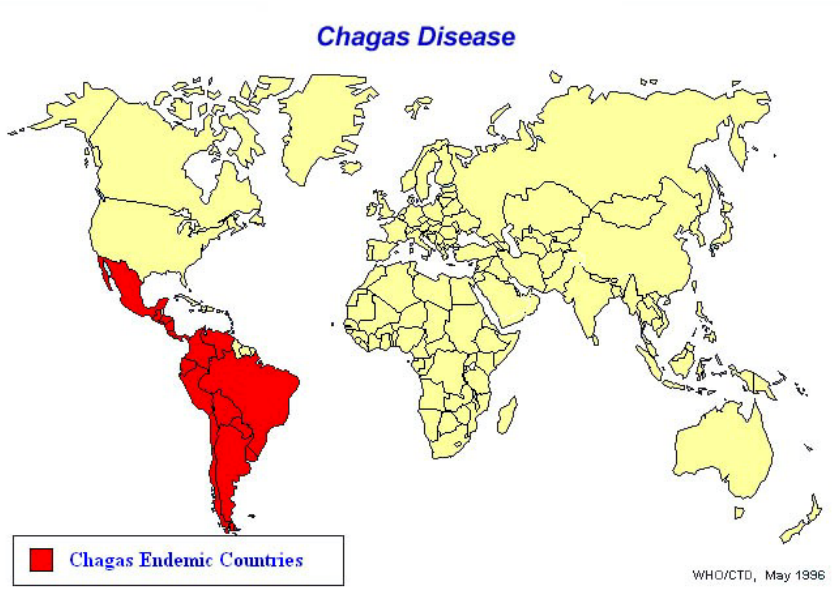

Figure 1.3: Geographical distribution of Chagas disease (WHO, 2002).

Furthermore, due to recent significant population migration from endemic countries towards developed countries, the threat of the disease is expanding to reach areas outside the traditional geographic boundaries (WHO, 2002).

Chronic Chagas disease affects a significant number of individuals in Latin America, mostly the poorest of the poor. The overall prevalence of human *Trypanosoma cruzi* infection is estimated at 16 – 18 million cases. Approximately 120 million people, i. e. 25 % of the inhabitants of Latin America, are at risk of infection.

1.2 Infection and disease

1.2.1 Leishmaniasis

Leishmaniasis is a vector-born disease that is transmitted by the bite of an infected female phlebotomine sandfly and caused by obligate intracellular protozoa of the genus *Leishmania*. Sandflies are primarily infected by biting an infected animal (i. e. rodents or dogs) or humans. A parasitized female sandfly takes a blood meal from a human host and injects the amastigote form of the parasite to the blood of the human host. In the amastigotic stage the parasites are infective and can affect different tissues depending in part on the *Leishmania* species (see Figure 1.4).

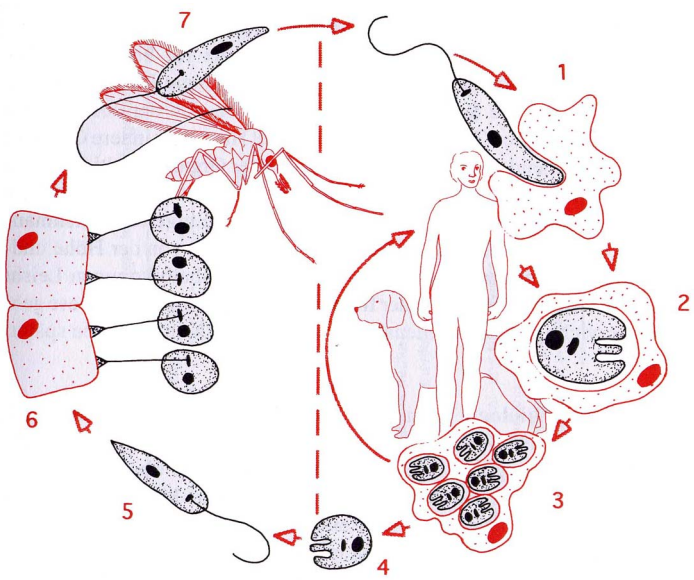

Figure 1.4: Leishmaniasis is transmitted by the bite of a female phlebotomine sandfly. The sandflies inject the infective stage, promastigotes, during a blood meal. Promastigotes are phagocytized by macrophages (1) and transform into amastigotes (2). Amastigotes multiply (3) and are released to the circulation, where they can infect different tissues (back to 1) or infect sandflies during a blood meal of an infected host

(4). In the gut of the fly they transform to promastigotes (5), attach to the epithel of the gut (6) transform to the infective stage and migrate to the proboscis later on (7) (Lucius and Loos-Frank, 1997).

The leishmaniasis can be classified into four main forms. The factors determining the form of disease include leishmanial species, geographic location and immune response of the host.

1. Visceral leishmaniasis (kala-azar) is characterized by irregular bouts of fever, substantial weight loss, swelling of the spleen and liver and anaemia. Visceral leishmaniasis is the most severe form of the disease which, if untreated, has a mortality rate of almost 100 %.

2. Cutaneous leishmaniasis is the most common form and characterized by one to 200 sores on the skin. The sores can change in size and appearance over time, which self-heal within a few months but leave unsightly scars.

3. Mucocutaneous leishmaniasis begins with skin ulcers which spread, causing dreadful and massive tissue destruction, especially of the nose and the mouth.

4. Diffuse cutaneous leishmaniasis produces disseminated and chronic skin lesions resembling those of lepromatous leprosy and is difficult to treat (WHO, 2003d).

For treatment, first-line drugs are pentavalent antimonials. Recently, resistance to drugs has been reported, requiring the use of more toxic drugs as the second-line drugs, amphotericin B and Ambisome. Most available drugs are costly, require long treatment regimes and are becoming more and more ineffective. Another strategy is to control the vector, but vector and reservoir host control measures are expensive, requiring good infrastructures and maintenance. Infection can be prevented by avoidance of sandfly bites through use of repellents or insecticides (WHO, 2003d).

1.2.2 African trypanosomiasis

Domestic and wild animals are the reservoir of *T. b. rhodesiense*. They can also be infected by *T. b. gambiense*, though the precise role of this reservoir is not well known. Infection starts with a blood meal on a mammalian host. An

infected tsetse fly (genus *Glossina*) injects metacyclic trypomastigotes into skin tissue. The life-cycle can start (see Figure 1.5).

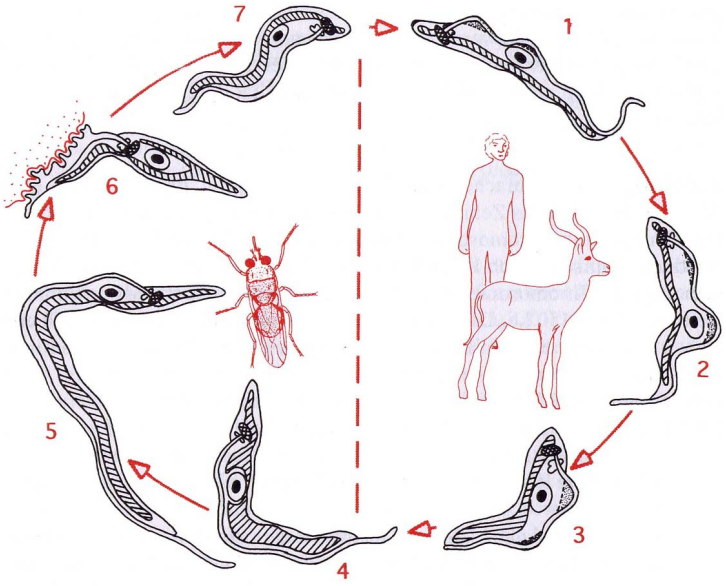

Figure 1.5: The tsetse fly injects the metacyclic trypomastigotes during a blood meal (1). They transform into bloodstream trypomastigotes (2) and replicate by binary fission. The tsetse fly can get infected by taking a blood meal from an infected host (3). The procyclic trypomastigotes (4) transform into mesocyclic trypomastigotes (5) in the gut of the fly. Later, when they reach the saliva they transform to epimastigotes, attached to the saliva (6). At the end they transform to infective trypomastigotes (7). The cycle in the fly takes approximately 3 - 5 weeks (Lucius and Loos-Frank, 1997).

The disease occurs in two forms: a chronic one caused by *T. b. gambiense*, which occurs in west and central Africa; and an acute form, caused by *T. b. rhodesiense*, which occurs in eastern and south Africa. The chronic infection lasts for years, while the acute form may last for only weeks before death occurs, if treatment is not administered. The early phase entails bouts of fever, headaches, pain in the joints and itching. The second, known as the neurological phase, begins when the parasite crosses the blood-brain barrier and infects the central nervous system. This is when the characteristic signs and symptoms of the disease appear: confusion, sensory disturbances and poor coordination. Disturbance of the sleep cycle, which gives the disease its name, is the most important feature. If the patient does not receive treatment before the onset of the second phase, neurological damage is irreversible even after treatment (WHO, 2003d).

If the disease is diagnosed early, the chances of cure are high. Suramine and Pentamidine are used as first phase drugs and Melarsoprol and Eflornithine

are used as treatment in the second phase of infection. In short, most drugs are old, difficult to administer in poor conditions, toxic, and by no means always successful (WHO, 2003d).

1.2.3 Chagas disease

There are various strains of *Trypanosoma cruzi* (*T. cruzi*), which differ in terms of epidemiology, pathogenicity, response to treatment, biochemistry or immunogenicity. The tendency is to assign all isolated strains into two major groups, defined as I and II. *T. cruzi* I is extremely widespread within the sylvatic cycle, highly associated with opossums and may represent the original form of *T. cruzi*. *T. cruzi* II seems primitively associated with rodents and with *Triatoma infestans*. Of more than 100 recognized triatome species, only about ten are widespread colonizers of human dwellings and are highly anthropophilic (Prata, 2001).

Parasites can be transmitted to humans in three ways:

1. By blood-sucking triatomes, which live in cracks and crevices of poor-quality houses, usually in rural areas. They emerge at night to bite and suck blood. The faeces of the insect, left after a blood meal, contain parasites, which can enter the wound usually when it is scratched or rubbed (see Figure 1.6).

2. Through blood transfusion with infected blood. The risk of acquiring the infection after transfusion is about 20%.

3. The third and most important route is the congenital one. The likelihood of congenital transmission in children of chagasic mothers ranges from 1 – 10 %. This type of transmission may also occur outside endemic areas.

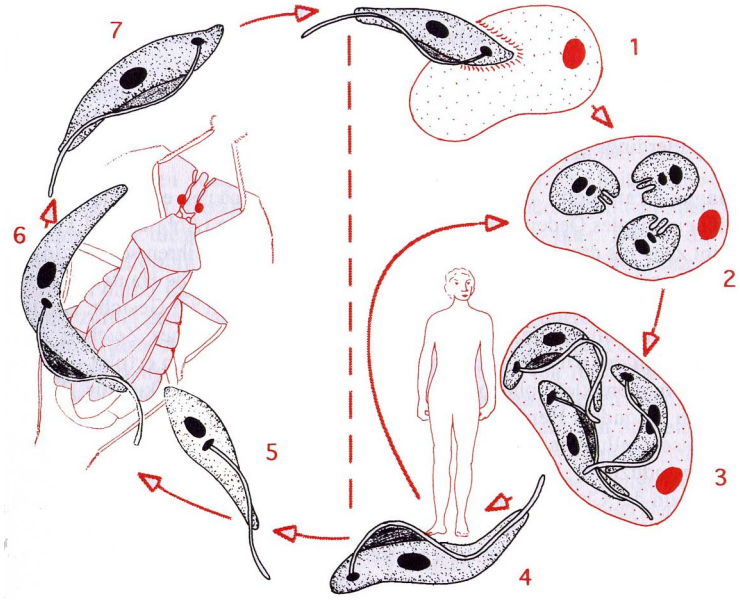

Figure 1.6: Inside the host the trypomastigotes invade cells (1), where they differentiate into amastigotes (2). They multiply and transform to trypomastigotes (3) and are then released into the circulation as bloodstream trypomastigotes (4). They infect a variety of tissues and transform back to amastigotes (back to 2). The bugs become infected by sucking human or animal blood that contains circulating parasites (5). The ingested trypomastigotes transform into epimastigotes in the vector´s midgut (6) and differentiate into infective metacyclic trypomastigotes in the hindgut (7) (Lucius and Loos-Frank, 1997).

Usually a small sore develops at the bite where the parasite enters the body. If this is near the eye, the eyelid, becomes swollen (known as Romaña´s sign). Within a few days, fever and swollen lymph nodes may develop. This initial acute phase may cause illness and death, especially in young children. More commonly, patients enter a symptomless phase lasting several months or years. During that time the parasites are invading most organs of the body, often causing heart, intestinal and oesophageal damage and progressive weakness. In 32 % of those infected people, fatal damage to the heart and digestive tract occurs (WHO, 2003b).

Two drugs, nifurtimox and benznidazol, are capable of curing at least 50 % of recent infections. These products are active in the acute and short-term chronic phase. However, they have little or no activity in long-term chronic forms of the disease. As well, both drugs have serious and frequent side-effects so their use has been limited.

1.3 Phagocytes and oxidative stress

As described in chapter 1.2 the promastigotes of the order Kinetoplastida are phagocytized by macrophages and transform into non-motile, oval amastigotes with retracted flagella. They are obligate intracellular pathogens that are major causes of human diseases and deaths worldwide. Such intracellular pathogens need specialized survival strategy to survive in the mammalian host.

Phagocytes are the first line of defense against invading pathogens, killing and disposing them with impressive efficiency. They produce a battery of reactive oxidizing agents, which also cause harm on the nearby tissues. These oxidants are generated by four enzymes: NADPH oxidase, superoxide dismutase, nitric oxide synthase and myeloperoxidase (Babior, 2000).

NADPH oxidase is a membrane-bound enzyme that catalyzes the production of superoxide (O_2^-) from oxygen and NADPH:

$$2\ O_2 + NADPH \rightarrow 2\ O_2^- + NADP^+ + H^+$$

It is dormant in the resting phagocyte but comes to life, when the cell is activated (i. e. by phagocytized bacteria or inflammatory polypeptides).

Superoxide dismutase catalyzes the conversion of O_2^- to H_2O_2 and oxygen.

$$2\ O_2^- + 2\ H^+ \rightarrow\ O_2 + H_2O_2$$

It is called a dismutation, because the substrate (O_2^-) reacts with itself to give an oxidized product (i. e. oxygen) and a reduced product (i. e. H_2O_2).

Nitric oxide synthase catalyzes the production of nitric oxide (NO) from arginine, oxygen and NADPH (Beckman and Koppenol, 1996).

$$\text{Arginine} + \text{oxygen} + NADPH \rightarrow NO + \text{citrulline} + NADP^+$$

There are two general varieties of NO synthase: constitutive and inducible. The constitutive form is a low-activity enzyme that produces small amounts of NO as signaling molecules (Murad, 1994). It is found in vascular endothelium and in the central nervous system. The inducible form is a high-activity enzyme that is produced by phagocytes, when they are suitably stimulated (Weinberg *et al.*, 1995).

Myeloperoxidase catalyzes the oxidation of halide ions (Cl^-, Br^-, I^-) to hypohalous acids at the expense of hydrogen peroxide.

$$Cl^- + H_2O_2 \rightarrow OCl^- + H_2O$$

The H_2O_2 employed in this reaction is produced by the dismutation of O_2^-. The enzyme can oxidize any of the three halide ions listed above and in addition can oxidize thiocyanate (SCN^-) (Babior, 2000).

H_2O_2 is able to generate the most aggressive $^\bullet OH$ in the presence of transition metals. Simultaneously, hydroperoxides of unsaturated fatty acids will be directly formed by activated lipoxygenases and cyclooxygenases or may be generated indirectly by $^\bullet O_2^-/H_2O_2$-driven unspecific lipid peroxidation (Brigelius-Flohé *et al.*, 2002).

Those responses to everything recognized as foreign are meant to eliminate intruded pathogens, but have also harmful side-effects to the host´s tissue. Both, the affected host and the pathogen had to develop strategies for the elimination of reactive oxygen intermediates (ROI) and reactive nitrogen intermediates (RNI). These strategies vary for phylogenetically diverse species, which offers the opportunity of selective inhibition of the pathogen´s defense mechanism, without affecting the host´s self-protection (Budde and Flohé, 2002).

1.4 Self-protection of the mammalian host

The best known H_2O_2 eliminating enzyme is catalase, which dismutates H_2O_2 to H_2O and molecular oxygen (Schonbaum and Chance, 1976; Wood *et al.*, 2003b). But in all mammalian cells catalase appears to be largely restricted to the peroxisomes, where it is involved in detoxifying the H_2O_2 derived from the peroxisomal metabolism. Equally efficient as catalase are the selenium-containing glutathione peroxidases (GPx) (Flohé *et al.*, 1972; Günzler *et al.*, 1972). Beneath H_2O_2 they detoxify a wide range of organic hydroperoxides (Flohé and Brigelius-Flohé, 2001). Five variants of glutathione peroxidases (GPx-1 - GPx-5) are known in mammals to date. GPx-5 is the only known non-selenium containing peroxidase. They have all in common, that they detoxify hydroperoxides at the expense of NADPH via glutathione (GSH) and glutathione reductase, with the exception of GPx-3, which additionally uses glutaredoxin and thioredoxin (Trx). Another H_2O_2 reducing enzyme family are the peroxiredoxins (Prx). Many organisms produce more than one isoform,

including at least six Prxs identified in mammalian cells (PrxI - PrxVI) (Hofmann *et al.*, 2002; Wood *et al.*, 2003b). They share a common reactive Cys residue in the N-teminal region, are capable of serving as a peroxidase, and involve thiols like thioredoxin or glutathione as the electron donors. These Prx family members are located in the cytosol, mitochondria, peroxisomes or plasma, that are all sites of ROI production (Fujii and Ikeda, 2002) (see Figure 1.7).

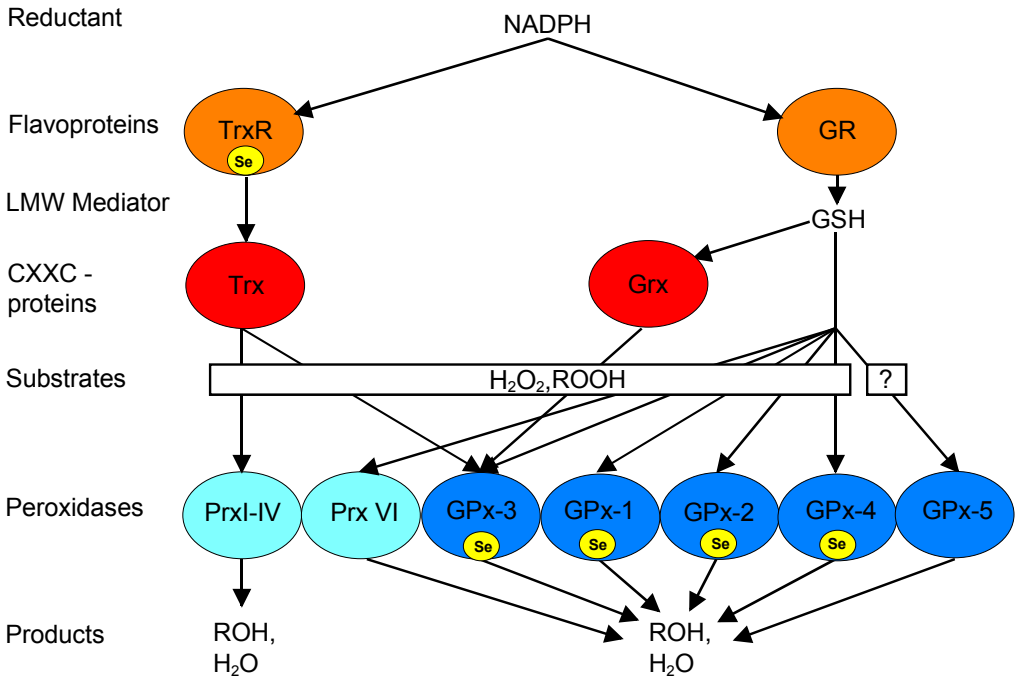

Figure 1.7: Thiol-mediated hydroperoxide metabolism in mammals. Homologous proteins are shown in identically marked circles. Se indicates redox-active selenium. TrxR, thioredoxin-reductase; GR, glutathione reductase; Trx, thioredoxin; Grx, glutaredoxin; Prx, peroxiredoxin; GPx, glutathione peroxidase (Budde and Flohé, 2002).

1.5 Detoxification of hydroperoxides in trypanosomatids

As the production of reactive oxygen intermediates (ROI) is an important microbicidal strategy used by the mammalian host against invading pathogens, the localization of the parasites within the host and the biochemical mechanisms used to detoxify ROI is a fundamental aspect of the host-parasite interaction. There are pronounced differences between the antioxidant machinery of trypanosomatids and other eukaryotes. Trypanosomatids lack catalase and selenium-containing glutathione peroxidases (Flohé *et al.*, 1999). As much as 70 % of their glutathione is converted to the N^1,N^8-bis-

(glutathionyl)-spermidine adduct, trypanothione (Fairlamb and Cerami, 1992). Trypanothione [$T(SH)_2$] is maintained in the reduced state by a trypanothione reductase (TR), a member of the disulfide reductase family, with high sequence homology to glutathione reductase (Fairlamb and Cerami, 1992). The downstream part of the trypanosomatid peroxide metabolism is quite distinct from the analogous mammalian system. The component accepting the reduction equivalents from trypanothione is tryparedoxin (TXN), which is related to the thioredoxin family. Tryparedoxin itself is a substrate for the tryparedoxin peroxidase (TXNPx), which reduces H_2O_2 and organic hydroperoxides (Gommel *et al.*, 1997; Nogoceke *et al.*, 1997) (see Figure 1.9)

Trypanothione reductase is common to *Chrithidia*, *Trypanosoma* and *Leishmania* species (Fairlamb and Cerami, 1992), but has also been detected in nonparasitic *Euglena gracilis* (Montrichard *et al.*, 1999). The enzyme was crystalized from two species, *T. cruzi* (Krauth-Siegel *et al.*, 1987) and *C. fasciculata* (Hunter *et al.*, 1990; Kuriyan *et al.*, 1991) and studied extensively by radiographic analysis, steady-state kinetics and rational mutagenesis (Fairlamb and Cerami, 1992). Moreover, the results of disruption of the TR gene in *T. brucei* has confirmed their absolute necessity for the survival of the parasites in macrophages (Krieger *et al.*, 2000). Blocking the TR activity by a dominant-negative approach in *L. donovani* resulted in a down-regulation of the TR activity up to 85 % (Tovar *et al.*, 1998). A conditioned knock-out of trypanothione reductase in *T. brucei brucei* resulted in increased sensitivity to H_2O_2 exposure, loss of virulence and arrest of proliferation (Krieger *et al.*, 2000). That data complies with previous failures to obtain any viable clones in which the trypanothione reductase gene was knocked out constitutively (Dumas *et al.*, 1997).

Trypanothione is the essential redox mediator in trypanosomatids comprising the genera *Crithidia*, *Leishmania* and *Trypanosoma* (Fairlamb and Cerami, 1985). It is provided by de novo synthesis from spermidine, glutathione and ATP (Henderson *et al.*, 1990; Koenig *et al.*, 1997; Oza *et al.*, 2002; Comini *et al.*, 2003) and regenerated from its oxidized cyclic disulfide form by trypanothione reductase (see Figure 1.8).

$$GSH + Spermidine \xrightarrow{ATP/Mg2+;\ GspS} N^1(or\ N^8)\text{ -glutathionyl-spermidine (Gsp) (1)}$$

$$Gsp + GSH \xrightarrow{ATP/Mg2+;\ TryS} T(SH)_2\ (2)$$

Figure 1.8: Synthesis of trypanothione: The first step (1) of the reaction is catalyzed by glutathionyl-spermidine synthetase (GspS) and the second step (2) of the reaction is catalyzed by an enzyme called trypanothione synthetase (TryS).

The two distinct enzymes had been isolated from *C. fasciculata* having GspS or TryS activity (Smith *et al.*, 1992; Koenig *et al.*, 1997). So it was a big surprise to find a single gene in *T. cruzi*, *T. brucei brucei* and *C. fasciculata*, which encodes for a protein with both, GspS and TryS activity (Oza *et al.*, 2002; Comini *et al.*, 2003; Comini *et al.*, 2003, unpublished)

Tryparedoxins (TXNs) are redox-active proteins which were discovered first in *C. fasciculata* (Nogoceke *et al.*, 1997; Montemartini *et al.*, 1998a; Guerrero *et al.*, 1999), later identified in *T. cruzi* (Lopez *et al.*, 1997), *T. brucei* (Lüdemann *et al.*, 1998), and *Leishmania infantum* (Castro H. *et al.*, 2003, unpublished). They differ from typical thioredoxins by their active site motif WCPPCR. CXXC motifs in general are characteristics of proteins reversible catalyzing the reduction of disulfides and are common in the thioredoxin superfamily. Due to several insertions up to 5 kDa, TXNs are considerable larger than thioredoxins. Functionally, TXN transfers reduction equivalents from trypanothione to tryparedoxin peroxidase, which is a peroxiredoxin. Apart from being a reducing substrate for TXNPx, TXN was shown to support also ribonucleotide reductase of *T. brucei*, thus being relevant for DNA synthesis (Dormeyer *et al.*, 2001; Krauth-Siegel and Schmidt, 2002) (see Figure 1.9).

Peroxiredoxins have received considerable attention in recent years as a new expanding family of thiol-specific antioxidant proteins (Chae *et al.*, 1994a; Chae *et al.*, 1994b). They exert their protective antioxidant role in cells through their peroxidase activity, whereby hydrogen peroxide, peroxynitrite and a wide range of organic hydroperoxides are reduced and detoxified (Poole and Ellis, 1996; Bryk *et al.*, 2000; Hofmann *et al.*, 2002). Indeed, these enzymes are truly ubiquitous, having been identified in yeast, plant and animal cells, including both protozoan an helminth parasites, and most, if not all, eubacteria and archaea. Peroxiredoxins use redox-active cysteines to reduce peroxides and were originally divided into two categories, the 1-Cys and the 2-Cys peroxiredoxins, based on the number of cysteinyl residues directly involved in catalysis. The TXNPxs belong to the 2-Cys Prx in analogy to peroxiredoxins of

other species, the alkyl hydroperoxide reductase (AhpC) of bacteria (Wood *et al.*, 2002), thioredoxin peroxidase of yeast (Chae *et al.*, 1994a) and some mammalian peroxiredoxins (Chae *et al.*, 1999). The reaction center of tryparedoxin peroxidase of Kinetoplastida is presumed to be build-up by two identical, invertedly orientated subunits. The oxidized proximal cysteine (C52) first reacts with the distal one (C173´) of the co-reacting second inverted subunit of the oligomeric enzyme (Budde *et al.*, 2003a), before specific reduction can start.

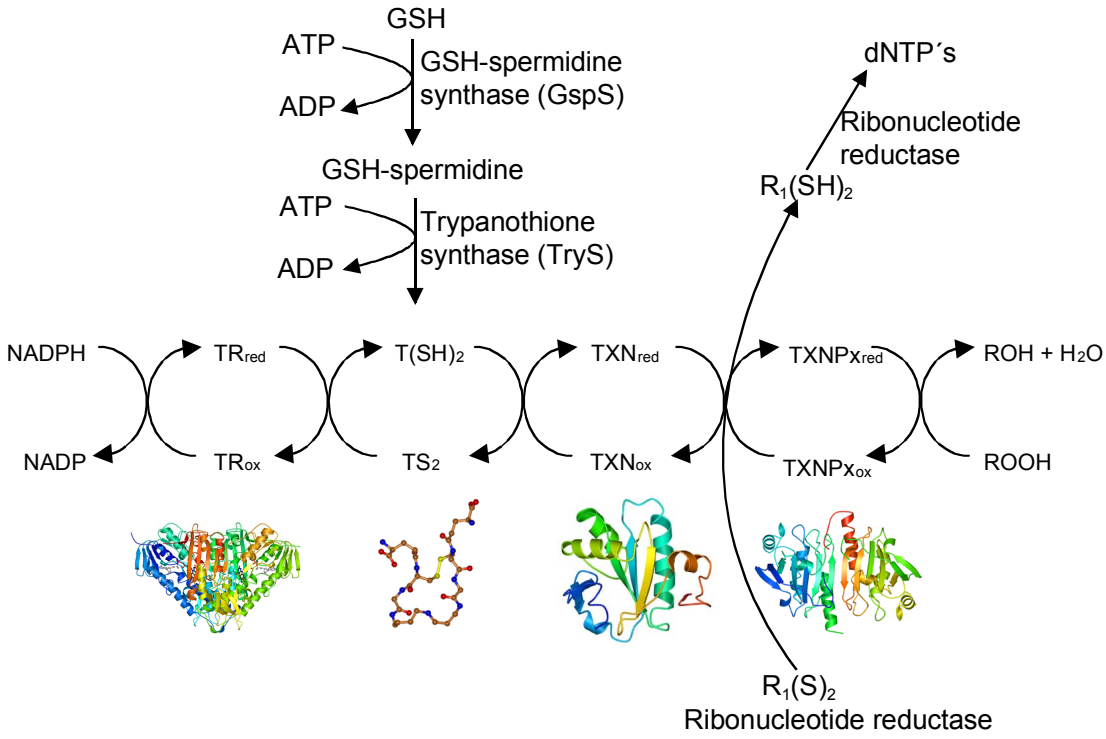

Figure 1.9: The unique hydroperoxide detoxification cascade in Kinetoplastida. The terminal peroxidase [tryparedoxin peroxidase (TXNPx)] reduces hydroperoxide at the expense of NADPH. Tryparedoxin (TXN) reduces tryparedoxin peroxidase (TXNPx) and is itself reduced by trypanothione [$T(SH)_2$]. Oxidized trypanothione is recycled by trypanothione reductase (TR). Trypanothione is synthesized by glutathione-spermidine synthase (GspS) and trypanothione synthase (TryS) at the expence of two molecules of ATP. In some cases both reactions are triggered by one enzyme. The synthesis of deoxyribonucleotides (dNTPs) by ribonucleotide reductase is linked to the peroxide detoxification mechanism in *T. brucei* as this reaction is catalyzed by tryparedoxin.

It was shown by immunohistochemistry, that the localization of TXN and TXNPx of *C. fasciculata* is restricted to the cytosol. But recently, peroxiredoxins with mitochondrial targeting sequences have been reported in

T. cruzi (Wilkinson *et al.*, 2000b), *L. infantum* (Wilkinson *et al.*, 2000a; Castro *et al.*, 2002a), and *T. brucei* (Tetaud *et al.*, 2001).

1.6 Objectives of the study

In Kinetoplastida, tryparedoxin peroxidases are the terminal peroxidases of a unique cascade of oxidoreductases that reduce hydroperoxides at the expense of NADPH. Enzymatic characterizations were reported for the cytosolic form of TXNPxs of *Crithidia fasciculata* (Nogoceke *et al.*, 1997), *Leishmania major* (Levick *et al.*, 1998), *Trypanosoma cruzi* (Guerrero *et al.*, 2000a), *Leishmania donovani* (Flohé *et al.*, 2002a), and *Leishmania infantum* (Castro unpublished), but no one for the *Trypanosoma brucei* species.

The objectives of this study was to characterize the hydroperoxide detoxification system of *T. brucei brucei*. The main part of this work will focus on the TXNPx of *Trypanosoma brucei brucei*, which is nearly identical to the TXNPx of *T. b. rhodesiense*.

1. Like other TXNPxs, the *Tb*TXNPx (tryparedoxin peroxidase of *Trypanosoma brucei brucei*) has to be tested for different peroxides including organic and lipid hydroperoxides.

2. The tryparedoxin peroxidase nature of the *Tb*TXNPx has to be clarified by using thioredoxin of *E. coli* or glutathione as reductants.

3. A kinetic pattern for *Tb*TXNPx, *Li*TXNPx and *Li*TXN will be evaluated in this thesis and compared to the previous investigations of related enzymes.

4. Specifically we will investigate the question, how oxidation and reduction or substrate binding affect the molecular size and shape of *Tb*TXNPx and the mitochondrial TXNPx of *Leishmania infantum* (*Li*mTXNPx).

5. We wanted to clarify the question, if all ten binding sites of the decameric *Tb*TXNPx are accessible for its substrates or not.

6. The reaction mechanism of the reductive part of the TXNPx, should be compared with the hypothetical thesis.

7. Models of TXN interacting with trypanothione will be supported by mutagenesis studies and measurements of TXN with an inhibitory pseudosubstrate.

2 Methods and materials

2.1 Chemicals

Most chemicals used in this study were of the highest purity grade available and were obtained from:

- J. T. Baker B. V., Denventer, Netherlands
- Merck, Darmstadt, Germany
- Serva Feinbiochemica GmbH & Co., Heidelberg, Germany
- Sigma-Aldrich, Taufenkirchen, Germany

2.2 Parasite strain and culture procedure

The procyclic *Trypanosoma brucei brucei* strain PC 117 (VSG variant 117 from the cell line MITat 1.4) was kindly provided by Dr. Friedemann Hesse (GBF, Braunschweig, Germany).

The promastigotes were cultivated under logarithmic growth conditions (2 x 10^4 to 1 x 10^7 parasites per ml) at 27 °C in supplemented 1 x MEM-medium (Duszenko *et al.*, 1992) (see Table 2.1). Cell growth was monitored by counting the parasites in a Neubauer chamber.

Table 2.1: Composition of completed 1 x MEM-medium for cultivation of procyclic trypanosomes:

minimum essential medium (MEM), pH 7.4	
10 x MEM (Invitrogen, Karlsruhe, Germany)	100 ml/l
100 x non-essential amino acid solution (Sigma-Aldrich, Taufenkirchen, Germany)	10 ml/l
HEPES for cell culture (Roth, Karlsruhe, Germany)	7140 mg/l (30 mM)
L-Phenylalanine (Sigma-Aldrich, Taufenkirchen, Germany)	68 mg/l (0.6 mM)
L-Ornithine/HCl (Sigma-Aldrich, Taufenkirchen, Germany)	10 mg/l (59 µM)
Adenosine (Sigma-Aldrich, Taufenkirchen, Germany)	12 mg/l (45 µM)
L-Glutamine (Invitrogen, Karlsruhe, Germany)	10 ml/l (2 mM)
Sodium-pyruvat (Sigma-Aldrich, Taufenkirchen, Germany)	220 mg/l (2 mM)
L-Proline (Serva, Heidelberg, Germany)	600 mg/l (5.2 mM)
Hemin (ICN, Costa Mesa, CA, USA)	25 mg/l (0.25 mM) solved in 0.1 N NaOH
Fetal calve serum (heat inactivated for 30 min. at 60 °C, Biochrom KG, Berlin, Germany)	10 % (v/v)

2.3 Bacterial strains and culture procedure

2.3.1 Bacterial strains

E. coli strains used in this study are listed in Table 2.2:

Table 2.2: *E. coli* strains and their characteristics:

***E. coli* strain**	**genotype and relevant phenotype**	**reference**
E. coli Tuner (DE3)	F$^-$ *ompT hsdS$_B$* (r_B^- m_B^-) *gal dcm lacY1* (DE3)	Novagen (Madison, WI, USA)
E. coli BL21 (DE3)	F$^-$ *ompT hsdS$_B$* (r_B^- m_B^-) *gal dcm* (DE3)	Novagen (Madison, WI, USA)
E. coli Nova Blue	*endA1 hsdR17*(r_{K12}^- m_{K12}^+) *supE44 thi-1 recA1* *gyrA96 relA1 lac*[F´*proA*$^+$*B*$^+$ *lacI*^{q}*ZΔM15*::Tn*10*(Tc^R)]	Novagen (Madison, WI, USA)
E. coli DH5α	*supE44 ΔlacU*169(Φ80 *lacZ* ΔM15) *hsdR17 recA1 endA1 gyrA96 thi*-1 *re*lA1	(Hanahan, 1983)
E. coli SURE	*e14*$^-$ *(McrA*$^-$*) Δ(mcrCB-hsdSMR-mrr)*171 *endA1 supE44 thi-1 gyrA96 relA1 lac recB recJ sbcC umuC*::Tn5 (Kan^r) *uvrC* [F´*proAB lacI*^{q}*ZΔ*(M15 Tn*10* (Tet^r)]	Stratagene (Amsterdam, Netherlands)

2.3.2 Plasmids

Plasmids used in this study are summarized in Table 2.3.

Table 2.3: Plasmids and their properties:

plasmids	properties	reference
pET-22b(+)	IPTG-inducible expression vector (5.5 kb), T7 promoter, T7 terminator, C-terminal His-tag, lac operator, pBR322 ori, ampicillin resistent	Novagen (Madison, WI, USA)
pET-24a(+)	IPTG-inducible expression vector (5.3 kb), T7 promoter, T7 terminator, C-terminal His-tag, lac operator, pBR322 ori, kanamycin resistent	Novagen (Madison, WI, USA)
pET-28c(+)	IPTG-inducible expression vector (5.4 kb), T7 promoter, T7 terminator, N-terminal His-tag with thrombin restriction site, lac operator, pBR322 ori, kanamycin resistent	Novagen (Madison, WI, USA)

2.3.3 Cultivation of *E. coli*

E. coli strains DH5α, *Nova blue* and SURE were used for plasmid transformation and replication. The strains BL21(DE3) and Tuner(DE3) were used for expression of recombinant proteins under the control of the T7 RNA-

polymerase promoter. The cells were cultured at 25 – 37 °C in LB medium on a rotary shaker operated at 160 rpm (Certomat U, B. Braun, Melsungen, Germany), in Erlenmeyer flasks filled up with not more than 20 % of their total volume. For strains carrying plasmids, selection was performed by addition of 200 µg/ml ampicillin or 100 µg/ml kanamycin to the medium. For short term storage strains were conserved on agar plates at 4 °C for one month; for long term storage a liquid culture containing 50 % glycerol was stored at –80 °C.

Table 2.4: Composition of the Luria-Bertani (LB) medium. The pH was adjusted to pH 7.4 with 5 N NaOH. For the preparation of agar plates 1.5 % Agar (Difco, Detroit, MI, USA) was supplemented to the liquid LB-medium.

Bacto-Tryptone (Difco, Detroit, MI, USA)	10 g
Bacto-Yeast extract (Difco, Detroit, MI, USA)	5 g
NaCl p.a.	10 g
dest. H_2O	ad 1 l

2.4 Methods used in molecular biology

Most of the molecular biology methods used in this study were according to Sambrook *et al.* (2001).

2.4.1 Isolation of genomic DNA from *T. brucei brucei*

Genomic DNA was prepared from the late logarithmic phase of the promastigote culture (5 x 10^7 parasites). The cells were disrupted in a Mikro-dismembranator S (Braun, Melsungen, Germany), containing 100 µl glass beads (425 – 500 µm diameter, Sigma-Aldrich, Taufenkirchen, Germany). The cell suspension was applied to a QIA-shredder (Qiagen, Hilden, Germany) to remove the glass beads and the DNA was afterwards purified with the DNeasy tissue kit (Qiagen, Hilden, Germany).

2.4.2 Purification of DNA

1/10 volume of 3 M sodium acetate (pH 4.8) and 2 volume of 95 % ethanol (p. a.) were added to the DNA solution, mixed briefly and incubated on ice for 10 min. The sample was centrifuged for 30 min at 20,000 x g. The DNA pellet was

washed two times with 70 % ethanol (centrifuged for 15 min at 4 °C and 20,000 x g), air-dried and dissolved in an appropriate volume of deionized water or TE buffer (pH 8.0)(see Table 2.5) and stored at –20 °C.

Table 2.5: Composition of TE-buffer:

10 mM Tris-HCl
1 mM EDTA

2.4.3 Quantification of nucleic acids

2.4.3.1 Measurement of absorbance

The concentration-dependent absorbance of nucleotids at 260 nm can be used to estimate the concentration of DNA solutions. The nucleic acid solution was diluted 1:50 or 1:100 with water. 100 µl (water as reference) was added into a quarz cuvette, absorbance was measured at 260 nm and 280 nm. An OD_{260} of 1 roughly equals 50 µg/ml double stranded DNA. A carefully prepared nucleic acid solution has a ratio of OD_{260}/OD_{280} between 1.5 to 2.0.

2.4.3.2 Quantification in agarose gels

Alternatively to the method described above, the concentration of nucleic acids can be determined by staining the agarose gel with SYBR gold (10,000 x concentrated in DSMO, Molecular Probes Inc., Leiden, Netherlands). A defined amount of mass ladder (Gibco BRL, Karlsruhe, Germany) was used as a standard to run a gel in parallel with the DNA in question. The gel was documented with a digital camera and analyzed (E.A.S.Y. RH-3 system, Herolab, Wiesloch, Germany).

2.4.4 Oligonucleotides

Oligonucleotides were obtained desalted and lyophilized from Metabion (Martinsried, Germany), resolved to a concentration of 100 pmol/µl and used without further purification. Primers used in this study are listed in Table 7.1.

2.4.5 Polymerase chain reaction (PCR)

The PCR was performed in a total volume of 50 – 100 µl solution with either *Taq* DNA Polymerase or ProofStart DNA Polymerase (Qiagen, Hilden, Germany). The protocol used for DNA amplification is listed in Table 2.6.

Table 2.6: PCR reaction composition:

0.5 –1 µg / 10-500 ng	chromosomal template DNA / plasmid DNA
2.5 units	DNA polymerase
200 µMol	each dNTP
0.5 - 1 µMol	5´- primer
0.5 –1 µMol	3´- primer
1 x buffer	Qiagen PCR buffer containing 15 mM $MgCl_2$
up to 50 or 100 µl	sterile deion. water

The reaction was carried out in a T3 Thermocycler (Biometra, Göttingen, Germany) as follows: 95 °C 1 min, annealing temperature 1 min 72 °C 3 min (40 cycles) and 72 °C for 15 min elongation step.

2.4.6 DNA digestion with restriction endonucleases

Restriction enzymes and reagents for cloning procedures were purchased from MBI Fermentas (St. Leon-Rot, Germany). In each restriction reaction an amount of 3 units enzyme were used for 1 µg DNA. The amount of buffer (ionic strength), temperature and duration of the reaction depended on the specific application.

2.4.7 Agarose gel electrophoresis of DNA

The size of DNA fragments or entire plasmids was determined by analysis on 0.8 – 1 % agarose gels. The necessary amount of agarose was dissolved in 1 x TBE buffer (Table 2.7). DNA was loaded with an appropriate dilution in a 6 fold loading buffer (MBI Fermentas, St. Leon-Rot, Germany) onto the gel using 1 x TBE as running buffer. The electrophoresis was performed at 80 - 100 Volt

in a Wide Mini-Sub Cell or a DNA Sub Cell gel chamber (BioRad, Munich, Germany). The agarose gel was stained in a SYBR gold solution (1:10,000 in TBE) for 30 min and analyzed under UV light.

Table 2.7: Composition of 1 x TBE buffer:

89 mM Tris-base
89 mM boric acid
2 mM EDTA

2.4.8 DNA extraction from agarose gels

For DNA extraction from an agarose gel, the QIAquick Gel Extraction Kit from Qiagen (Hilden, Germany) was used. Elution of the DNA was accomplished either with elution buffer (10 mM Tris-HCl, pH 8.5) or sterile deionized H_2O.

2.4.9 DNA sequencing

Nucleotide sequencing of DNA was carried out using an ABI PRISM Dye Terminator Cycle Sequencing Ready Reaction Kit (Perkin-Elmer, Shelton, CT, USA). Samples containing fluorescence-labeled dideoxynucleotid terminators were processed on a 373A Applied Biosystems DNA Sequencing System (Applied Biosystems, Darmstadt, Germany). Homology analysis between sequences was performed using the Vector NTI Suite 6.0 (InforMax. Inc., Oxford, UK) multiple sequence alignment program.

2.4.10 Ligation

For the ligation of cohesive termini, the molar ratio of insert/plasmid was approximately 3:1 in T4 DNA ligase buffer, using 1 Weiss unit T4 ligase (Roche, Mannheim, Germany) per 1 µg DNA in 20 µl. The reaction was carried out at 16 °C over night. For electroporation into *E. coli* the traces of salts were removed by dialysis. A volume of 20 µl ligation reaction was dropped on a filter membrane (0.025 – 0.05 µM, Millipore, Schwalbach, Germany) floating on deionized H_2O and dialyzed for 20 minutes.

2.4.11 Transformation of DNA into *E. coli*

2.4.11.1 Electroporation

A single clone of *E. coli* was transferred from an LB-agar plate to 20 ml LB medium and shaken at 37 °C over night. A volume of 500 ml was inoculated with 5 ml of this over-night culture and cultured at 37 °C for 2 – 5 hours until an OD_{600} of 0.6 to 0.9 was reached. The cells were cooled on ice for 30 min and harvested at 4 °C, 5,000 x g for 15 min (centrifuge: RC5C, Kendro, Hanau, Germany) and washed once with 500 ml, once with 250 ml ice-cold deionized H_2O and with 10 ml cold sterile glycerol (10 %, w/v). The pellet was resuspended with 2 ml glycerol (10 %, w/v), dispensed in 50 µl aliquots and immediately frozen in liquid nitrogen. The competent cells were stored at –70 °C. For the electroporation, 50 µl electrocompetent cells were mixed with 0.1 – 1 µg dialyzed DNA and transferred into a precooled electroporation cuvette (0.2 cm, BioRad, Munich, Germany). The electroporation was performed at 2.5 kV, 200 Ω and 25 µF (*E.coli* Pulser, BioRad, Munich, Germany). Cells were resuspended in 1 ml LB medium, left shaking at 37 °C for 1 hour and then plated on selective solid medium.

2.4.11.2 TSS Transformation

This method was performed according to Chung *et al.* (1989). 50 ml LB medium were inoculated with 1/100 of a freshly prepared over-night culture of *E. coli* and grown for about 1.5 hours until the OD_{600} was 0.5 to 0.7. For each transformation 1 ml culture was transferred to an Eppendorf cup and centrifuged for 30 sec at 20,000 x g at room temperature. The cell pellet was resuspended in ice cold 100 µl TSS (Table 2.8) and incubated for 30 min on ice with 0.1 – 1 µg DNA. After adding 0.9 ml LB medium, containing 1 % glucose the mixture was incubated for an hour at 30 °C and cells were plated on selective solid medium.

Table 2.8: Composition of TSS (Transformation and storage solution). The solution was filter-sterilized and stored in 2 ml aliquots at –20 °C.

50 ml	2 x LB medium pH 6.5
10 g	PEG 6000
5 ml	DMSO
5 ml	$MgCl_2$ or $MgSO_4$
up to 100 ml	add deion. water

2.4.12 Site-directed mutagenesis

For site-directed mutagenesis, a first PCR [40 cycles, 47 °C annealing temperature; Proof Start Taq (Qiagen, Hilden, Germany)] was performed with the pET22b(+) plasmid containing the wild type gene as template. The common pET22b(+)-T7 promoter primer and one of the modified reverse primers and the pET22b(+)-terminator primer and one of the modified forward primers (see Table 7.1) were used for the first PCR. The PCR products corresponding to overlapping 5´ and 3´ fragments were purified on a 1 % agarose gel and eluted (chapter 2.4.7). In the second PCR the products of the first PCR were used as megaprimers and as templates using both pET22b(+) T7 primers. The PCR products were digested with the appropriate restriction endonucleases and ligated into an expression vector. To verify the mutation and to check for extra mutations the plasmid was sequenced as described in chapter 2.4.9.

2.4.13 Preparation of plasmid DNA

Single clones were picked for simultaneous inoculation of a master-plate and a 3 ml culture of LB medium (Miniprep) or 50 to 150 ml LB medium (Midiprep), all incubated over-night at 37 °C. Both plasmid preparations were performed according to either the manual of QIAprep Spin Miniprep Kit or HiSpeed Plasmid Midi Kit (Qiagen, Hilden, Germany).

2.5 Biochemical methods

2.5.1 SDS polyacrylamide gel-electrophoresis (SDS-PAGE)

SDS polyacrylamid gels were used for determining the molecular weight of denaturated proteins and to check the efficiency of the protein purifications. In the majority of cases 15 % acrylamid was used for SDS-PAGE, which was conducted as described by Laemmli (Laemmli, 1970) and performed with the minigel-system (11 x 7 x 0.1 cm; Biometra, Göttingen, Germany; see Table 2.9). All samples were diluted 1:2 with double concentrated loading buffer and denaturated at 95 °C for 10 minutes. Electrophoresis was performed at 60 V, for collecting the samples in the stacking gel, and was increased to 140 V, for separating the proteins in the running gel. A broad-range molecular weight marker (MBI Fermentas, St. Leon-Rot, Germany) was loaded next to the protein samples for evaluating the molecular weight of the denaturated proteins.

Table 2.9: Solutions for SDS-PAGE:

2 x SDS loading buffer	**SDS electrophoresis buffer**
100 mM Tris –HCl, pH 6.8	25 mM Tris-base
200 mM DTT	250 mM glycin
4 % (w/v) SDS	0.1 % (w/v) SDS
0.2 % (w/v) bromphenolblue	
20 % glycerol	
4 x Upper Tris (stacking gel buffer)	**4 x Lower Tris (running gel buffer)**
0.5 M Tris-HCl pH 6.8	1.5 M Tris-HCl pH 8.8
0.4 % (w/v) SDS	0.4 % (w/v) SDS

stacking gel (4%)	**running gel (15%)**
0.7 ml Rotiphorese Gel 30 (Roth, Karlsruhe, Germany)	7.5 ml ml Rotiphorese Gel 30 (Roth, Karlsruhe, Germany)
1.25 ml stacking gel buffer	3.8 ml running gel buffer
3 ml deionized H_2O	3.6 ml deionized H_2O
12 µl TEMED	18 µl TEMED
6 µl 40 % (w/v) APS	12 µl 40 % (w/v) APS

2.5.2 Staining methods

2.5.2.1 Hot Coomassie staining

In the majority of cases the Coomassie staining method, with a detection limit of 0.1 µg protein per band, was used. Polypeptides separated by SDS-PAGE were fixed for 30 min in a fixing solution (40 % (v/v) ethanol, 10 % (v/v) acetic acid, 50 % H_2O). The staining solution [2 tablets PhastGel Blue R (Amersham Biosciences, Freiburg, Germany) in 1 l fixing solution] was heated to 55 - 60 °C and the gel was stained for 30 min. After staining the gel was destained in a destainer-bath, model 556 (BioRad, Munich, Germany), containing 25 % (v/v) ethanol, 8 % (v/v) acetic acid and 67 % H_2O.

2.5.2.2 Silver staining

The silver staining of SDS-PAGE gels was performed with the Silver Stain Plus kit from BioRad (Munich, Germany). Silver staining is 30 – 50 fold more sensitive than the staining by Coomassie blue dye.

2.5.3 Western blotting

This method was used as an analytical method for immunological detection of proteins on nitrocellulose membranes. The samples to be analyzed were separated by SDS-PAGE (see chapter 2.5.1). Electrophoretically separated proteins were blotted to an Immobilon PVDF-membrane (Millipore, Karlsruhe, Germany) by a Trans-Blot Semi-Dry Transfer Cell (BioRad, Munich,

Germany). Before blotting, the membrane was wetted in methanol and equilibrated with the gel in transfer buffer (Table 2.10) for 15 min. The blotting was performed at 15 V for 30 min at 4 °C. After protein transfer the membrane was incubated over night at 4 °C in blocking solution [TBS-Tween (Table 2.10) containing 3 % (w/v) BSA] in order to reduce unspecific antibody binding to the membrane itself. The membrane was washed once for 15 min in TBS-Tween and twice for 5 min in TBS-Tween at room temperature and was then incubated for 1 hour with a dilution of 1:1000 – 1:5000 of the antiserum in TBS-Tween. The membrane was again washed as described before and incubated for one hour with an alkaline-phosphatase conjugated anti-rabbit IgG (Sigma-Aldrich, Taufenkirchen, Germany) diluted 1:30,000 in TBS-Tween. The washing procedure was repeated before incubating the membrane with the substrate for alkaline phosphatase (Western Blue Stabilized Substrate for alkaline phosphatase, Promega Co., Mannheim, Germany) until a signal appeared. Reaction was stopped by rinsing the blot with water.

Table 2.10: Solutions used for Western blot:

Transfer buffer
48 mM Tris-base
39 mM glycin
0.037 % (w/v) SDS
20 % methanol (freshly added)
TBS-Tween (Tris Buffered Saline)
50 mM Tris-base
137 mM NaCl
3 mM KCl
0.05 % (v/v) Tween 20
the pH was adjusted to 7.0

2.5.4 Determination of the protein concentration

2.5.4.1 Method of Bradford

Protein concentration was determined by the method of Bradford (Bradford, 1976) using the BioRad Protein Assay (BioRad, Munich, Germany) and bovine serum albumin (BSA) as a standard. The protein preparation was diluted with H_2O to the final volume of 800 µl and mixed with 200 µl Bradford reagent. After 15 min of incubation at room temperature the absorbance was determined at λ = 595 nm using 800 µl H_2O with 200 µl Bradford reagent as a blank. The protein concentration was obtained from the absorbance using a calibration curve with BSA as standard.

2.5.4.2 Determination of protein concentration by analysis of the amino acid composition

Amino acid analysis is the most efficient method for determining the quantity of a protein actually in a sample. The protein was hydrolyzed into its component and the quantities of the amino acids was determined. By using this data, the molecular weight, and the sequence of the protein, it is possible to calculate how much protein was really present in the sample. The analysis of the amino acid composition was performed by Rita Getzlaff (GBF, Braunschweig, Germany) with Amino Acid Analysis System Model 420A (Applied Biosystems, Darmstadt, Germany).

2.5.5 Desalting and buffer-exchange of protein solutions

The buffer of protein solutions was changed by gelfiltration using a Sephadex G 25 (Amersham Bioscience, Freiburg, Germany) column. For small amounts of protein, desalting was performed following the instructions for PD-10 columns (Amersham Bioscience, Freiburg, Germany).

2.5.6 Concentration of protein solutions

For the concentration of protein samples the products Vivaspin 6, Vivaspin 20 and Vivacell 70 (Sartorius, Göttingen, Germany) were used. The appropriate molecular weight cut off was chosen for each protein and concentrating was performed following the instructions.

2.5.7 N-terminal amino acid sequencing

The protein of interest was separated by SDS-PAGE (see chapter 2.5.1), blotted to an Immobilon PVDF-membrane (Millipore, Schwalbach, Germany) and stained in a freshly prepared cold Coomassie solution (see chapter 2.5.2.1) until the bands could be seen. The band of interest was cut out, washed in water and used for sequencing. The N-terminal amino acid protein sequencing was performed with the protein-sequencer 473A (Applied Biosystems, Taufenkirchen, Germany) by Rita Getzlaff (GBF, Braunschweig, Germany).

2.5.8 MALDI-TOF

The molecular masses of purified proteins were analyzed by matrix-assisted laser desorption and ionization time-of-flight (MALDI-TOF) mass spectrometry at the GBF (Braunschweig, Germany) by a Bruker Reflex-MALDI-TOF or by Bruker Autoflex (Bremen, Germany).

2.6 Biosynthesis and purification of recombinant proteins

2.6.1 Master seed bank

A master seed bank was created for each expression strain, to have the same starting conditions for each culture. Bacterial stocks containing each plasmid with the subcloned gene were prepared from a single colony and stored at –80 °C in LB medium containing 43.5 % (v/v) glycerol.

2.6.2 Induced expression of recombinant proteins

Genes of interest were cloned into the pET expression system of Novagen (Madison, WI, USA) under the control of an isopropyl-thio-β-D-galactopyranoside (IPTG) induceable T7 RNA polymerase promoter. *E. coli* cells in this study were precultured shaking at 180 rpm over night at 37 °C in Luria-Bertani medium containing the appropriate antibioticum and 1 % glucose. The main culture was inoculated with an OD_{600} of 0.1 and grown until an OD_{600} of 0.6 to 0.9 was reached. At this point the main culture was induced with 1 mM IPTG and further incubated, shaking at 25 °C until optimal expression of the protein was performed. *E. coli* cells were harvested at 5000 x g for 15 min at 4 °C and stored at –20 °C until they were used for further experiments. Expression experiments were either performed in Erlmeyer

flasks or, for bigger amounts of protein, in a 5 l Biostat B Fermentor (B. Braun, Melsungen, Germany).

Table 2.11: List of overexpressed recombinant proteins:

recombinant protein	plasmid	antibiotica resistence	*E. coli* strain	induction time
*Tb*TXNH6	pET22b(+)	ampicillin	Tuner (DE3)	4 hours
*Tb*H6TXN	pET28c(+)	kanamycin	BL21(DE3)	overnight
*Tb*TXNC43SH6	pET22b(+)	ampicillin	BL21(DE3)	overnight
*Tb*TXNC40AH6	pET22b(+)	ampicillin	BL21(DE3)	overnight
*Tb*TXNC40SH6	pET22b(+)	ampicillin	BL21(DE3)	overnight
*Tb*H6TXNC43S	pET28c(+)	kanamycin	BL21(DE3)	overnight
*Tb*H6TXNPx	pET28c(+)	kanamycin	BL21(DE3)	6 hours
*Tb*TXNPxH6	pET24a(+)	kanamycin	BL21(DE3)	5 hours
*Tb*TXNPx	pET22b(+)	ampicillin	Tuner(DE3)	6 hours
*Cf*TXN2R129D	pET24a(+)	kanamycin	BL21(DE3)	5 hours
*Cf*TXN2E73R	pET24a(+)	kanamycin	BL21(DE3)	4 hours
*Ld*TXNPxC173S	pET24a(+)	kanamycin	BL21(DE3)	5 hours

2.6.3 Preparation of crude cell extract

All cell extracts were handled on ice in each preparation step. *E. coli* cells were resuspended in 10 % of the original culture volume in buffer A, which was used for the pre-equilibration of the column used for further purification. The cells were disrupted by sonication (30 sec for volumes up to 1 ml and 3 times 1 min for volumes up to 200 ml) and centrifuged twice at 20,000 x g at 4 °C to remove the cell debris.

2.6.4 Protein chromatographic methods

For all chromatographic operations the FPLC systems BioLogic Workstation or BioLogic Duo Flow (BioRad, Munich, Germany) were used. All buffers were degassed under vacuum and filtrated through a 0.2 µm membrane filter (Sartorius, Göttingen, Germany).

2.6.4.1 Immobilized-metal affinity chromatography (IMAC)

The purification was mainly performed as described in The QIA*expressionist* (Fifth edition, Qiagen, Hilden, Germany)

For the purification of His-tag fusion proteins, the cells were lysed in buffer A [50 mM NaH_2PO_4, 300 mM NaCl, pH 8 (see chapter 2.6.3)].The supernatant was applied on a Ni^{2+}-nitrilotriacetic acid (Ni-NTA) superflow agarose (Qiagen, Hilden, Germany) column, washed with 10 volumes of buffer A and eluted with a gradient from 0 – 100 % of buffer B (buffer A containing 500 mM imidazol).

2.6.4.2 Purification of the native *Tb*TXNPx

2.6.4.2.1 S-Sepharose

S-Sepharose is a strong cation exchanger. The isoelectric point of *Tb*TXNPx is 6.36. Therefore the *Tb*TXNPx were found in the flow through using a buffer at pH 7.6.

The cells were lysed in 10 mM sodium phosphate buffer pH 7.6 containing 20 mM DTT (freshly added; lysis buffer). The supernatant was applied to a chromatographic column (5 cm x 7.5 cm) packed with 150 ml S-Sepharose fast flow (Amersham Bioscience, Mannheim, Germany) previously equilibrated in the lysis buffer. The flow through was collected and further purified on Source Q.

2.6.4.2.2 Source Q

Source Q is a strong anion exchanger containing a quaternary ammonium anion. The *Tb*TXNPx was bound to the matrix and could be eluted with a salt gradient.

The flow through of the S-Sepharose was applied to a Source Q column (Amersham Bioscience, Mannheim, Germany), equilibrated with 10 mM sodium phosphate buffer pH 7.6 containing 20 mM DTT (buffer A). After

washing the column with 5 column volumes of buffer A, fractions containing *Tb*TXNPx were eluted by two bed volumes of 5 % buffer B (= buffer A containing 1 M NaCl).

2.6.4.2.3 Hydroxyapatite

The fractions eluted from Source Q were loaded to a chromatographic column containing 50 ml (2.6 cm x 9.4 cm) hydroxyapatite matrix (Macro-Prep Ceramic Hydroxyapatite, BioRad, Munich, Germany) equilibrated with 10 mM sodium phosphate buffer pH 7.6 containing 20 mM DTT (buffer A). The column was washed with 250 ml buffer A and eluted stepwise with 250 ml 60 % and 250 ml 100 % of 0.4 M potassium phosphate buffer pH 7.6 (buffer C). The fractions, corresponding to the elution with 60 % buffer C, that contained purified *Tb*TXNPx were pooled and stored in 50 mM sodium phosphate buffer pH 7.6 at 4 °C.

2.6.4.3 Gel filtration chromatography on a Superdex 200

Estimation of the molecular size of the native enzyme or the intermediate (see chapter 2.7.12) were performed by gel filtration chromatography on a Superdex 200 HR 10/30 (Amersham Bioscience, Mannheim, Germany). High molecular weight standard (Amersham Bioscience, Mannheim, Germany), consisting of tyreoglobulin (699 kDa), ferritin (440 kDa), catalase (232 kDa), aldolase (158 kDa), BSA (66 kDa) and myoglobulin (17.6 kDa), were used for column calibration.

Reduced *Tb*TXNPx was chromatographed in 10 mM sodium phosphate buffer, 20 mM DTT, pH 7.6. Eluted peroxidase was identified by activity measurements (see chapter 2.7.10) and SDS-PAGE gel electrophoresis (see chapter 2.5.1) under reducing and denaturating conditions.

Oxidized *Tb*TXNPx and intermediate (see chapter 2.7.11 and 2.7.12) were chromatographed in 10 mM sodium phosphate buffer, pH 7.6 without DTT.

2.6.5 Cleavage of the N-terminal His-tag with thrombin

The cleavage of the N-terminal His-tag was performed with the Thrombin Cleavage Capture Kit (Novagen, Madison, WI, USA). 1.7 U of thrombin were used for 1 mg protein and incubated at RT overnight. After the reaction, the biotinylated thrombin was removed by adding 16 µl strepavidin agarose per

unit thrombin. The cleavage was confirmed by SDS-PAGE (see chapter 2.5.1), MALDI-TOF analysis (see chapter 2.5.8) and N-terminal Edman degradation (see chapter 2.5.7).

2.7 Analytical methods

2.7.1 Determination of TXN activity

Specific tryparedoxin activity was performed according to Nogoceke *et al.* (1997) as described in detail by Flohé *et al.* (2002b). The test system contained 150 µM NADPH, 1 U/ml TR, 20 µM $T(SH)_2$, 10 µM *Tb*H6TXNPx, 100-1500 nM *Tb*TXNH6, up to 33 µM *Tb*TXN-mutants, and 73 µM *t*-bOOH in 50 mM Tris, 1 mM EDTA pH 7.6 in a final volume of 500 µl. After preincubation (25 °C for 15 min) the reaction was started by the addition of peroxide and the NADPH consumption was monitored continuously at 340 nm at the Specord 2000 photometer (SAFAS, Monte Carlo, Monaco).

2.7.2 Determination of TXNPx activity

Specific tryparedoxin peroxidase activity was performed as described in chapter 2.7.1, using 450 µM NADPH, 1 U/ml TR, 130 µM $T(SH)_2$, 20 mM *Tb*H6TXN, 50 – 200 nM *Tb*H6TXNPx and 73 µM *t*-bOOH in 50 mM Tris, 1 mM EDTA pH 7.6 in a final volume of 500 µl.

2.7.3 Determination of peroxide concentration

H_2O_2, *t*-bOOH and cumene hydroperoxide were purchased from Sigma-Aldrich (Taufenkirchen, Germany). Phosphatidyl choline hydroperoxide and linoleic acid hydroperoxide, both prepared by soybean lipoygenase-catalyzed oxidation of the corresponding lipids, were kindly provided by R. Brigelius-Flohé (Potsdam, Germany). Hydroperoxide concentrations were determined enzymatically with glutathione peroxidase (Sigma-Aldrich, Taufenkirchen, Germany; bovine GPx-1, 0.2 mg/ml) or a phospholipid hydroperoxide glutathione peroxidase (GPx-4) preparation of rat testis as described by Ursini *et al.*(1985) and Flohé *et al.* (1989).

2.7.4 Determination of TXNPx activity with different peroxides

TXNPx reactivity was determined accordingly to chapter 2.7.2.

2.7.5 Determination of glutathione peroxidase activity

The activity was investigated in a test system analogous to chapter 2.7.2 replacing TR by bakers yeast glutathione reductase (8.0 U/ml; Sigma-Aldrich, Taufenkirchen, Germany) and trypanothione plus TXN by 3.3 mM glutathione. After the preincubation time of 15 min at 25 °C the reaction was started by 73 µM *t*-bOOH.

2.7.6 Glutamine synthetase protection assay

This assay monitores the oxidative denaturation of glutamine synthetase by H_2O_2 generated in an aerobic solution of $FeCl_3$ and DTT. Peroxidases, that are able to consume H_2O_2, delay the process of denaturation by using DTT as an unspecific reducing substrate. The assay contains 0.072 µg (= 0.77nM) glutamine synthetase (GS), 10 mM DTT, 1.2 mM $FeCl_3$, 25 µM peroxidase, and 50 mM HEPES pH 7.4 in 50 µl. Every sample was incubated for 0, 10, 20, 30 min. at 30 °C, before the glutamine synthetase denaturation was started by adding 400 µl of GSAL (100 mM HEPES, 0.4 mM ADP, 150 mM L-Glutamine, 10 mM potassium arsenate, 20 mM hydroxylamine, 0.4 mM $MnCl_2$ x 2 H_2O). The mixtures were incubated for 20 min. at 37 °C and stopped with 400 µl GSSAL (0.2 M $FeCl_3$ x 6 H_2O, 0.12 M trichloric acid, 0.2 M HCl, 50 mM HEPES). The positive control contained 1 mM EDTA, instead of peroxidase, to complex the $FeCl_3$. The colored reaction was measured at OD_{540}.

2.7.7 Inhibition of TXN by bis-(ophthamyl)-spermidine

TXN activity was monitored by NADPH consumption in a reconstituted trypanothione peroxidase system as described by Flohé *et al*. (2002b). For inhibition studies, the assay was performed in 500 µl reaction volume containing 10 µM *Cf*H6TXNPx or *Tb*H6TXNPx, 225 µM NADPH (Sigma, Taufenkirchen, Germany), 1 U/ml TR, 10 µM *Cf*TXN2H6, *Cf*TXN1H6 or *Tb*H6TXN, respectively, in 50 mM Tris, 1 mM EDTA pH 7.6, containing $T(SH)_2$ (Bachem, Heidelberg, Germany) in concentrations of 0.6 to 1.3 µM and the pseudosubstrate in a range from 400 to 1500 µM. The mixture was preincubated at 25 °C for 15 minutes before the reaction was started by adding 70 µM *t*-bOOH.

2.7.8 Determination of thioredoxin activity

In the test for the thioredoxin peroxidase activity TR was replaced by thioredoxin reductase of *E. coli* (Sigma-Aldrich, Taufenkirchen, Germany),

TXN by *E. coli* thioredoxin (Sigma-Aldrich, Taufenkirchen, Germany) and trypanothione was omitted. The reaction was performed as described in chapter 2.7.2.

2.7.9 Steady-state kinetic of *Tb*H6TXNPx

The kinetic pattern of *Tb*H6TXNPx was analyzed with *Tb*TXNH6, in concentrations of 0.6 µM, 0.8 µM, 1 µM, 1.3 µM and 2 µM, and *t*-bOOH, in a range of 5 - 65 µM, as substrates. The concentration of *Tb*H6TXNPx was 0.5 µM, which was chosen high enough to allow the reaction to be proceed within less than 10 min. Under these conditions the spontaneous reaction could be disregarded. The data thus obtained were further analyzed according to Dalziel (1957).

2.7.10 Preparation of reduced *Tb*TXNPx for gel filtration chromatography

For the estimation of the molecular size of native, reduced *Tb*TXNPx, purified protein was incubated with 260 mM DTT for ten minutes at room temperature and separated on a Superdex 200 column, pre-equilibrated with 10 mM sodium phosphate buffer, 20 mM DTT pH 7.6 (Amersham Bioscience, Mannheim, Germany) as described in chapter 2.6.4.3.

2.7.11 Preparation of oxidized *Tb*TXNPx for gel filtration chromatography

For size determination of oxidized *Tb*TXNPx, the enzyme was incubated with 300 µM *t*-bOOH at room temperature for 30 min in 10 mM sodium phosphate buffer pH 7.6. The estimation of the molecular size was performed on an equilibrated and calibrated Superdex 200 as described in chapter 2.6.4.3.

2.7.12 Purification of a dead-end intermediate by gel filtration chromatography

A dead-end intermediate was obtained by incubating 80 µM *Tb*TXNPx, 160 µM *Tb*TXNC43S and 200 µM *t*-bOOH for 30 min at room temperature. The reaction mixture containing an excess of *Tb*TXNC43S was separated by gel filtration on a Superdex 200 as described in chapter 2.6.4.3

2.7.13 Determination of acessible reaction centers of the decameric *Tb*TXNPx

2.7.13.1 Determination by SDS-PAGE

The density of silver-stained bands on a 15 % SDS-gel containing different concentrations of *Tb*TXNPx and *Tb*TXNC43S were compared with the density of the bands rising from the intermediate. The gel was scanned by an Electrophoresis Documentation and Analysis System 120 and analyzed by 1D Image Analysis Software Windows Version 3.0 (Kodak Digital Science, Rochester, NY, USA)

2.7.13.2 Determination by chromatography

The intermediate was reduced by 100 µM β-Mercaptoethanol, and the tryparedoxin peroxidase was separated from the *Tb*TXNC43S by gel chromatography as described in chapter 2.6.4.3. Protein concentrations of the peak areas were calculated from E_{280} and the respective extinction coefficients ($\varepsilon_{TXNC43S\ 280}$ = 0.92 mg^{-1} cm^{-1}; $\varepsilon_{TXNPx\ 280}$ = 0.42 mg^{-1} cm^{-1}) calibrated by amino acid analysis (see chapter 2.5.6).

2.8 Electron microscopic studies

Purified protein was absorbed to a carbon foil and negatively stained in 4 % uranylacetat pH 4.5 (Valentine *et al.*, 1968). Samples were analyzed by Dr. Lünsdorf (GBF, Braunschweig, Germany) with an energy-filtered transmission electron microscope (EFTEM) CEM 902 (Zeiss, Oberkochen, Germany). Images were directly registered with a cooled 1024 x 1024 CCD-camera (Proscan, Scheuring, Germany) and digitally optimized for sharpness and contrast with Corel Photopaint (Corel Corporation, Ottawa, Canada).

2.9 3D-Reconstruction

For 3D-reconstruction, negatively stained *Tb*TXNPx or *Tb*TXNPx/*Tb*TXNC43S intermediate complexes were analyzed by EFTEM. The 3D-reconstruction of the images was performed by Dr. Hecht (GBF, Braunschweig, Germany) with the EMAN software package (Ludtke *et al.*, 1999).

2.10 Molecular Modeling

The structural model of the intermediate was based on the coordinates of oxidized peroxiredoxin HBP23 (Hirotsu *et al.*, 1999) and tryparedoxin I of *C.*

fasciculata (Hofmann *et al.*, 2001). Models for the corresponding *T. brucei* enzymes were generated using Modeller 6v1 (Sali and Blundell, 1993) and a sequence alignment generated with Clustalx (Thompson *et al.*, 1997). The initial model of the intermediate was selected from docking calculation using Ftdock (Gabb *et al.*, 1997). The resulting model was manually adjusted to the EM-based electron density using O (Jones *et al.*, 1991). The models were done by Dr. Hofmann (GBF, Braunschweig, Germany).

2.11 Check of protein nativity by circular dichroism

CD-spectras were recorded under N_2-atmosphere at ambient temperature on a J-600 spectropolarimeter (Jasco, Gross-Umstadt, Germany) from 260 to 180 nm. Proteins were measured at a concentration of 0.3 mg/ml in 10 mM potassium phosphate buffer pH 7.9 in 0.5 mm Suprasil quarz cuvettes (Helma, Jena, Germany). For every spectrum 32 single scans were recorded (401 datapoints, step resolution 0.2 nm, scan speed 10 nm/min), averaged, and the resulting curves were smoothed using a high frequency filter and corrected for the solvent. Secondary structure content was quantified using the program Varselec (Manavalan and Johnson, 1987).

2.12 RNA interference

2.12.1 Cultivation of bloodstream cell line *T. brucei 13-90*

The bloodstream cell line *13-90* (a gift from Dr. George Cross, Rockefeller University, New York, NY, USA) was propagated in HMI-9 completed medium (Gibco BRL, Karlsruhe, Germany) supplemented with 10 % heat inactivated fetal calve serum, 2.5 µg/ml neomycine, and 5 µg/ml hygromycine. Cells were cultivated at 37 °C in 5 % CO_2-atmosphere.

2.12.2 Transfection of *T. brucei 13-90*

The bloodstream form of *T. brucei* was harvested at 1400 x g at 37 °C, washed in pre-warmed cytomix (120 mM KCl, 2 mM EGTA, 0.15 mM $CaCl_2$, 10 mM potassium phosphate buffer pH 7.6, 25 mM HEPES, 5 mM Mg Cl_2, 0.5 % glucose, 1 mM hypoxanthine) and resuspended in a concentration of 1 x 10^7 cells/400 µl cytomix. Transfection was performed with 10 µg *Not*I linearized p2T7 plasmid DNA per cuvette, using one puls from a BTX T 820 electroporator (Qbiogene GmbH, Heidelberg, Germany) at 1.5 kV, 175 Ω, and 200 µF. After transfection cells were transferred to 50 ml HMI-9 completed

medium and incubated over night. After 12 hours, selection was carried out by addition of 4 µg/ml phleomycin to the medium.

2.12.3 ^{3}H-labeled thymidine incorporation

Cells containing *Tb*TXN RNAi constructs were diluted to a final concentration of 1 x 10^5 cells/ml. ^{3}H-labeled thymidine was added to the medium of an uninduced culture and a culture, induced with 1 µg/ml tetracycline, in a concentration of 5 µCi/ml. After 0, 8, 24, 32 and 48 hours 1 ml of culture was pelleted at 20,000 x g and washed with TDB (5 mM KCl, 80 mM NaCl, 1 mM $MgSO_4$, 20 mM Na_2HPO_4, 2 mM NaH_2PO_4, 20 mM glucose). Proteins were precipitated by adding 5 % TCA for 10 min. The DNA was washed with H_2O and resuspended in 0.3 M NaOH and added to 2.5 ml ECO Plus (Rotiszint ECO plus, Roth, Karlsruhe, Germany). The solution was incubated over night and the incorporated ^{3}H-labeled thymidine was measured by a β-counter (LS 6500, Beckmann, Würzburg, Germany).

3 Results

3.1 The *T. brucei brucei* peroxidase system

3.1.1 Preparation of the system components

The system components to be studied, *Tb*TXN and *Tb*TXNPx, were obtained by heterologous expression of the pertinent genes in *E. coli* BL21(DE3) or Tuner(DE3). The gene of TXN of *T. brucei brucei* (Acc.No. AJ006403) had before been identified by Lüdemann *et al.* (1998) and could easily be obtained by PCR. The gene was cloned and expressed in the pET28c(+) vector to yield a protein with an N-terminal His-tag (*Tb*H6TXN) or in the pET22b(+) vector to yield a C-terminal His-tagged protein (see chapter 2.6.2). A considerable proportion of the expression product was initially found in the pellet, but with progressing time after induction sufficient amounts appeared in the soluble fraction to disregard the insoluble part (see Figure 3.1).

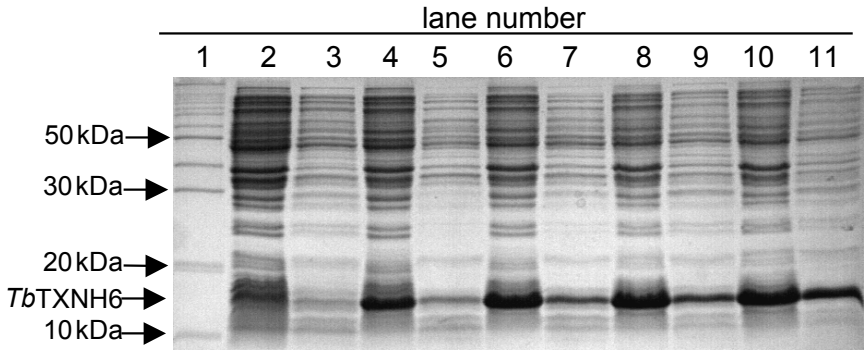

Figure 3.1: The synthesis of *Tb*TXNH6 in *E. coli* BL21(DE3) transfected with recombinant pET22b(+) upon induction by 1 mM IPTG, analyzed by SDS-PAGE, is shown. lane 1: molecular weight marker (MBI Fermentas, St. Leon-Roth, Germany); lane 2 and 3: cell pellet and supernatant before induction; lane 4 and 5: cell pellet and supernatant one hour after induction with 1 mM IPTG; lane 6 and 7: 2 hours after induction; lane 8 and 9: 3 hours after induction; lane 10 and 11: four hours after induction.

The expression products were isolated by His-bind chelate chromatography (see chapter 2.6.4.1). The N-terminal His-tag was removed by thrombin at a single cleavage site located between the His-tag and the genuine *Tb*TXN sequence, leaving three amino acids at the N-terminus (Gly-Ser-His). Product identity was confirmed by MALDI-TOF analysis and Edman degradation. The homogenous protein thus obtained and certificated had the expected size of

18,053 Da for the *Tb*H6TXN and 16,282 Da for the *Tb*TXN cleaved with thrombin (see Figure 3.2).

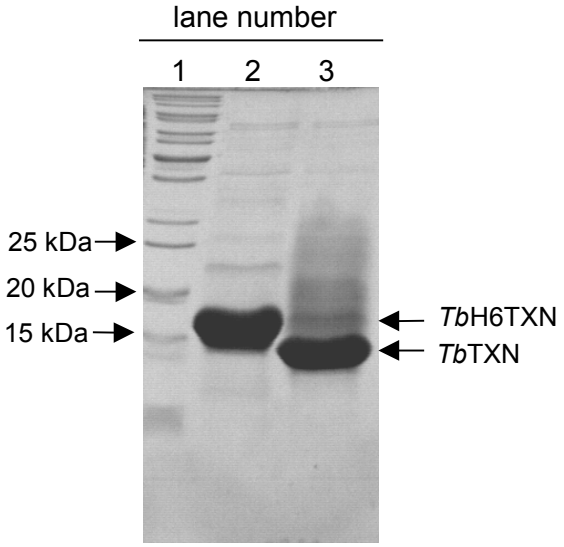

Figure 3.2: *Tb*H6TXN and *Tb*TXN after chelate chromatography on a His-bind column. lane 1: molecular weight marker (MBI Fermentas, St. Leon-Roth, Germany) lane 2: purified *Tb*H6TXN; lane 3: purified *Tb*TXN after thrombin cleavage.

The ability to substitute for TXN of *Crithidia fasciculata* in a reconstituted trypanothione peroxidase system, first established by Nogoceke *et al.* (1997), proved nativity of *Tb*H6TXN (not shown). Molecular mutants (see below) were obtained accordingly.

The gene encoding TXNPx in *T. brucei brucei* was unknown, but could be anticipated to be closely related to a DNA sequence of *T. brucei rhodesiense* proposed to encode an “antioxidant protein” (el-Sayed *et al.*, 1995). With primers designed accordingly (see chapter 2.4.4) a full-length coding sequence was obtained from the genomic DNA of *T. brucei brucei* that was identical, except for primer-independent amino acid residues at least, with the *T. brucei rhodesiense* homologue (see Figure 3.3). The amino acid sequence showed typical characteristics of a tryparedoxin peroxidase and displayed high similarity to TXNPx of *Leishmania donovani* (*Ld*TXNPx), *Leishmania major* (*Lm*TXNPx), *Trypanosoma cruzi* (*Tc*TXNPx), and *Crithidia fasciculata* (*Cf*TXNPx). With 199 residues *Tb*TXNPx corresponds precisely to the cytosolic TXNPxs of *L. donovani*, *T. cruzi* and *L. major*, which are slightly longer than that of *C. fasciculata*, but markedly shorter than the putative mitochondrial variants of *T. brucei brucei*, *T. cruzi* or *L. infantum* (see Figure 3.3).

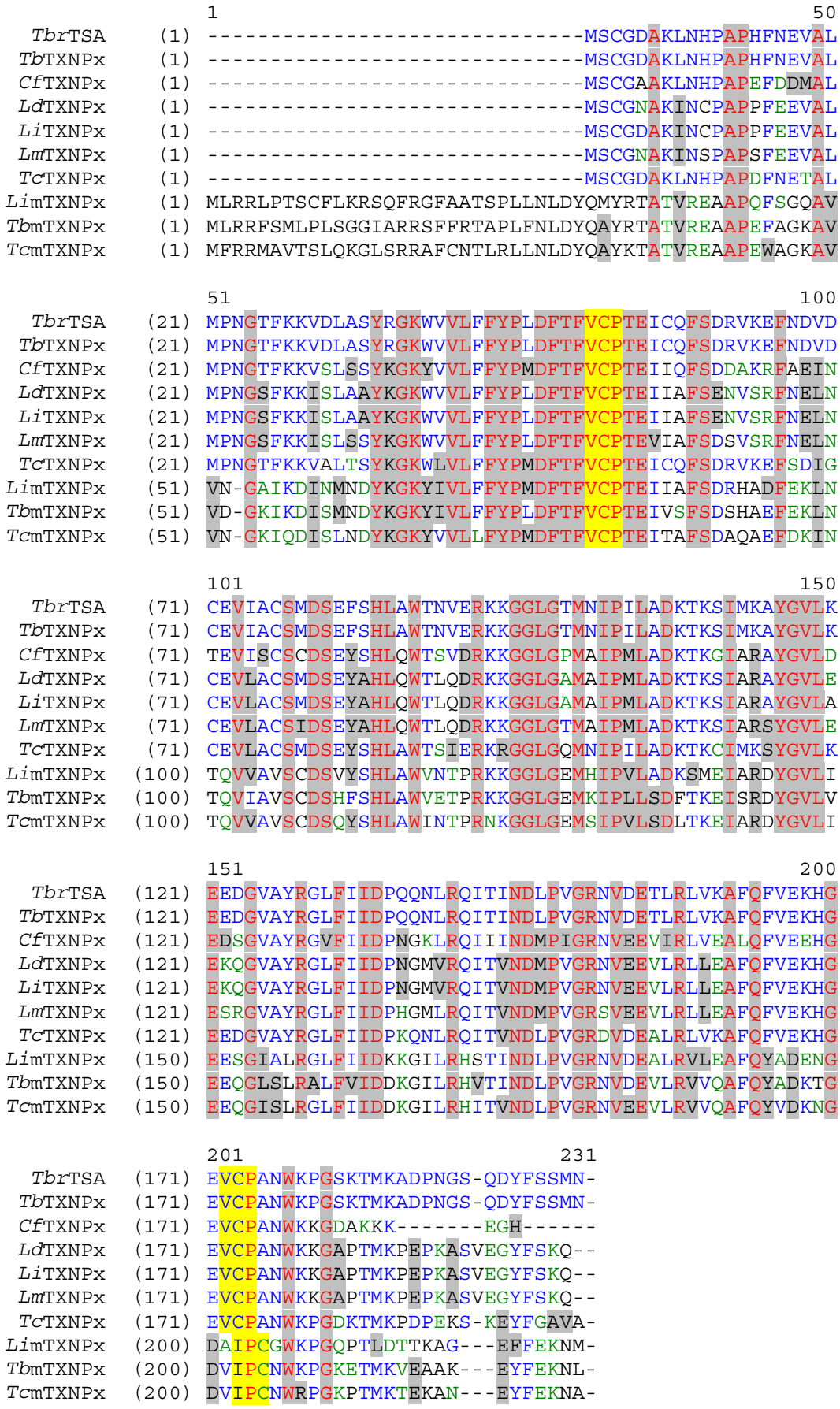
1 50
TbrTSA (1) ----------MSCGDAKLNHPAPHFNEVAL
TbTXNPx (1) ----------MSCGDAKLNHPAPHFNEVAL
CfTXNPx (1) ----------MSCGAAKLNHPAPEFDDMAL
LdTXNPx (1) ----------MSCGNAKINCPAPPFEEVAL
LiTXNPx (1) ----------MSCGDAKINCPAPPFEEVAL
LmTXNPx (1) ----------MSCGNAKINSPAPSFEEVAL
TcTXNPx (1) ----------MSCGDAKLNHPAPDFNETAL
LimTXNPx (1) MLRRLPTSCFLKRSQFRGFAATSPLLNLDYQMYRTATVREAAPQFSGQAV
TbmTXNPx (1) MLRRFSMLPLSGGIARRSFFRTAPLFNLDYQAYRTATVREAAPEFAGKAV
TcmTXNPx (1) MFRRMAVTSLQKGLSRRAFCNTLRLLNLDYQAYKTATVREAAPEWAGKAV
51 100
TbrTSA (21) MPNGTFKKVDLASYRGKWVVLFFYPLDFTFVCPTEICQFSDRVKEFNDVD
TbTXNPx (21) MPNGTFKKVDLASYRGKWVVLFFYPLDFTFVCPTEICQFSDRVKEFNDVD
CfTXNPx (21) MPNGTFKKVSLSSYKGKYVVLFFYPMDFTFVCPTEIIQFSDDAKRFAEIN
LdTXNPx (21) MPNGSFKKISLAAYKGKWVVLFFYPLDFTFVCPTEIIAFSENVSRFNELN
LiTXNPx (21) MPNGSFKKISLAAYKGKWVVLFFYPLDFTFVCPTEIIAFSENVSRFNELN
LmTXNPx (21) MPNGSFKKISLSSYKGKWVVLFFYPLDFTFVCPTEVIAFSDSVSRFNELN
TcTXNPx (21) MPNGTFKKVALTSYKGKWLVLFFYPMDFTFVCPTEICQFSDRVKEFSDIG
LimTXNPx (51) VN-GAIKDINMNDYKGKYIVLFFYPMDFTFVCPTEIIAFSDRHADFEKLN
TbmTXNPx (51) VD-GKIKDISMNDYKGKYIVLFFYPLDFTFVCPTEIVSFSDSHAEFEKLN
TcmTXNPx (51) VN-GKIQDISLNDYKGKYVVLLFYPMDFTFVCPTEITAFSDAQAEFDKIN
101 150
TbrTSA (71) CEVIACSMDSEFSHLAWTNVERKKGGLGTMNIPILADKTKSIMKAYGVLK
TbTXNPx (71) CEVIACSMDSEFSHLAWTNVERKKGGLGTMNIPILADKTKSIMKAYGVLK
CfTXNPx (71) TEVISCSCDSEYSHLQWTSVDRKKGGLGPMAIPMLADKTKGIARAYGVLD
LdTXNPx (71) CEVLACSMDSEYAHLQWTLQDRKKGGLGAMAIPMLADKTKSIARAYGVLE
LiTXNPx (71) CEVLACSMDSEYAHLQWTLQDRKKGGLGAMAIPMLADKTKSIARAYGVLA
LmTXNPx (71) CEVLACSIDSEYAHLQWTLQDRKKGGLGTMAIPMLADKTKSIARSYGVLE
TcTXNPx (71) CEVLACSMDSEYSHLAWTSIERKRGGLGQMNIPILADKTKCIMKSYGVLK
LimTXNPx (100) TQVVAVSCDSVYSHLAWVNTPRKKGGLGEMHIPVLADKSMEIARDYGVLI
TbmTXNPx (100) TQVIAVSCDSHFSHLAWVETPRKKGGLGEMKIPLLSDFTKEISRDYGVLV
TcmTXNPx (100) TQVVAVSCDSQYSHLAWINTPRNKGGLGEMSIPVLSDLTKEIARDYGVLI
151 200
TbrTSA (121) EEDGVAYRGLFIIDPQQNLRQITINDLPVGRNVDETLRLVKAFQFVEKHG
TbTXNPx (121) EEDGVAYRGLFIIDPQQNLRQITINDLPVGRNVDETLRLVKAFQFVEKHG
CfTXNPx (121) EDSGVAYRGVFIIDPNGKLRQIIINDMPIGRNVEEVIRLVEALQFVEEHG
LdTXNPx (121) EKQGVAYRGLFIIDPNGMVRQITVNDMPVGRNVEEVLRLLEAFQFVEKHG
LiTXNPx (121) EKQGVAYRGLFIIDPNGMVRQITVNDMPVGRNVEEVLRLLEAFQFVEKHG
LmTXNPx (121) ESRGVAYRGLFIIDPHGMLRQITVNDMPVGRSVEEVLRLLEAFQFVEKHG
TcTXNPx (121) EEDGVAYRGLFIIDPKQNLRQITVNDLPVGRDVDEALRLVKAFQFVEKHG
LimTXNPx (150) EESGIALRGLFIIDKKGILRHSTINDLPVGRNVDEALRVLEAFQYADENG
TbmTXNPx (150) EEQGLSLRALFVIDDKGILRHVTINDLPVGRNVDEVLRVVQAFQYADKTG
TcmTXNPx (150) EEQGISLRGLFIIDDKGILRHITVNDLPVGRNVEEVLRVVQAFQYVDKNG
201 231
TbrTSA (171) EVCPANWKPGSKTMKADPNGS-QDYFSSMN-
TbTXNPx (171) EVCPANWKPGSKTMKADPNGS-QDYFSSMN-
CfTXNPx (171) EVCPANWKKGDAKKK-------EGH------
LdTXNPx (171) EVCPANWKKGAPTMKPEPKASVEGYFSKQ--
LiTXNPx (171) EVCPANWKKGAPTMKPEPKASVEGYFSKQ--
LmTXNPx (171) EVCPANWKKGAPTMKPEPKASVEGYFSKQ--
TcTXNPx (171) EVCPANWKPGDKTMKPDPEKS-KEYFGAVA-
LimTXNPx (200) DAIPCGWKPGQPTLDTTKAG---EFFEKNM-
TbmTXNPx (200) DVIPCNWKPGKETMKVEAAK---EYFEKNL-
TcmTXNPx (200) DVIPCNWRPGKPTMKTEKAN---EYFEKNA-

Figure 3.3: Alignment of the "thiol specific antioxidant" protein from *T. brucei rhodesiense* (*Tbr*TSA acc. No. U26666.1) and tryparedoxin peroxidase of *T. brucei brucei* (*Tb*TXNPx acc. No. AF283104) with known tryparedoxin peroxidases. Conserved residues are shown in red and the active site cysteines embedded in the VCP or IPC, in the cases of mitochondrial TXNPxs, motifs are shown in yellow. Those conserved in one or more subfamilies are colored and not conserved residues are shown in black. *Cf*TXNPx, *C. fasciculata* TXNPx (acc. No. AF020947); *Ld*TXNPx, *L. donovani* TXNPx (acc. No. AF225212), *Li*TXNPx, *L. infantum* TXNPx (acc. No. AY058210); *Lm*TXNPx; *L. major* TXNPx (acc. No. AF069386); *Tc*TXNPx, *T. cruzi* TXNPx (acc. No. CAA09922); *Li*mTXNPx, mitochondrial TXNPx of *L. infantum* (acc. No. AY058209); *Tb*mTXNPx, mitochondrial TXNPx of *T. brucei brucei* (acc. No. AF196570); *Tc*mTXNPx, mitochondrial TXNPx of *T. cruzi* (acc. No. AJ006226)

Like all known cytosolic TXNPx species the *Tb*TXNPx contains two conserved cysteines (C52 and C173) each embedded in a Val-Cys-Pro (VCP) motif, which differs from Ile-Pro-Cys (IPC) motif that composes the conserved second cysteine of mitochondrial TXNPxs.

Expression was achieved with different pET vectors, pET24a(+) yielding the unmodified protein (*Tb*TXNPx)(see Figure 3.4), pET22b(+) designed to add a C-terminal His-tag (*Tb*TXNPxH6) and pET28c(+) resulting an N-terminal His-tag (*Tb*H6TXNPx) (see Figure 3.4).

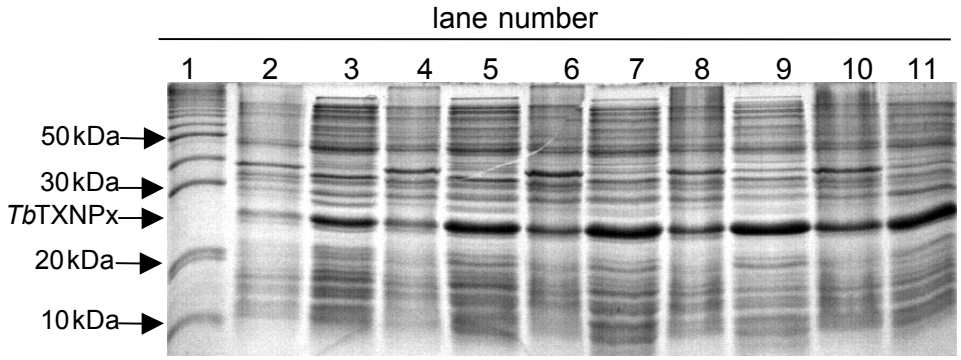

Figure 3.4: Expression pattern of the unmodified *Tb*TXNPx. lane 1: molecular weight marker (MBI Fermentas, St. Leon Roth, Germany); lane 2 and 3: cell pellet and supernatant before induction; lane 4 and 5: cell pellet and supernatant one hour after induction with 1 mM IPTG; lane 6 and 7: cell pellet and supernatant two hours after induction; lane 8 and 9: cell pellet and supernatant three hours after induction; lane 10 and 11: cell pellet and supernatant four hours after induction.

*Tb*H6TXNPx was primarily found in the soluble fraction and could be purified in one step by chelate chromatography. Removal of the His-tag in *Tb*H6TXNPx by thrombin proved to be impossible likely due to inaccessibility of the

cleavage site in the oligomeric protein. Therefore the unmodified protein, *Tb*TXNPx, was purified by chromatographic techniques that had been successfully applied to the purification of authentic TXNPx from *C. fasciculata* (Nogoceke *et al.*, 1997). N-terminal Edman degradation complied with the expected sequence up to position 22. Confirmation of the right size was done by MALDI-TOF analysis, 24,698 Da for *Tb*H6TXNPx, 22,534 Da for the unmodified *Tb*TXNPx and 23,599 Da for the C-terminally His-tagged protein *Tb*TXNPxH6, as well as by SDS gel electrophoresis and Western blot analysis with anti *Cf*TXNPx antibodies (see Figure 3.5).

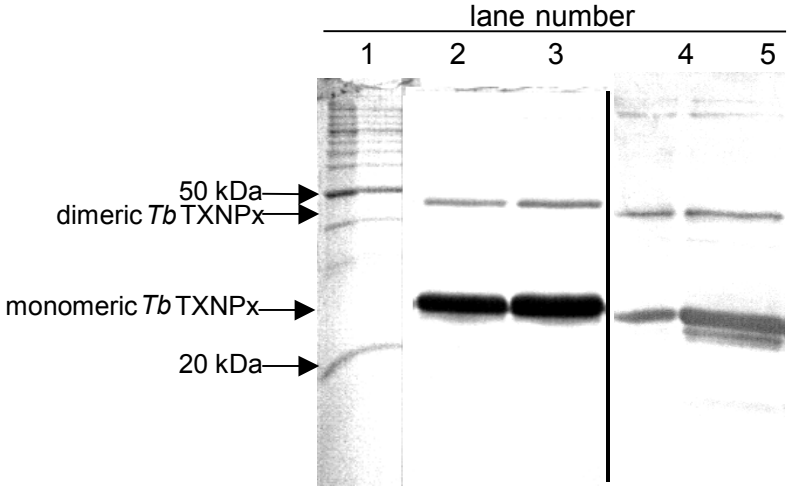

Figure 3.5: Purified *Tb*TXNPx as monomer and dimer verified by Western Blot. lane 1: molecular weight marker (MBI Fermentas, St. Leon-Roth, Germany); lane 2 and 3: Coomassie stained *Tb*TXNPx; lane 4 and 5: Western blot of *Tb*TXNPx with rabbit anti *Cf*TXNPx antibodies.

After purification, both, *Tb*TXNPx and *Tb*H6TXNPx, proved to be active tryparedoxin peroxidases with TXNs from different species, while *Tb*TXNPxH6 was completely inactive (data not shown). The specific TXNPx activity, when analyzed by our routine procedure (see chapter 2.7.2) with tertiary-butyl-hydroperoxide (*t*-bOOH), was 17 ± 0.8 U/mg for *Tb*H6TXNPx and 9 ± 1.6 U/mg for *Tb*TXNPx. These values lie in the same order of magnitude as those of authentic *Cf*TXNPx (Nogoceke *et al.*, 1997), *Cf*TXNPxH6 (Montemartini *et al.*, 1998b), and *Tc*TXNPx (Guerrero *et al.*, 2000a).

3.1.2 Basic characteristics of *Tb*H6TXNPx

The tryparedoxin peroxidase nature of the *T. brucei* peroxiredoxin is underscored by its specificity for the homologous *Tb*TXNH6 as reductant. As Kinetoplastida also contain typical thioredoxins (Reckenfelderbäumer *et al.*,

2000), analogous experiments were performed offering up to 5.9 µM thioredoxin of *E. coli* as reducing substrate. *Tb*H6TXNPx proved to catalyze the reaction between the thioredoxin of *E. coli* and *t*-bOOH, that is due to the similarity of active site motif (CXXC). $T(SH)_2$ or glutathione did not yield any measurable activity with *Tb*H6TXNPx (see Table 3.1).

Enzyme	Reductants	spec. act. (%)
*Tb*TXNPx	TR/$T(SH)_2$/TXN	(100)
*Tb*TXNPx	TrxR/Trx	19
*Tb*TXNPx	GR/GSH	0

Table 3.1: Relative activities of TXNPx for different thiol substrates. TR, trypanothione reductase of *T. cruzi*; $T(SH)_2$, trypanothione (Bachem, Weil am Rhein, Germany); TXN, *Tb*TXNH6 of *T. brucei*; TrxR, thioredoxin reductase of *E. coli*; Trx, thioredoxin of *E. coli*; GR, glutathione reductase of *E. coli*; GSH, glutathione.

The substrate *t*-bOOH is conveniently used to characterize TXNPx, because its spontaneous reaction with trypanothione and tryparedoxin is slow enough to be ignored in most experimental settings. With *Tb*H6TXNPx it does not react as fast as the predominant natural substrate H_2O_2. Like TXNPxs from other species, *Tb*H6TXNPx proved to be a broad-spectrum peroxidase acting with H_2O_2 and organic hydroperoxides including complex lipid hydroperoxides (see Table 3.2). Cumene hydroperoxide, frequently used as a model for natural lipophilic hydroperoxides, is also reduced by *Tb*H6TXNPx. But naturally occurring lipid hydroperoxides such as 13-hydroperoxy octodecadienoic acid (LOOH) and soybean lipoxygenase-peroxidized phosphatidyl choline (PCOOH) are accepted with much lower rates and, like with *Li*mTXNPx and *Ld*TXNPx, fast inactivation by these substrates could be observed (Castro *et al.*, 2002a; Flohé *et al.*, 2002a). The relative specific activities for the lipid hydroperoxides listed in Table 3.2 correspond to initial velocities measured at the highest enzyme concentrations that could technically be monitored.

Enzyme	*t*-bOOH	LOOH	PCOOH	H_2O_2	COOH	Reference
***Tb*H6TXNPx**	100	10.4*	1.7*	140	45*	
***Cf*TXNPx**	100	43	19	43	n.d.	Nogoceke *et al.*, 1997
***Lm*H6TXNPx**	100	n.d.	n.d.	459	0	Levick *et al.*, 1998
***Li*mH6TXNPx**	100	8.4*	4.0*	105	60	Castro et al., 2002a
***Ld*H6TXNPx**	100	18	3.3*	209	97	Flohé *et al.*, 2002a

Table 3.2: Relative specificity of *Tb*H6TXNPx with different peroxides as substrates. The activities with *t*-butyl hydroperoxide (*t*-bOOH) were set to 100 %. LOOH, PCOOH, and COOH mean linoleic acid hydroperoxide, phosphatidyl cholin hydroperoxide and cumene hydroperoxide, respectively. Specificities reported for TXNPxs of other species are added for comparison. *Cf*, *C. fasciculata*; *Lm*, *L. major*; *Ld*, *L. donovani*; *Li*, *L. infantum*. * Means fast inactivation by substrate.

3.1.3 Steady-state kinetics of *T. brucei* TXNPx

Based on extensive studies on TXNPxs of other species (Nogoceke *et al.*, 1997; Guerrero *et al.*, 2000a; Flohé *et al.*, 2002a) and related 2-Cys-peroxiredoxins (Baker *et al.*, 2001), a “ping-pong” or “enzyme substitution” mechanism was expected. The kinetic pattern of these enzymes observed in steady-state-kinetic analysis complied with the general Dalziel equation of a two-substrate reaction (Dalziel, 1957), wherein the term $\Phi_{1,2}/[A]\,[B]$ was zero.

$$\frac{[E_0]}{v} = \Phi_0 + \frac{\Phi_1}{[A]} + \frac{\Phi_2}{[B]} + \frac{\Phi_{1,2}}{[A]\,[B]}$$

Equation 3.1: Dalziel equation for a two-substrate reaction. $[E_0]$ is the total enzyme concentration; v the initial velocity at pertinent substrate concentration [A] and [B] and Φ_0, Φ_1, Φ_2, and $\Phi_{1,2}$ are kinetic coefficients characterizing a particular enzyme.

In view of experimental difficulties in obtaining reliable initial velocities for the reduction of natural lipid hydroperoxides, the kinetic behavior of *Tb*H6TXNPx was only investigated with the most convenient substrate, *t*-bOOH, which was shown not to inactivate the enzyme within 20 minutes. As an additional measure of precaution, the enzyme concentration was chosen high enough to allow completion of the reaction within less than 10 min.

A ping-pong pattern, similar to previous investigations on related enzymes (Nogoceke *et al.*, 1997; Guerrero *et al.*, 2000a; Baker *et al.*, 2001; Flohé *et al.*, 2002a), could be expected from the type of catalysis (Hofmann *et al.*, 2002). In that case the term $\Phi_{1,2}$/[A] [B], that characterizes a central complex mechanism, should be zero. The kinetic analysis of *Tb*H6TXNPx surprised with irregularities similar to those that had previously been observed with a mitochondrial TXNPx of *L. infantum* (Castro *et al.*, 2002a). The primary Dalziel plot, that shows the reciprocal hydroperoxide concentration at different fixed TXN concentrations, does neither yield linear slopes nor can the slopes measured at different cosubstrate concentrations be rated to be strictly parallel. The set of data was obtained by single curve progression analysis. Initial velocities were read from the substrate consumption curves that correspond to 12 residual substrate concentrations giving distant abscissa points in the double reciprocal plot. Thereby a balanced and unibased statistical weight of the individual velocities over a substrate range between 95 % and 5 % of the starting concentration was to be guaranteed. A minimum of three data sets were generated.

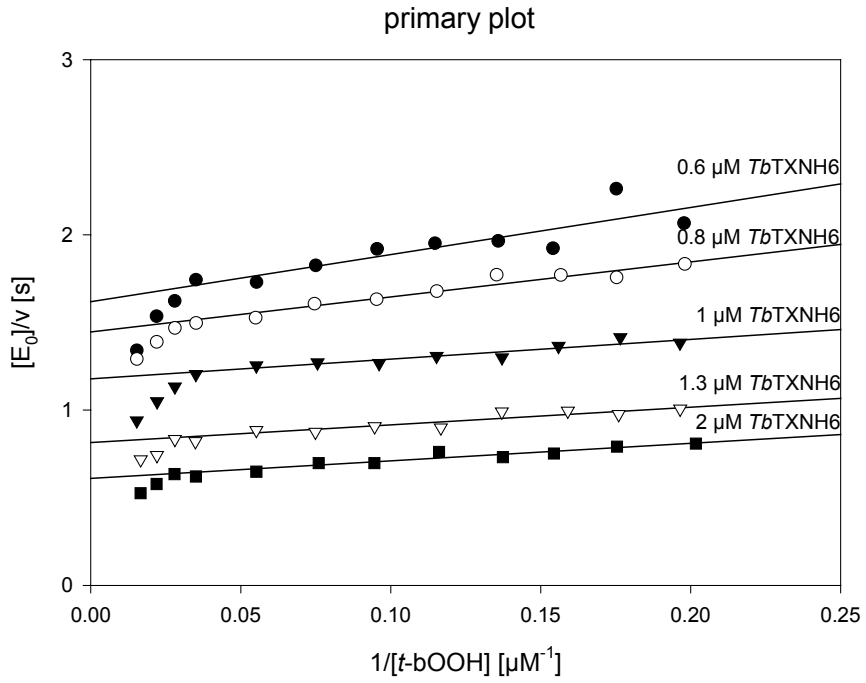

Figure 3.6: Steady-state kinetics of *Tb*H6TXNPx. Substrate turnover by *Tb*H6TXNPx was monitored continuously by NADPH consumption in a coupled test system as described in chapter 2.7.9 at 25 °C and pH 7.6 with *t*-bOOH as substrate and *Tb*TXNH6 as cosubstrate. Three sets of data were analyzed according to Dalziel (1957). Example of primary Dalziel plot showing enzyme normalized inverse initial velocities ($[E_0]/v$) in dependence of reciprocal hydroperoxide concentrations at different *Tb*TXNH6 concentrations that were kept constant by continuous regeneration. Note the biphasic slopes; only the flatter parts were used for data processing.

As is at least evident from the upper curves in Figure 3.6, the slopes are clearly biphasic being steeper at high hydroperoxide concentrations. Qualitatively, the same phenomenon is seen in the curves obtained at higher TXN concentrations. Unfortunately, the two phases of the curves could not be assessed with the same accuracy for technical reasons. Only the flatter slopes, that are observed over a wide range of lower peroxide concentrations, could be used for further data processing such as the calculations of the Dalziel coefficients and the kinetic constants. Replotting the ordinate intercepts of the Dalziel primary plot (the reciprocal enzyme-normalized apparent maximum velocities for infinite concentrations of *t*-bOOH = [A]) against the reciprocal concentrations of cosubstrate *Tb*TXNH6 (=[B]) yields Φ_0 as ordinate intercepts and Φ_2 being the slope of the secondary plot (see Figure 3.7).

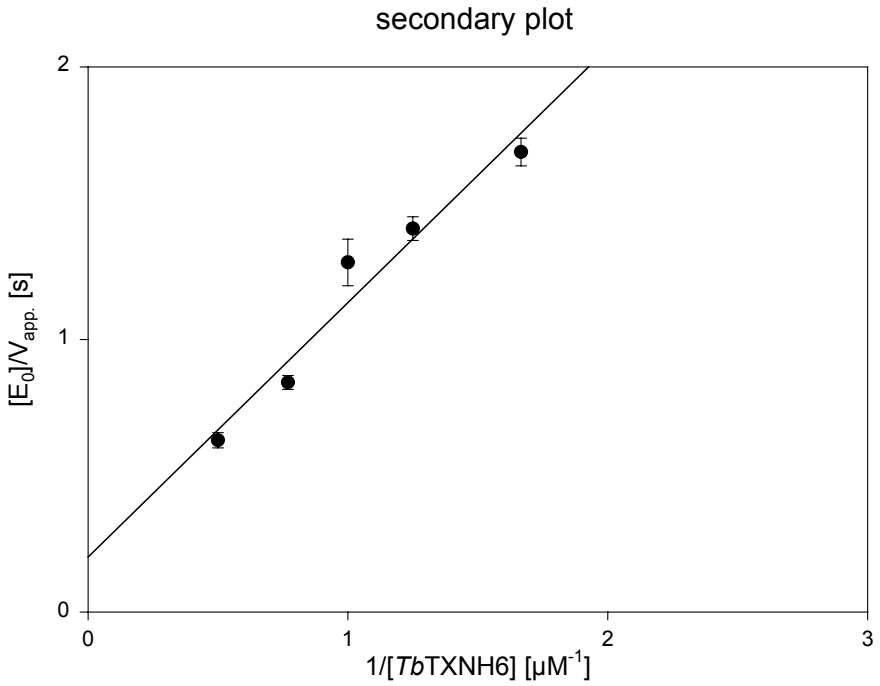

Figure 3.7: Secondary plot of ordinate intercepts ($[E_0]/V_{app.}$) of the primary plots against reciprocal cosubstrate (*Tb*TXNH6) concentrations.

As the regression lines in the primary plot of *Tb*H6TXNPx converge and are not parallel as expected, the term $\Phi_{1,2}/[A]\,[B]$ is different from zero, which is highly unusual for a peroxidase (Flohé and Brigelius-Flohé, 2001). The coefficients Φ_1 and $\Phi_{1,2}$ are obtained by replotting the slopes of the primary plots against 1/[*Tb*TXNH6] as ordinate intercepts and slope, respectively (see Figure 3.8).

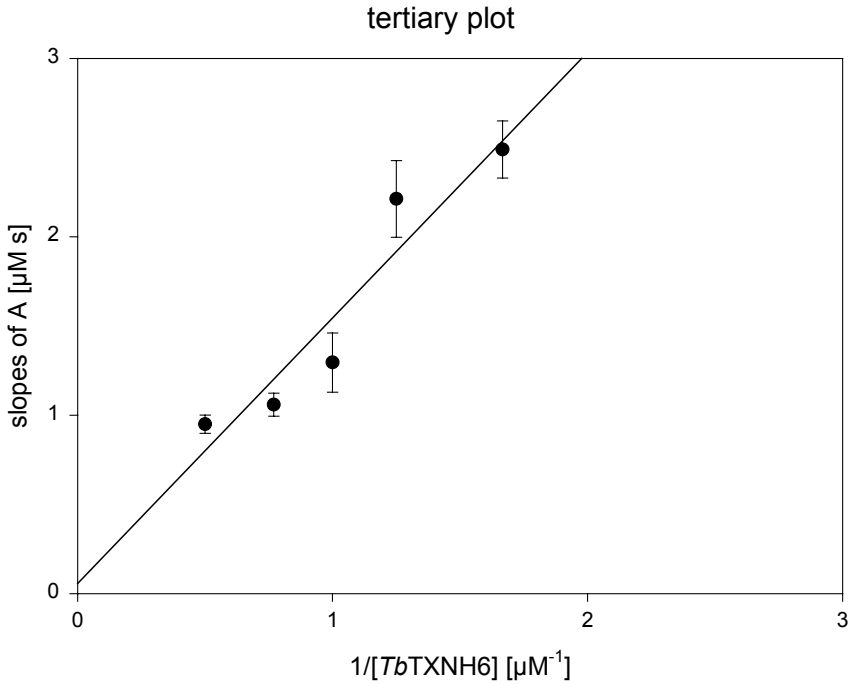

Figure 3.8: Tertiary Dalziel plot of averaged slopes ($\Phi_{1app.}$) of primary plots versus reciprocal cosubstrate concentration (*Tb*TXNH6).

The Dalziel coefficients and kinetic constants, as obtained from the Dalziel plots are compiled in Table 3.3.

Enzyme	Φ_0 [s]	Φ_1 [s µM]	Φ_2 [s µM]	$\Phi_{1,2}$ [s µM^2]	$K_{M\ ROOH}$ [µM]	$K_{M\ TXN}$ [µM]	$k_{cat.}$ [s^{-1}]	Reference
***Cf*TXNPx**	0	5.3	0.51	0	∞	∞*	∞	Nogoceke *et al.*, 1997
***Tc*TXNPxH6**	0.60	30.9	1.0	0	51.8	1.66#	1.7	Guerrero *et al.*, 2000
***Ld*H6TXNPx**	0.14	4.2	0.48	0	30.5	3.4*	7.2	Flohé *et al.*, 2002a
***Li*H6mTXNPx**	0.03	0.26	0.85	0.83	9.15	31.90#	33.3	Castro *et al.*, 2002a
***Tb*H6TXNPx**	0.20	0.06	0.93	1.49	0.28	4.64x	5.0	

Table 3.3: Dalziel coefficients and kinetic constants of *Tb*H6TXNPx compared with TXNPxs of other species. *Cf*, *C. fasciculata*; *Tc*, *T. cruzi*; *Ld*, *L. donovani*; *Li*m, mitochondrial TXNPx of *L. infantum*. * TXN is *Cf*TXN1H6; # TXN is *Cf*TXN2H6; x TXN is *Tb*H6TXN.

Compared with other TXNPxs, *Tb*H6TXNPx appears to be an unusually active peroxiredoxin-type peroxidase. The extrapolated Φ_1 is comparatively low which implies that the reaction constant k'_1 for the reaction of the reduced enzyme with the peroxide is accordingly high, since by definition Φ_1 equals $1/k'_1$. The value of the net forward rate constant for *Tb*H6TXNPx corresponds with the values obtained from the selenium-containing glutathione peroxidases of mammals (Flohé and Brigelius-Flohé, 2001). The steep parts of the slopes of the primary plot (see Figure 3.6) could be taken as a very rough approximation for the Φ_1 values resulting from a conformation change of the enzyme due to strongly oxidizing conditions. They would indicate a very low k'_1. This could be interpreted to result from impaired accessibility of the reaction center to the hydroperoxide. The reciprocal value of the extrapolated Φ_2 can only describe the reaction constant for the reaction of the oxidized TXNPx with the cosubstrate TXN. Φ_0 is defined as the reciprocal value of the velocity at infinite concentrations of both substrates, *t*-bOOH and TXN, that

means k_{cat}. A finite k_{cat} is not uncommon for peroxiredoxins (Montemartini *et al.*, 1999; Guerrero *et al.*, 2000a; Flohé *et al.*, 2002a). The meaning of $\Phi_{1,2}$ remains elusive. In a central complex mechanism both substrates are bound to the enzyme to build a ternary complex and $\Phi_{1,2}$ is the coefficient related to this process. Since such complex mechanisms can be ruled out for 2-Cys-peroxiredoxins in general, it may be guessed that here $\Phi_{1,2}$ reflects substrate-induced conformational changes that modulate the affinity to the cosubstrate.

3.1.4 Reaction mechanism of TXNPx

Like most peroxiredoxins, TXNPx possesses a reactive cysteine residue in its N-terminal domain, which is imbedded in a VCP motif (C52) and repeated in its C-terminal domain (C173) (see Figure 3.3). As has become evident from structural data (Hirotsu *et al.*, 1999; Alphey *et al.*, 2000), the C52 builds a disulfide bridge to C173´ of a second subunit. Two possible reaction centers are build by two subunits within the homooligomeric enzyme. The reducing thiol substrate, here reduced tryparedoxin, then attacks the disulfide bond at the C173, with its only solvent exposed Cys40 of the active site, and the catalysis can proceed (as outlined in Figure 3.9).

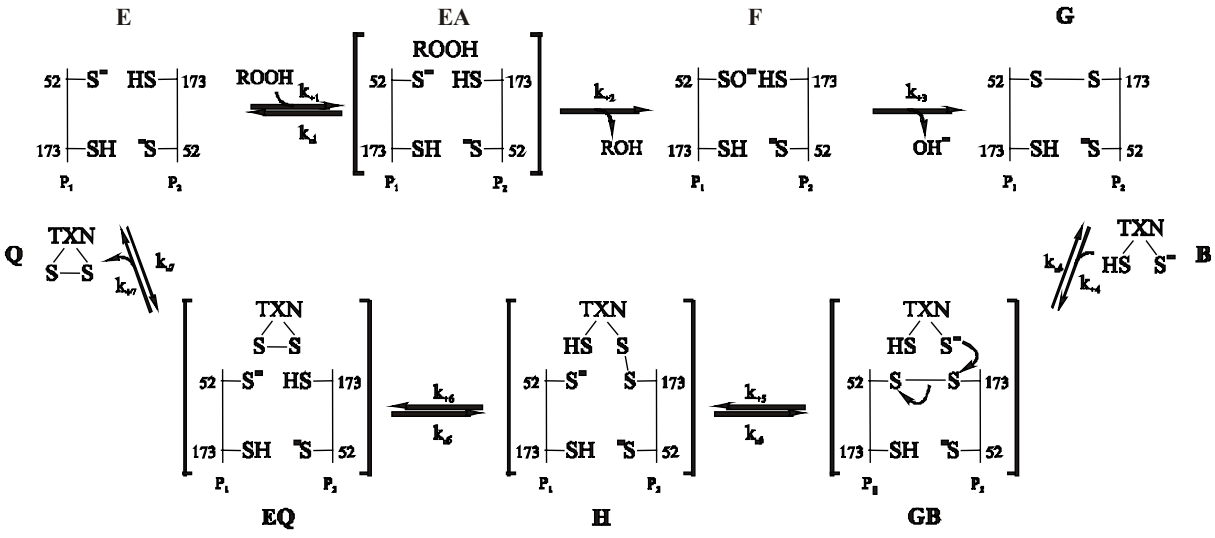

Figure 3.9: Scheme of the reaction mechanism of TXNPx. TXN, tryparedoxin; ROOH, hydroperoxide; ROH, alcohol; E, ground state enzyme; F, G, and H, catalytic intermediates; P_1 and P_2, first and second subunit of the dimeric protein. The sulfhydryl group of Cys40 in *Tb*TXN is shown to be dissociated (B) to emphasize its presumed nucleophilic attack on the disulfide bridge of oxidized TXNPx. Identical reactions may occur within the second pair of SH groups of the intersubunit active site (not shown) (Flohé *et al.*, 2002b; Hofmann *et al.*, 2002)

The present view of the catalytic cycle, as illustrated in Figure 3.9, was originally deduced from previous investigations of the homologous yeast thioredoxin peroxidase (Chae *et al.*, 1994b) and the first established X-ray structure of a peroxiredoxin, that of human ORF6 (Choi *et al.*, 1998), now reclassified as a non-selenium glutathione peroxidase.

3.1.4.1 Necessity of conserved cysteines

The proposed reaction mechanism of 2-Cys-peroxiredoxins is supported by experimental evidence. The TXNPxs of Kinetoplastida decreased or abolished dramatically their specific activity when the distal conserved cysteine was changed to a serine (see Table 3.4).

Data relevant to reacting cysteines		**Relative activity (%)**
Peroxidase	**Reductant**	
*Cf*TXNPx	*Cf*TXN2	(100)
*Cf*TXNPxC52SH6	*Cf*TXN2	0
*Cf*TXNPxC173SH6	*Cf*TXN2	4.2
*Ld*H6TNPx	*Cf*TXN2H6	(100)
*Ld*H6TXNPxC52S	*Cf*TXN2H6	0
*Ld*H6TXNPxC173S	*Cf*TXN2H6	0.02
*Tb*H6TXNPx	*Tb*H6TXN	(100)
*Tb*H6TXNPxC52S	*Tb*H6TXN	0
*Tb*H6TXNPxC173S	*Tb*H6TXN	5.2

Table 3.4: Exchange of the two conserved active site cysteines of TXNPx by serine of *Cf*, *C. fasciculata* (Montemartini *et al.*, 1999); *Ld*, *L. donovani* (Flohé *et al.*, 2002a), and *Tb*, *T. brucei* (Budde *et al.*, 2003a).

Exchange of the C52 versus serine abolishes the activity in *C. fasciculata*, *L. donovani* and *T. brucei* completely, while a marginal activity is left when the C173 is mutated. The view that the C52 is the residue that is oxidized by the peroxide substrate is supported by the findings that the C173S muteins of *L.*

donovani TXNPx (Flohé *et al.*, 2002a) and TrxPx of *Saccharomyces cerevisiae* (Chae *et al.*, 1993), retained activity in the glutamine synthetase protection assay and the C52S muteins did not (see chapter 3.2.2). The conclusion is further provided by molecular models based on homology considerations and site-directed mutagenesis. The mutagenesis studies on *C. fasciculata* (Montemartini *et al.*, 1999) and *L. donovani* (Flohé *et al.*, 2002a) proved, that the residues R128 and T49 are essential for activity. The catalytic triad activates the thiol in the proximal domain of TXNPx. (Flohé *et al.*, 2002a; Hofmann *et al.*, 2002) (see Figure 3.10).

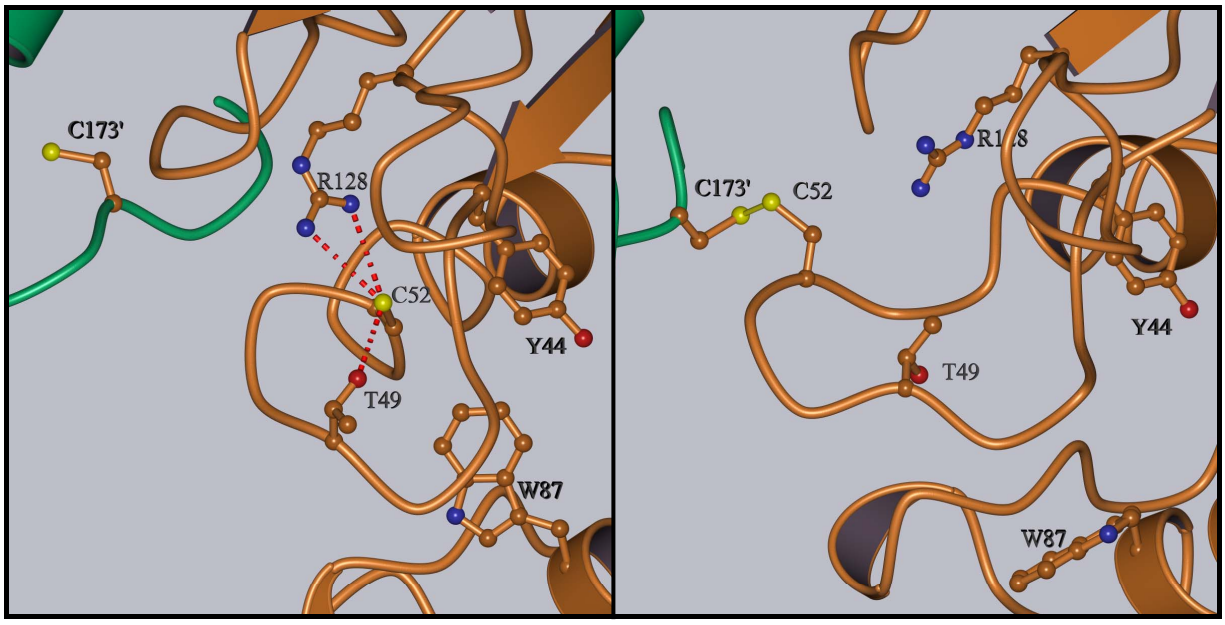

Figure 3.10: Modeling of the catalytic cycle of TXNPx. In the reduced TXNPx the sulfur of C52 in the center of the catalytic triad is activated by R128 and T49 (left panel). Upon oxidation C52 reacts with C173´ of a second inverted subunit to form a disulfide bond in the intersubunit active site (right panel).

3.1.4.2 Oligomeric nature of TXNPx

Although a peroxiredoxin dimer theoretically forms a functional unit, higher aggregates appear to be preferred. The crystal structures of three 2-Cys-peroxiredoxins have revealed decameric forms, built of five homodimers: the reduced tryparedoxin peroxidase from *C. fasciculata* (Alphey *et al.*, 1999b), the thioredoxin peroxidase B from human erythrocytes (Schröder *et al.*, 2000) and the oxidized form of alkyl hydroperoxide reductase from *S. typhimurium* (Wood *et al.*, 2002). Normally the dimeric form of peroxiredoxins tend to be inactive as observed with TXNPx of *C. fasciculata*, when diluted (Flohé *et al.*, 2002b). Exception are the AhpCs of *S. typhimurium* (Wood *et al.*, 2002) and *M.*

tuberculosis (T. Jäger, unpublished data), because they tend to form active dimers when oxidized and decamers in the reduced state.

Therefore the molecular weight of *Tb*TXNPx and the influence of the redox state on the molecular weight were investigated.

As commonly observed with 2-Cys-peroxiredoxins, a trace of dimeric *Tb*TXNPx was always detectable in SDS gels under reducing conditions (see Figure 3.5). The major band appeared at the molecular mass corresponding to one subunit (*Tb*TXNPx = 22,507 Da). The denaturating conditions of the SDS-PAGE and boiling for 10 min at 95 °C were not able to abrogate the dimer/dimer interactions of the oligomeric protein completely.

MALDI-TOF analysis of a freshly prepared *Tb*H6TXNPx gave a spectrum with mass peaks corresponding up to octamers that disclosed an unusually high affinity of the dimers to each other (see Figure 3.11). The dimer peak was most prominent, while the peak corresponding to the subunit size was small and could also represent a double charged dimer.

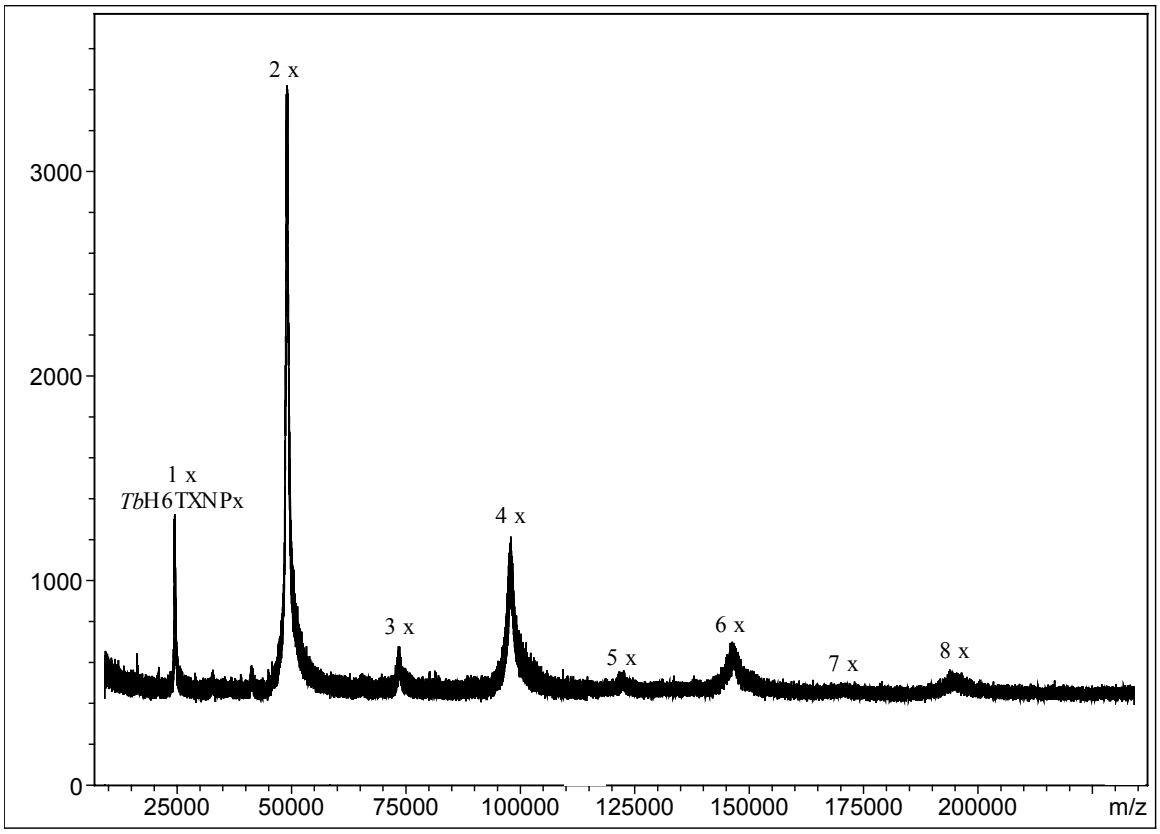

Figure 3.11: MALDI-TOF analysis of *Tb*H6TXNPx. The highest peak corresponds to the dimeric state and all even subunit multimers (tetra-, hexa-, and octamer peaks) appear substantially higher than that of the uneven numbers.

It is surprising that this non-covalent dimer/dimer interaction is evidently strong enough to resist laser desorption and ionization.

3.1.4.3 Influence of the redox-status on the molecular weight of *Tb*TXNPx

For studies of the influence of the redox-state on the molecular weight of the enzyme, reduced and oxidized *Tb*TXNPx were subjected to a Superdex 200 column for gel permeation. The effluents were analyzed for specific activity by the conventional assay (see chapter 2.7.2), for identity by SDS gel electrophoresis, and for the shape by electron microscopy.

The reduced protein seemed to elute homogeneously in a single peak (E_{280}), with paralleling activity. The peak fraction eluted with an apparent molecular weight of 236,400 Da that complies with the decamer size of *Tb*TXNPx (225,507 Da). The corresponding silver-stained SDS-gel displayed a major band corresponding to the subunit size of *Tb*TXNPx with a trace of dimer. Surprisingly the electron micrographs showed a non-homogenous fraction consisting of ring-shaped and pearl-chain-like structures (see Figure 3.12 A, middle panel). The ring-shaped structures were considered to represent the pentamers of dimers that were anticipated from X-ray crystalography of *Cf*TXNPx (Alphey *et al.*, 2000) or by electron microscopy for human TrxPx (Harris *et al.*, 2001) and *Li*mTXNPx (Castro *et al.*, 2002a).

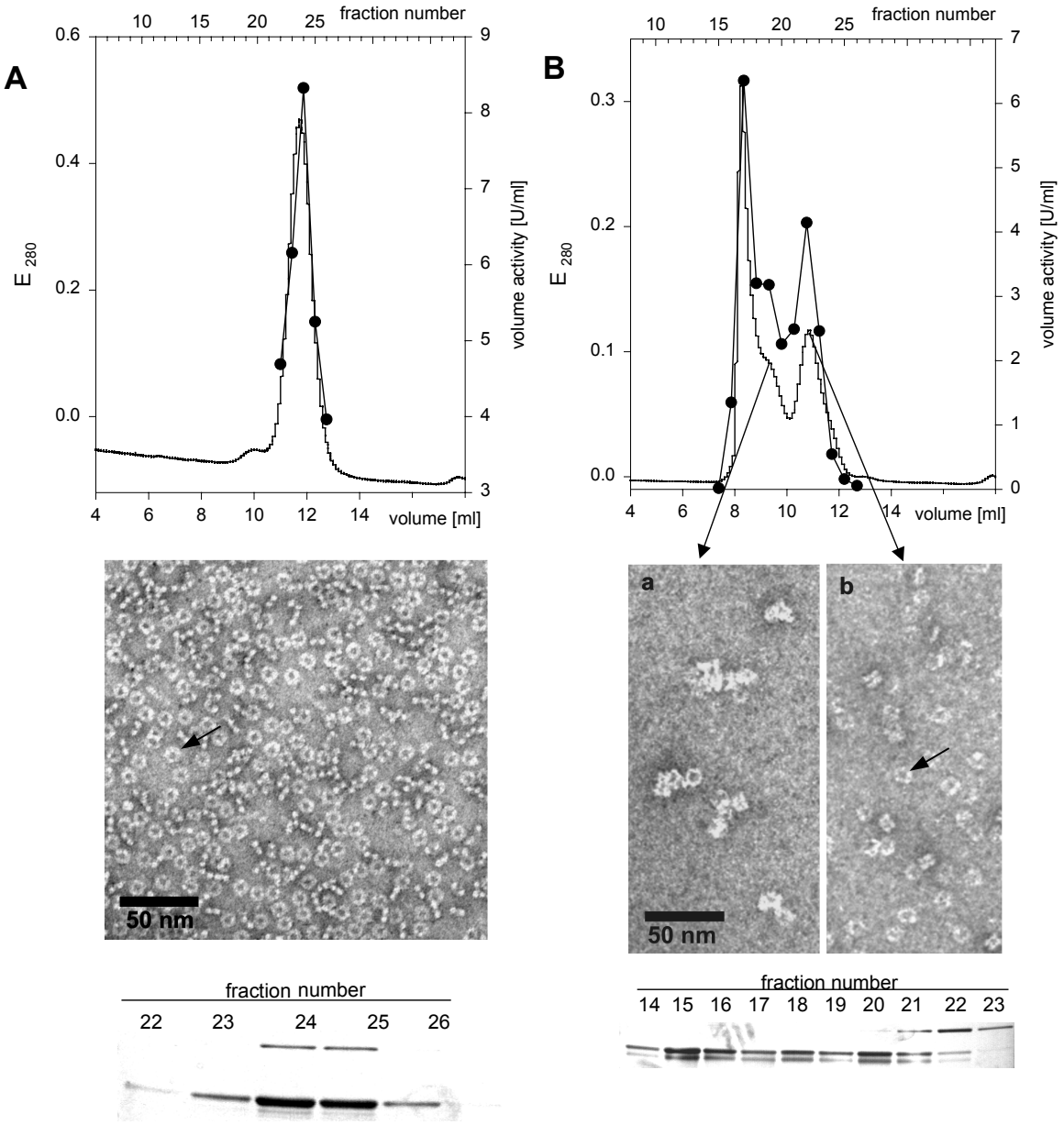

Figure 3.12: Status of oligomerization of reduced and oxidized *Tb*TXNPx. (A) The upper panel shows the elution profile of DTT-reduced *Tb*TXNPx in terms of proteinconcentration (E_{280}, solid line) and activity (U/ml, solid line with black dots). In the middle panel the appearance of the peak fraction in electron microscopy (uranylacetate-stained) is shown. Notice the mix of rings (black arrow) and open-chain structures. The lower part demonstrates the appearance of individual fractions in SDS-PAGE. (B) Same as (A) but oxidized with *t*-bOOH. The smaller SDS-bands co-eluting with *Tb*TXNPx are likely truncated forms thereof, as indicated by N-terminal sequencing. Also traces of dimers could be detected. The ring-shaped structure is indicated by a black arrow.

The oxidized enzyme (see Figure 3.12 B) eluted with a different pattern. The front peak eluted with the exclusion volume of the column, followed by a small shoulder and a discrete peak with a molecular weight similar to that of the reduced enzyme. All fractions showed activity, but the highest was measured in the fractions corresponding to the last peak. In the SDS gel the subunit band and an increase of the dimer with progressing retardation on the column was seen. Electron-microscopy revealed that the front peak consisted of highly aggregated material without any detectable structures (not shown). The shoulder contained clusters of discrete structural elements the nature of which became evident when inspecting the late peak material. Here isolated ring-shaped structure prevailed which were hardly distinguishable from those seen in the preparation of the reduced enzyme. Rarely side views of piled-up rings are seen. Open chain structures indicating sizes lower than decamers could not be detected. Higher order multimers, stacking into columns of various lengths could also be detected for mammalian PrxII (Harris *et al.*, 2001) and PrxIII (Kato *et al.*, 1985) which are typical 2-Cys-peroxiredoxins. In conclusion, the redox status of *Tb*TXNPx effects the dimer/dimer interaction. The tendency to form decameric rings is weakened by reduction and strengthened by oxidation. The oxidized enzyme also trends to form higher aggregates of decamers, which is accompanied by a decline in specific activity.

3.1.5 TXNPx/TXN interaction

TXNs may systemically be described as trypanothione:protein disulfide oxidoreductases. In the context of trypanosomal peroxide metabolism the disulfide substrate is the peroxiredoxin-type TXNPx. Beside their function as reducing equivalent to ribonucleotide reductase (Dormeyer *et al.*, 2001), they are the substrates of TXNPx. TXNs appear to be specifically reduced by $T(SH)_2$, as GSH and thioredoxins are poor substrates (see chapter 3.1.2) (Gommel *et al.*, 1997; Nogoceke *et al.*, 1997; Steinert *et al.*, 2000; Castro *et al.*, 2002a). The molecular basis of this specificity has become evident from molecular modeling (Hofmann *et al.*, 2001), site-directed mutagenesis (Steinert *et al.*, 2000; Hofmann *et al.*, 2001), and X-ray crystallography (Alphey *et al.*, 1999a; Hofmann *et al.*, 2001).

As discussed above (see chapter 3.1.4), TXNPx is an oligomeric enzyme and builds-up the reaction centers between two subunits. The conserved C52 residue is first oxidized by H_2O_2 to a sulfenic acid derivative (see Figure 3.9; intermediate F) and reacts with the conserved C173´ of a second invertedly

orientated subunit to build a intersubunit disulfide bridge (see Figure 3.9, intermediate G). The formation of the disulfide bridge is associated with considerable conformational changes that lead to exposure of the C173´ to the surface. Since the C40 of *Tb*TXN is the only accessible one from the solvent side, it attacks the disulfide bond of the oxidized *Tb*TXNPx resulting in an intermediate formation. The intermediate-state is resolved by formation of an intramolecular disulfide bridge between C40 and C43 of the tryparedoxin active site motif (WCPPCR), and an oxidized tryparedoxin and a reduced tryparedoxin peroxidase are released.

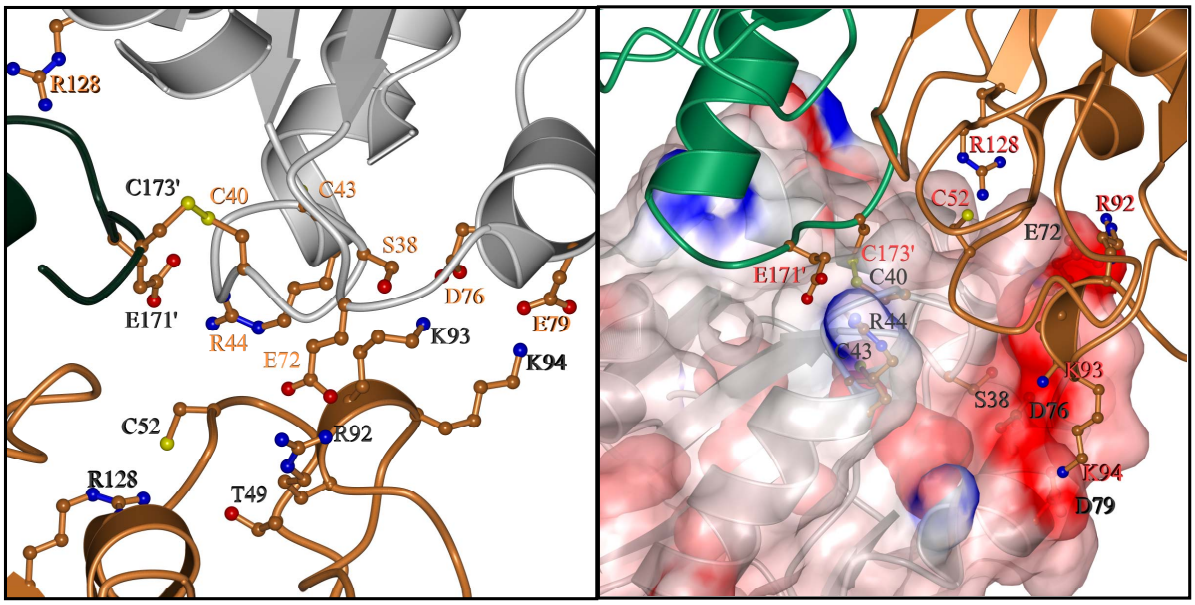

Figure 3.13: Model of the catalytic intermediate demonstrating potential TXNPx/TXN interactions. Docking of reduced *Tb*TXN (grey ribbon model) to oxidized *Tb*TXNPx (brown ribbon diagram subunit 1, black ribbon diagram subunit 2) suggests a nucleophilic attack of C40 of TXN on C173´ of the TXNPx that is facilitated by four ionic attractions (left panel). The resulting intermediate is devoid of sterical infringements and appears stabilized by multiple electrostatic attractions between TXNPx (ribbon diagram, residue names shown in red) and TXN [surface charges shown in red (negative) and blue (positive), residue designation in black].

Molecular events supporting the specific reaction of TXNPx with TXN were suggested by molecular modeling (see Figure 3.13). Negative charges of E72, D76 and D79 in *Tb*TXN are in the right position for electrostatic attraction to the positive charges of R92, K93 and K94 of the peroxidase, while R128 of the *Tb*TXN forms a salt bridge to E171 of *Tb*TXNPx. If arranged in that way the C40 can react with the C173 of the TXNPx (Hofmann *et al.*, 2002).

Data relevant for TXNPx/TXN interaction		Relative activity (%)
Peroxidase	**Reductant**	
*Tb*H6TXNPx	*Tb*H6TXN	(100)
*Tb*H6TXNPx	*Tb*TXNC40SH6	0
*Tb*H6TXNPx	*Tb*TXNC43SH6	0.2
*Tb*H6TXNPx	*Tb*H6TXND76K	48
*Tb*H6TXNPx	*Tb*H6TXND79K	111
*Tb*H6TXNPx	*Tb*H6TXN76K,D79K	52
*Tb*H6TXNPx	*Tb*H6TXNE72R	41
*Tb*H6TXNPx	*Tb*H6TXNR128D	9

Table 3.5: Relative activities of *Tb*H6TXN muteins in the TXNPx test as described in chapter 2.7.2.. Activity of *Tb*H6TXN is set to 100 %.

The validation of these assumption was checked by mutating the *Tb*TXN residues implicated and, indeed, charge inversion at the TXN residues, with the exception of the D79K exchange, significantly reduced activity (see Table 3.5).

3.1.5.1 Verification of TXN/TXNPx interaction by MS

A particular challenge was how to get information on the shape of a catalytic intermediate such as “H“ in Figure 3.9. The proposed catalytic intermediate, in which TXN is linked to the peroxidase could never be identified, because it is evidently processed too fast. A mutated substrate that still can react with the oxidized peroxidase but is no longer able to complete the catalytic cycle by thiol/disulfide exchange, could freeze in the state of a catalytic intermediate. To this end the hidden C43 was mutated to serine, while the solvent-exposed C40 was left unchanged. The mutein showed practically no activity (see Table 3.5). An intermediate was obtained by co-oxidation of the *Tb*TXNPx with the mutein *Tb*TXNC43S and separated from excess of *Tb*TXNC43S by gel permeation. The intermediate was cleaved by trypsin and chymotrypsin and peptides not bigger than 2500 Da were obtained that were detectable by ESI

(electronspray ionization mass spectrometry) analysis. A peak of a molecular mass from 1988.8 Da could be found which matched with the predicted size of the amino acid residues 36-44 of *Tb*TXNC43S (containing the active C40) linked by a disulfide bond to the fragment 169-177 of the *Tb*TXNPx (containing the active C173 imbedded in the C-terminal VCP motif).

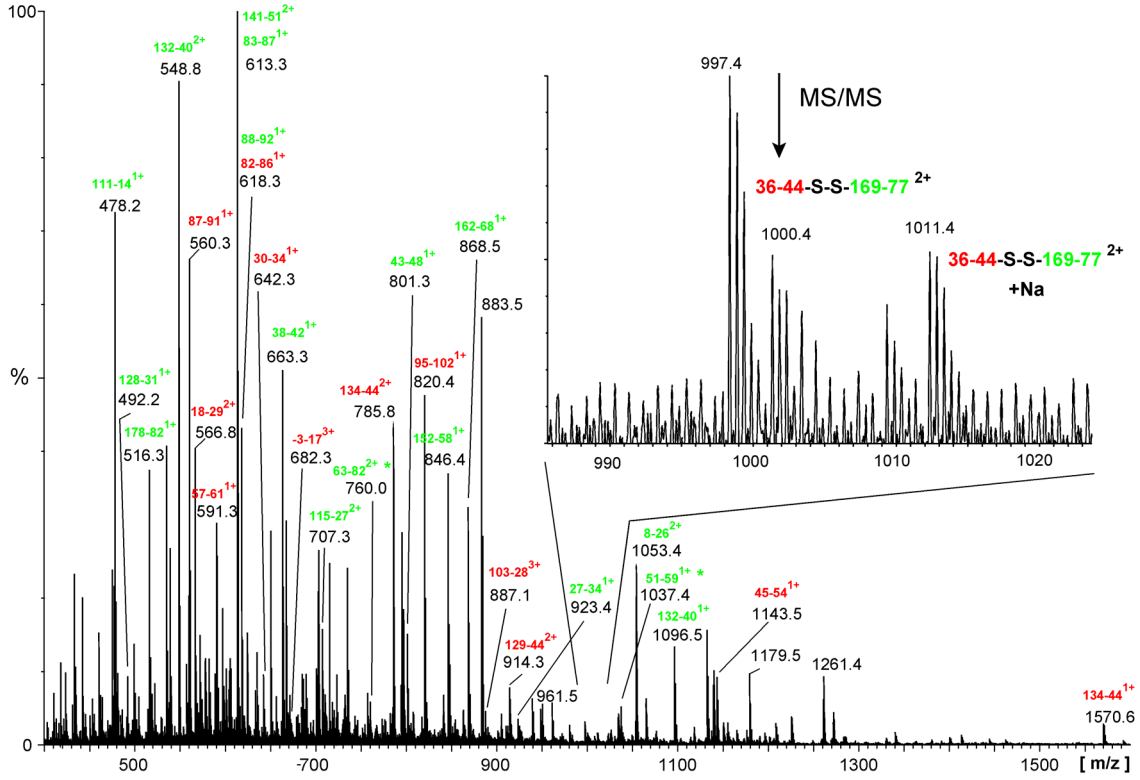

Figure 3.14: Mass spectrum of *Tb*TXNC43S/*Tb*TXNPx intermediate cleaved by trypsin and chymotrypsin. Both proteins were discovered with a sequence coverage of 82.3 % of *Tb*TXNC43S and that of *Tb*TXNPx with 80 %. The peptides of *Tb*TXNC43S are shown in red and of *Tb*TXNPx are shown in green. The insert shows the MS/MS analysis of the C40/C173-linked fragments.

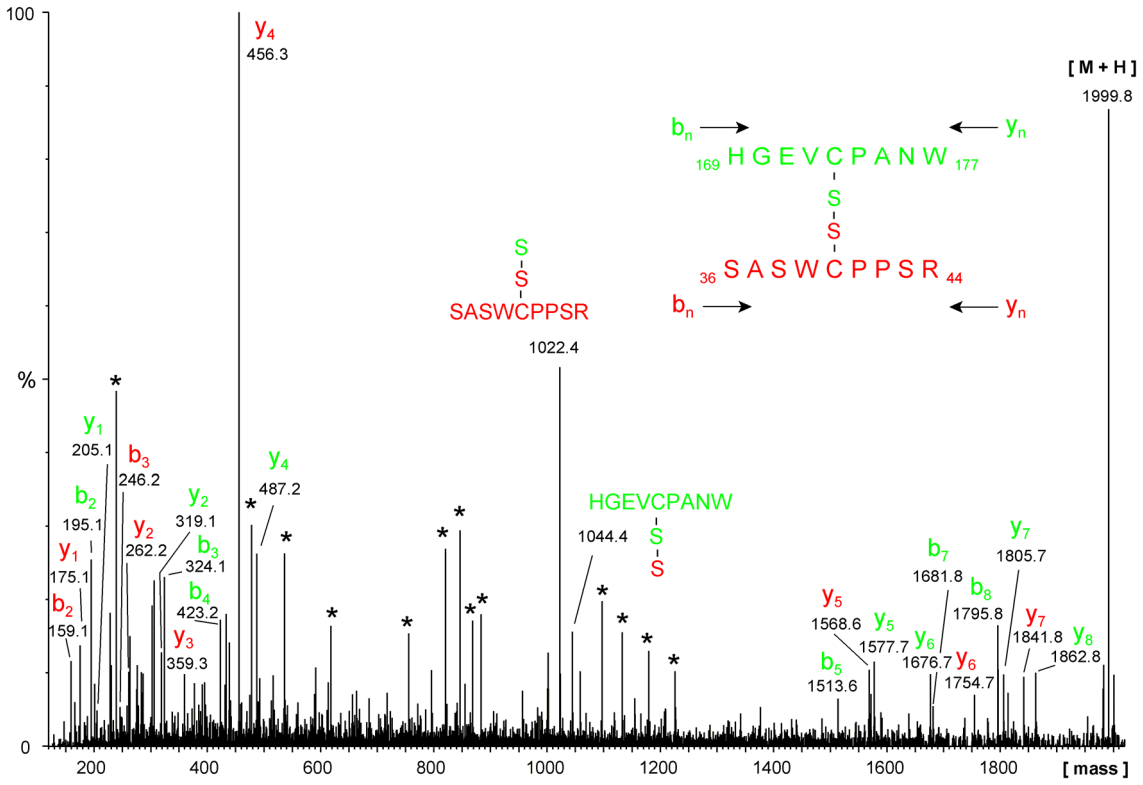

Figure 3.15: MS/MS sequencing of the disulfid-linked proteolytic fragment revealing the TXN/TXNPx interaction. The amino acid sequence of both peptide moieties could be deduced from two complementary series of N-terminal (b_n) and C-terminal (y_n) fragment ions depicted in green (HGV*C*PANW) and red (SASW*C*PPSR), respectively. Due to the low intensity of the parent ion, some signals resulting from a contamination of the instrument are also seen (marked by asteriks)

The peak eluting with the predicted size was analyzed by MS/MS and the sequences of the peptides 36-SASWCPPCR-44 and 169-HGEVCPANW-177 could be verified.

The results comply with the hypothetical reaction mechanism and with molecular models of TXN/TXNPx intermediates from *T. brucei brucei* or *C. fasciculata* (Flohé *et al.*, 2002a; Hofmann *et al.*, 2002; Budde *et al.*, 2003a). It is the first time that this interaction is corroborated. According to our data, the reductive part starts with an attack of the solvent exposed cysteine (C40) of the TXN on the distal conserved cysteine (C173´) of the peroxidase.

3.1.5.2 Reaction stoichiometry

From molecular modeling it was known that the decameric *Tb*TXNPx has ten putative reaction centers. If all ten binding-sites react with the substrate TXN at the same time remained elusive. Therefore the intermediate-state of

*Tb*TXNPx/*Tb*TXNC43S was reduced with β-Mercaptoethanol and the presence of both, *Tb*TXNPx and *Tb*TXNC43S was verified by SDS-gel electrophoresis. Appropriate calibration of the gel with the single components revealed that the intermediate contained one molecule of *Tb*TXNC43S per subunit of *Tb*TXNPx (see Figure 3.16). The stoichiometry was confirmed by gel permeation of the reductively cleaved *Tb*TXNPx/*Tb*TXNC43S intermediate (data not shown). The protein concentration of the peak areas were calculated from E_{280} and the respective extinction coefficients were calibrated by amino acid analysis ($\varepsilon_{TXNC43S\ 280}$ = 0.92 $mg^{-1}cm^{-1}$; $\varepsilon_{TXNPx\ 280}$ = 0.42 $mg^{-1}cm^{-1}$)

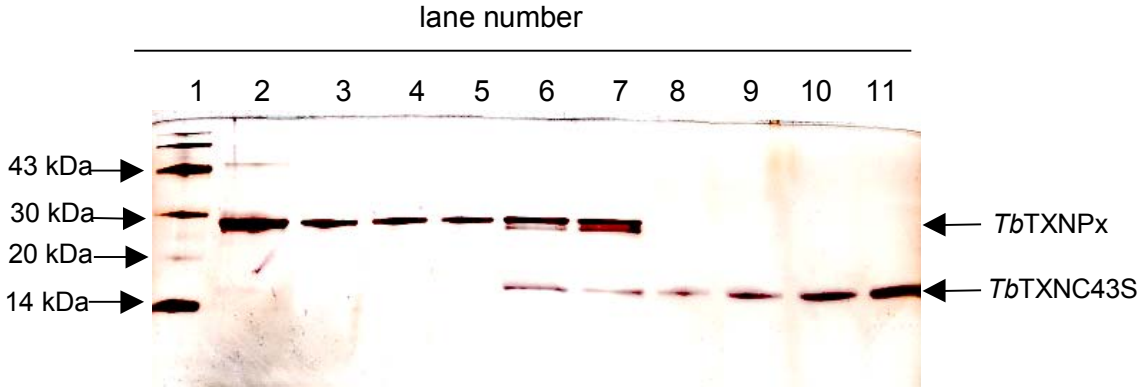

Figure 3.16: Denaturating SDS-PAGE showing different concentrations of *Tb*TXNPx, *Tb*TXNC43S and the intermediate. lane 1: molecular weight marker (GibcoBRL, Karlsruhe, Germany); lane 2: *Tb*TXNPx 32 pmol; lane 3: *Tb*TXNPx 16 pmol; lane 4: *Tb*TXNPx 8 pmol; lane 5: *Tb*TXNPx 4 pmol; lane 6 and 7: intermediate; lane 8: *Tb*TXNC43S 6 pmol; lane 9: *Tb*TXNC43S 12 pmol; lane 10: *Tb*TXNC43S 24 pmol; lane 11: *Tb*TXNC43S 48 pmol; After measuring the density of the bands the concentration of *Tb*TXNC43S in the intermediate was calculated to be 10.3 ± 4.21 pmol and the concentration of *Tb*TXNPx 10.5 ± 3.8 pmol.

3.1.5.3 Recovery of TXNPx activity from a dead-end intermediate by trypanothione

When *Tb*TXNPx thus modified with the dead-end substrate *Tb*TXNC43S, was tested for activity in the conventional assay, it expectedly proved to be inhibited, but gradually recovered when exposed to $T(SH)_2$ and the authentic TXN. The recovery is time-dependent and a specific activity up to 89% of the starting value was re-established within 30 min (see Table 3.6). That corroborates the assumption that the pseudosubstrate reacted in the anticipated way and did not damage the structure of the peroxidase.

time [min]	specific activity [%]
control without *Tb*TXNC43S	100
1	51
11	74
21	84
31	89

Table 3.6: Recovery of reactivity of *Tb*TXNPx after a dead-end intermediate was built. The assay mixture contained, 300 µM NADPH, 1 U/ml TR, 50 µM *Tb*TXNC43S, 10 µM *Tb*TXNPx and 70 µM *t*-bOOH, was pre-equilibrated for 15 min at 25 °C before 10 µM *Tb*TXN was added to the reaction mixture. The whole mixture was incubated for 1, 11, 21, 31 min before the reaction was started by addition of 130 µM $T(SH)_2$.

3.1.5.4 Electron microscopic studies of the dead-end intermediate

A model that reveals that all reaction centers of the decameric peroxidase may simultaneously react with the reducing substrate was created by Hofmann *et al.* (2002). Electron microscopy of the intermediate, which eluted with an apparent molecular weight beyond 300,000 Da from a gel chromatography column, showed almost exclusively ring-like structures which appeared larger and had adopted a pentangular shape. When the material was tested on a reducing SDS gel, bands corresponding to the sizes of *Tb*TXNPx and *Tb*TXNC43S were detected.

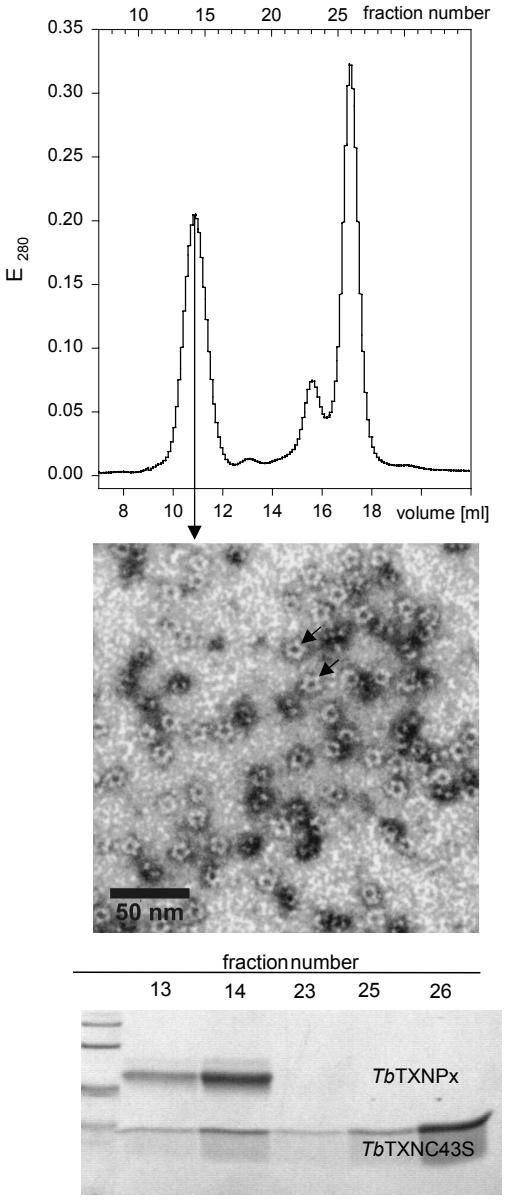

Figure 3.17: Elution profile and shape of pseudo-substrate-loaded decamer *Tb*TXNPx. *Tb*TXNPx co-oxidized with excess of *Tb*TXNC43S was subjected to gel permeation. The covalent intermediate of *Tb*TXNPx and *Tb*TXNC43S elutes with an apparent MW of 300,000 Da. Excess of *Tb*TXNC43S that is partially dimerized is separated (upper panel). The pentangular shape of the intermediate as appearing in electron microscopy, is shown in the middle panel and indicated by black arrows. Identity of the peaks is shown in the SDS-PAGE below.

The model of the intermediate has predicted almost equidistant attachment of the ten TXN molecules to the decameric peroxidase (Hofmann *et al.*, 2002), which appeared incompatible with the pentangular shape of the intermediate seen by electron microscopy. An idealized shape of the structure was obtained by averaging about 1,000 individual e. m. pictures. The resulting shape of

electron density was compared with a re-newed model of *Tb*TXN-loaded *Tb*TXNPx (see Figure 3.18). The idealized shape of unloaded reduced TXNPx forms an almost regular ring and fits to the predicted model as is shown in Figure 3.18.

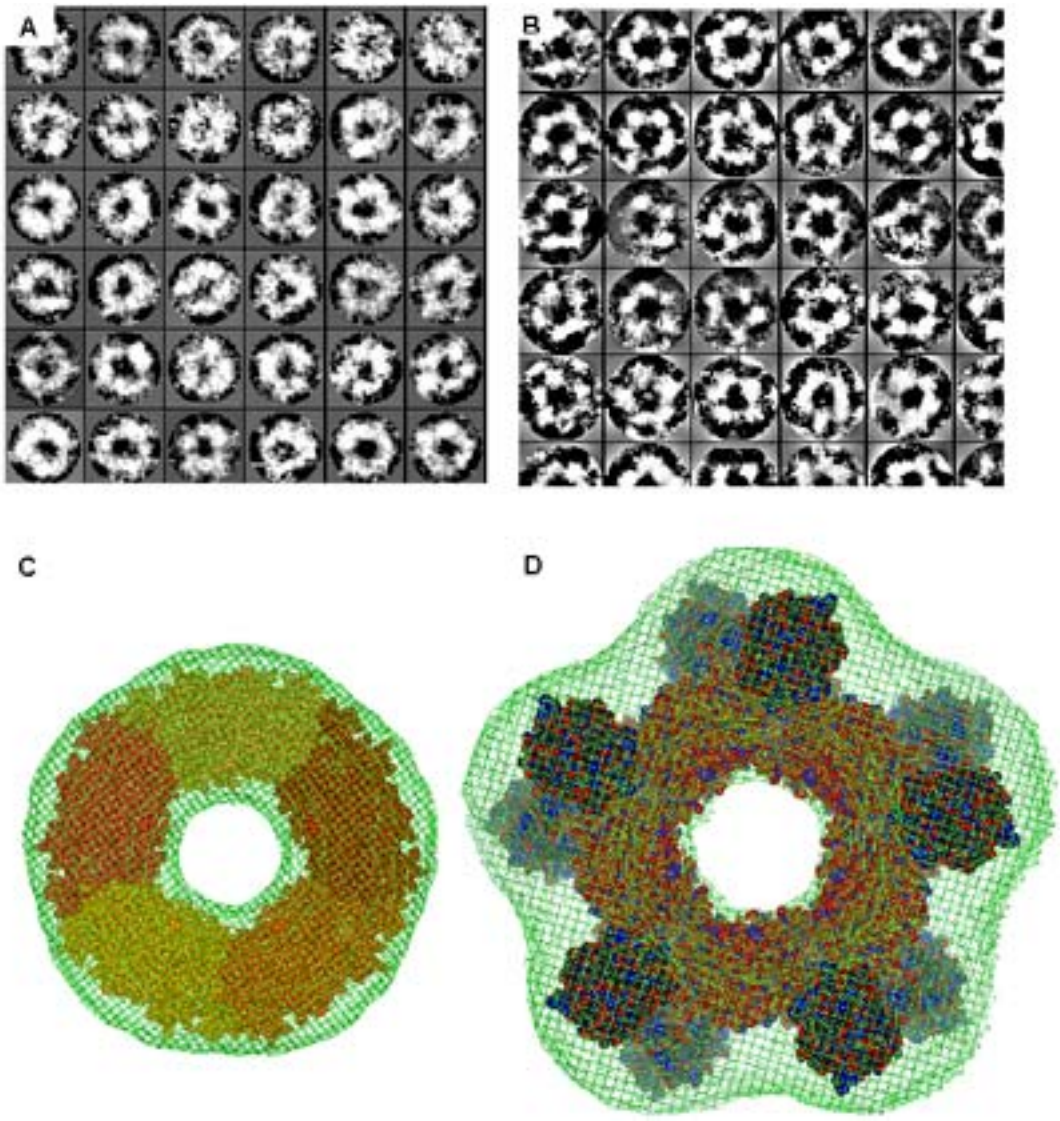

Figure 3.18: Comparing reduced *Tb*TXNPx in shape and model with intermediate (*Tb*TXNPx/*Tb*TXNC43S). (A) Panel of e. m. images obtained with DTT reduced *Tb*TXNPx. (B) Analogous panel of images obtained by co-oxidation of *Tb*TXNPx with *Tb*TXNC43S. (C) Idealized shape (green net) of reduced *Tb*TXNPx, as obtained by averaging individual e. m. pictures of (A), fitted to a space filling model of decameric *Tb*TXNPx. The five dimers are highlighted by different colors. (D) Shape of *Tb*TXNPx loaded with ten molecules of *Tb*TXNC43S, as derived from images in (B), fitted to the model of intermediate. The color code of the model is: orange, carbon atoms of *Tb*TXNPx; black, carbon atoms of *Tb*TXNC43S; blue, nitrogen; red, oxygen; yellow, sulfur.

As demonstrated in Figure 3.18, the fit of the models and the e. m.–derived shapes may be rated as highly satisfactory.

3.2 Results of related cooperative projects

The following chapters describe contributions to collaborative projects related to hydroperoxide metabolism of Kinetoplastida and other pathogens. Results are here briefly summarized in the context of the entire projects. The own contributions to each of the projects are indicated as footnotes at the end of the chapters.

3.2.1 Structures of *Cf*TXN revealing interaction with trypanothione*

Tryparedoxins are redox-active proteins which have been discovered in Trypanosomatids as thioredoxin-related proteins (Nogoceke *et al.*, 1997; Lüdemann *et al.*, 1998; Montemartini *et al.*, 1998a; Guerrero *et al.*, 2000b; Lopez *et al.*, 2000). TXN accepts its reduction equivalents from the unique redox mediator trypanothione, N^1, N^8-(bis)-glutathionylspermidine, and transfers them to tryparedoxin peroxidase, that can reduce hydroperoxides. Reduced trypanothione is consumed and regenerated by a NADPH-dependent flavoprotein, the trypanothione reductase.

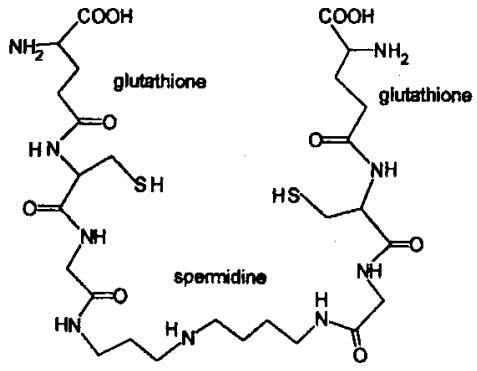

Figure 3.19: Structural formula of the bis-(glutathionyl)-spermidine conjugate trypanothione (Steenkamp, 2002).

A model for TXN/trypanothione interaction was developed based on the known structures of *Cf*TXN1 and *Cf*TXN2 (Hofmann *et al.*, 2001) and the following assumptions: (i) TXN displays ping-pong kinetics which implies independent interactions with both substrates ($T(SH)_2$ and TXNPx). The reduced TXN reacts with the oxidized TXNPx (Gommel *et al.*, 1997) and oxidized TXN is reduced by trypanothione. (ii) Since the thiol sulfur Cys41 is the only one

accessible from the solvent side, it must be considered to be attacked by an SH group of trypanothione. Therefore a mixed disulfide between TXN and trypanothione is achieved as a catalytic intermediate. (iii) Binding of the highly ionized substrate was presumed to be of electrostatic nature as in glutathione utilizing enzymes (Epp *et al.*, 1983; Karplus and Schulz, 1989; Aumann *et al.*, 1997). (iv) The differences to glutathione lie in the spermidine moiety and the carboxylate groups on both ends of trypanothione. Since permutation of the active site motif of *Cf*TXN2 did not adequately explain substrate specificity (Steinert *et al.*, 2000), it is assumed to be achieved by residues remote from the reaction center.

Screening of the surface of *Cf*TXN2 for exposed charged residues suitable to attract a trypanothione molecule that is bound to the Cys41 via a disulfide bridge, showed the guanidino group of R129 in an ideal position to bind the carboxyl group of the N^1-bound glutathionyl residue. The spermidine nitrogen can be brought in the vicinity of the Glu73 carboxylate of TXN. Further electrostatic forces between the N^1-bound glutathione and the residues Ile110-Pro111 analogous to experimental thioredoxin complexes (Qin *et al.*, 1995; Doublie *et al.*, 1998), stabilize the TXN/trypanothione complex (see Figure 3.20). The proposed model is consistent with functional characteristics of the *Cf*TXN2 variants of the residues Glu73 and Arg129, each having the charge inversed. When freshly prepared, both muteins E73R and R129D shared similar CD-spectra with the wild-type enzyme and thus confirmed native conformation under these conditions. The specific activities of the freshly prepared *Cf*TXN2H6-E73R and R129D muteins were 17 % and 2 % of that of the wild-type enzyme. The mutein E73R declined its activity to 12 %, when stored at 4 °C over one day, that goes parallel with a denaturation of the enzyme as could be confirmed by marked changes in the CD spectrum. The instability of *Cf*TXN2H6E73R and the marginal activity of the R129D mutein precluded a detailed kinetic analysis. The low activities of the freshly prepared muteins support the involvement of the residues Arg129 and Glu73 of the *Cf*TXN2 in trypanothione binding predicted by the model (see Figure 3.20).

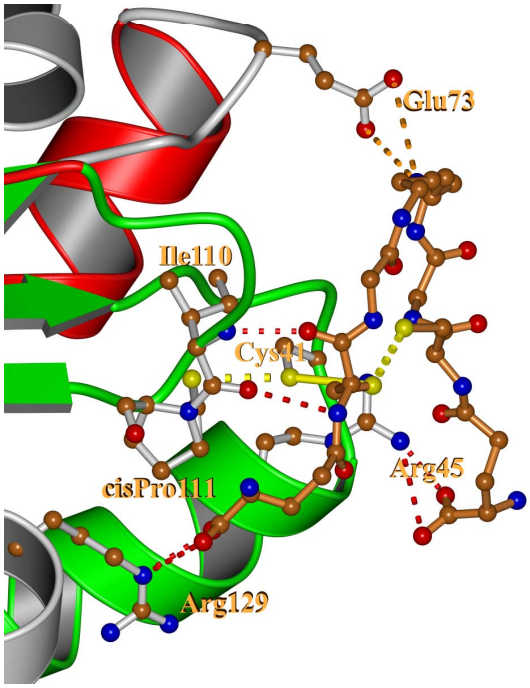

Figure 3.20: Modeling of trypanothione onto *Cf*TXN2 showing the presumed intermediate, where the sulfur of the N^1-glutathionyl residue of trypanothione has reacted with the sulfur of Cys41. Residues implicating the trypanothione binding are shown as balls and sticks and the corresponding *Cf*TXN2 is shown as a ribbon diagram.

* Own contributions to this chapter: Constructions and preparation of the muteins *Cf*TXN2E73R; *Cf*TXN2R129D; activity determination; verification of the amino acid exchange by tryptic cleavage and MALDI.

3.2.2 Tryparedoxin peroxidase of *Leishmania donovani* **

A novel peroxiredoxin was isolated from *L. donovani* (Flohé *et al.*, 2002a), the causative agent of fatal visceral Leishmaniasis. The TXNPx was investigated kinetically and subjected to molecular model-based mutagenicity for a better understanding of the catalytic events. Heterologous expression of the *Ld*TXNPx and variant genes in *E. coli* BL21(DE3) yielded proteins corresponding to the predicted size of 23,175 Da as was verified by MALDI-TOF spectrometry and gel electrophoresis. The native state of the variants were confirmed by CD spectra (The α-helix content of the wild-type *Ld*H6TXNPx was near 20 %). The N-terminally His-tagged proteins were easily purified in one step by nickel chelate chromatography.

*Ld*H6TXNPx proved to be an active peroxidase as it equally accepted *Cf*TXN1H6 and *Cf*TXN2H6. The specificity of *Ld*H6TXNPx for hydroperoxide

substrates, like that of other TXNPxs (Nogoceke *et al.*, 1997; Castro *et al.*, 2002a; Budde *et al.*, 2003a), is broad. It reacts with H_2O_2, *t*-bOOH, cumene hydroperoxide, linoleic acid hydroperoxide, and phosphatidyl choline hydroperoxide. Surprinsingly, the lipid hydroperoxides were incompletely reduced, as it was observed for *Li*mTXNPx (Castro *et al.*, 2002a) and *Tb*TXNPx (Budde *et al.*, 2003a), under standard test conditions due to substrate-induced inactivation with time (see Figure 3.21). While the reaction with *t*-bOOH always was complete (trace A), the reaction with phosphatidyl choline hydroperoxide slows down to marginal rates (trace B) (see Figure 3.21). Addition of *t*-bOOH at that time to the reaction confirmed that the enzyme activity has declined substantially (compare trace A and trace B). This suicide reaction was partially overcome by increasing the concentration of *Ld*H6TXNPx (trace C), but slowed down to marginal rates long before the Gpx-4-reactive hydroperoxy groups (trace F) have been consumed. The same kind of inactivation could be seen with linoleic acid hydroperoxide (trace D). When the enzyme concentration is high enough to allow a completed reaction within 10 s, the enzyme remains active (trace E). The activities of *Ld*H6TXNPx compared with other TXNPxs are listed in Table 3.2.

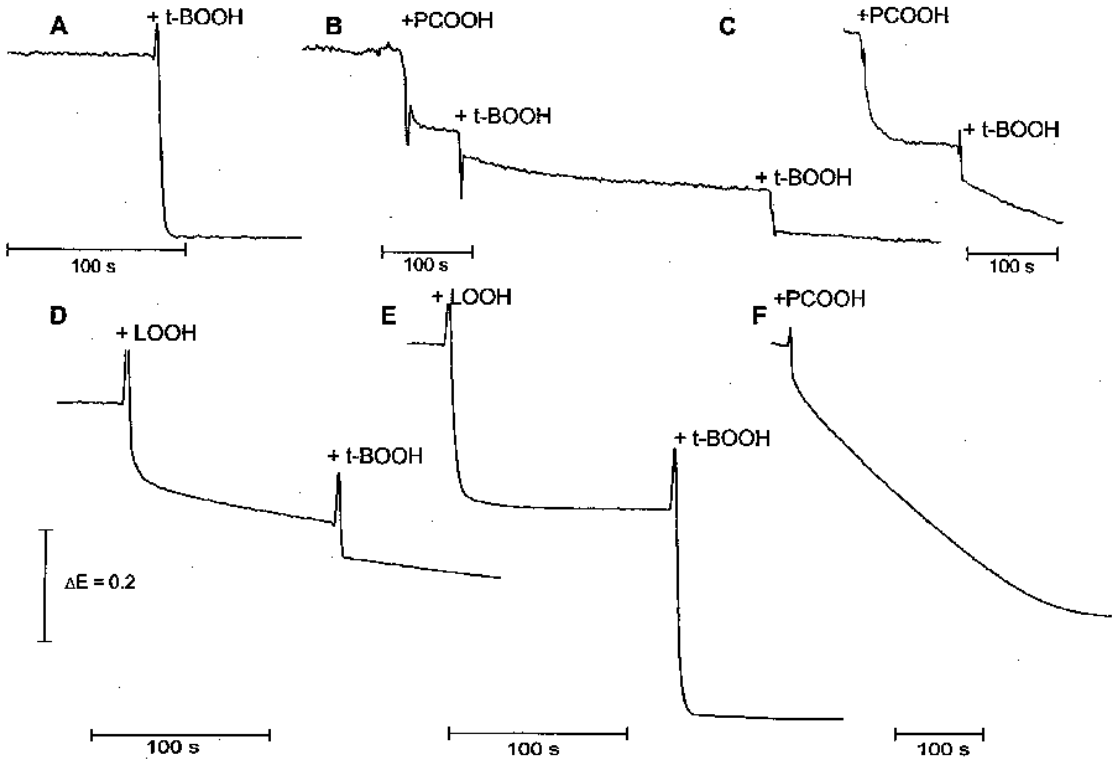

Figure 3.21: Original recordings of the *Ld*H6TXNPx reaction demonstrating substrate-induced inactivation. Activity assays are performed as described in chapter 2.7.4 but with 2.3 µM (traces A, B, and D) or 4.6 µM (traces C and E) *Ld*H6TXNPx. A difference of

absorbance ΔE = 0.441 corresponds to total consumption of hydroperoxide (70 µM in all experiments). The reduction of PCOOH (trace B) and peroxidized linoleic acid LOOH (trace D) by *Ld*TXNPx is incomplete due to inactivation, as evident from reduced activity with *t*-bOOH after pre-exposure to the lipid hydroperoxides. In trace C and E substrate-induced inactivity is partially overcome by increased enzyme concentration. Trace F demonstrates the determination of 70 µM PCOOH by means of GPx-4 reaction in an analogous test system described in chapter 2.7.3.

As observed in previous mutagenesis studies of *Cf*TXNPx (Montemartini *et al.*, 1999), an exchange of the active site cysteines to serines leads to abrogated (C52S) or marginal activities (C173S). *Ld*H6TXNPxC52S was also inactive in the glutamine synthetase protection assay (Kim *et al.*, 1988), but *Ld*TXNPxC173S showed considerable activity (see Figure 3.22).

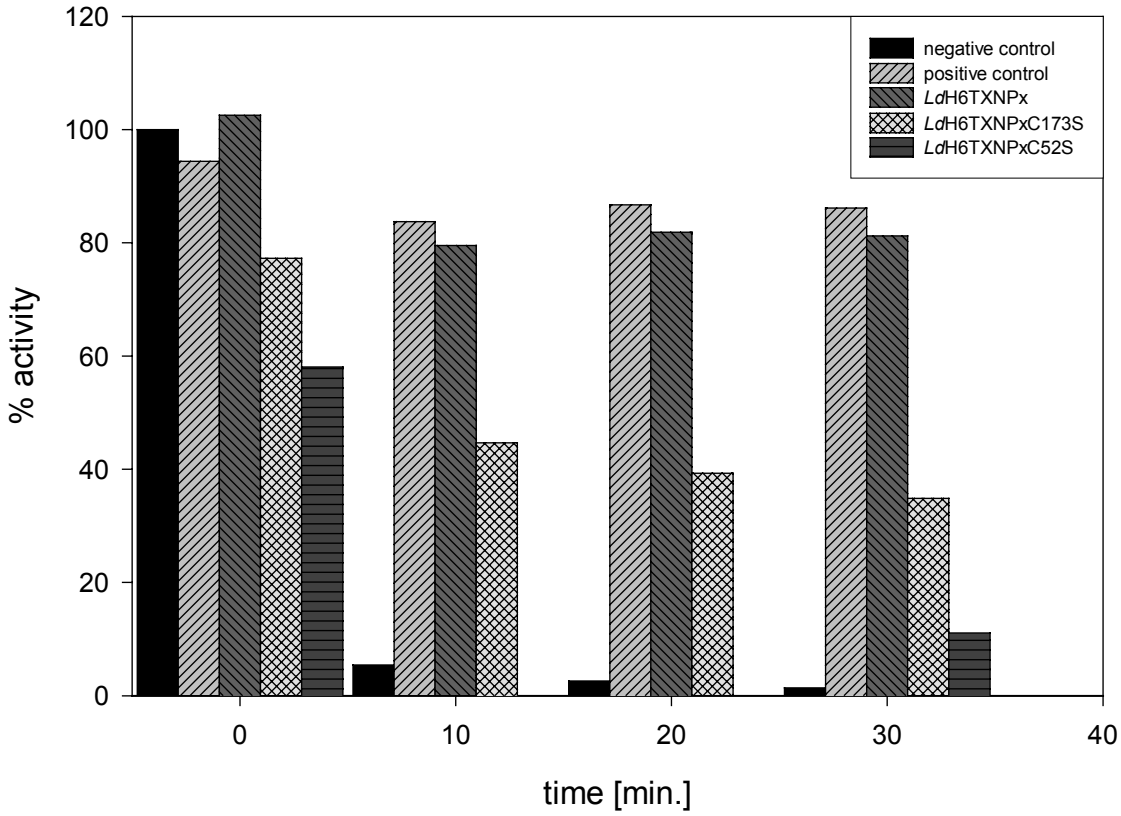

Figure 3.22: Protection of glutamine synthetase by *Ld*TXNPx and its variants against oxidative denaturation described by Kim *et al.* (1988). Data are presented as percentage of residual activity. The "negative control" contains no enzyme at all and in the "positive control" the catalytic iron ions are complexed by 1 mM EDTA. Samples were withdrawn in 30 s intervals, which implies that the decline of glutamine synthetase activity already seen with *Ld*H6TXNPxC173S and *Ld*H6TXNPxC52S at t_0 reflects glutamine synthetase activity after 90 and 120 s.

This assay monitores the oxidative denaturation of glutamine synthetase by H_2O_2 generated in an aerobic solution of $FeCl_3$ and dithiothreitol. Peroxiredoxins delay the process by reducing H_2O_2 using thiol as an unspecific reducing substrate (Netto and Stadtman, 1996). These finding support the view that C52 is the residue that is oxidized by the peroxide substrate. That conclusion was further supported by molecular models, based on the structure of *Cf*TXNPx (Alphey *et al.*, 2000), of the reduced *Ld*TXNPx. The *Ld*TXNPx models, supported by mutagenesis studies, proved to be extremely helpful in understanding the catalytic principles of the two active site cysteines (Flohé *et al.*, 2002a).

** Own contribution to this chapter: Detection of substrate-induced inactivation; Construction and preparation of the *Ld*H6TXNPxC173S mutein; investigations of *Ld*TXNPx muteins by glutamine synthetase protection assay.

3.2.3 AhpC of *Mycobacterium tuberculosis****

A peroxiredoxin, the AhpC of *M. tuberculosis*, became of interest, as it is overexpressed in strains that are resistant to isoniazid (Sherman *et al.*, 1996; Deretic *et al.*, 1997; Manca *et al.*, 1999).

The gene coding for the alkyl hydroperoxide reductase subunit C (AhpC) of *Mycobacterium tuberculosis* was amplified from genomic DNA, of the strain No. 4611 Reconquista from Argentine, that was a clinical isolate. The gene product was expressed heterologously in *E. coli* BL21(DE3) containing an N-terminal His-tag, and could easily be purified by a one step chelate chromatography. The activity as a peroxiredoxin-type peroxidase could be verified by glutamine synthetase protection assay as described by Kim *et al.* (1988). The protection of the glutamine synthetase against oxidative denaturation could be achieved by AhpC to 98 % of residual activity, after 30 min incubation. The search for possible reaction partners was done by T. Jäger.

*** Own contribution to this chapter: Construction of AhpC expression vector (Diploma thesis); large scale production; verification of activity.

3.2.4 Specificity and kinetics of a mitochondrial peroxiredoxin of *Leishmania infantum*$^{+}$

In *C. fasciculata* (Steinert *et al.*, 1999), *T. cruzi* (Lopez *et al.*, 2000) and *T. brucei* (Tetaud *et al.*, 2001) TXN and TXNPx were shown to be localized in the cytosol by immunohistochemistry. The cytosolic localization of the complete system appears to be ideal to protect the parasite against oxidative attack from outside. Kinetoplastida, like higher animals, are also able to produce endogenous H_2O_2, as byproduct of the mitochondrial energy metabolism (Boveris and Stoppani, 1977; Turrens and Cazzulo, 1987; Denicola-Seoane *et al.*, 1992). This endogenous oxidative stress cannot be balanced by the cytosolic peroxidase. In *L. infatum* two peroxiredoxin genes were identified. One coding for a cytosolic TXNPx (Castro *et al.*, 2002b) and the other, similar to the mitochondrial peroxiredoxins of *T. cruzi* (Wilkinson *et al.*, 2000b) and *T. brucei* (Tetaud *et al.*, 2001), was indeed shown to localize in this organelle (Castro *et al.*, 2002b).

The specificity for hydroperoxide substrates of *Li*mTXNPx is similar to those observed with *Tb*TXNPx (Budde *et al.*, 2003a), *Lm*TXNPx (Levick *et al.*, 1998), and *Ld*TXNPx (Flohé *et al.*, 2002a). The activity with lipid hydroperoxides is comparable weak and inactivation by these poor substrates could be objected (see chapter 3.2.2). The kinetic parameters deduced from *Li*mTXNPx are a $k_{cat.}$ of 37.0 s^{-1} and K_M values of 31.9 and 9.1 µM for *Cf*TXN2 and *t*-bOOH, respectively. Size and shape of the native enzyme was elucidated by light scattering, gel chromatography, and electron microscopic studies. The majority of *Li*mTXNPx molecules were recognized as ring-like structures, with an apparent molecular weight of 270 kDa, as was calculated for the decameric peroxidase. Therefore *Li*mTXNPx is assumed to preferentially adopt a state of oligomerization identical to that of *Cf*TXNPx in crystals (Alphey *et al.*, 2000). The kinetic pattern obtained for *Li*mTXNPx is similar to that observed for *Tb*TXNPx (Budde *et al.*, 2003a), deviating from the normal ping-pong pattern as observed for other TXNPxs. The regression lines of the primary Dalziel plot are converging and the coeffizient $\Phi_{1,2}$, that characterizes a ternary complex, is not zero (Castro *et al.*, 2002a). As judged by the chemical process and the knowledge of the structure, such a complex between the enzyme and both substrates is not assumed to be formed. These findings could possibly be attributed to a cooperativity of the reaction centers, as is not uncommon in oligomeric proteins (Koshland, 1970).

[+] Own contribution to this chapter: Instruction of H. Castro in chelate chromatography and spectroscopic techniques; know how transfer related to TXNPx kinetics; investigations of the native molecular weight of *Li*mTXNPx.

3.2.5 Kinetic pattern for *L. infantum* TXNPx and TXN[++]

For kinetic analysis the cytosolic form of TXNPx, modified with an N-terminal His-tag, from *L. infantum* (*Li*H6TXNPx) was prepared by Helena Castro (IBMC, Porto, Portugal) and the TXN1 from *L. infantum* (*Li*H6TXN1), cloned into the vector pET28c(+) to obtain an N-terminal His-tag, was provided from Marta Santos (IBMC, Porto, Portugal). As oxidizing substrate hydrogen peroxide was chosen, because *Li*H6TXNPx, in concentrations ≤ 2 µM, was inactivated by *t*-bOOH. The assay was essentially performed as described for *Tb*H6TXNPx and by Nogoceke *et al.* (1997), using 1.5 µM of *Li*H6TXNPx and 70 µM H_2O_2. As in that case the spontaneous reaction with $T(SH)_2$ can not be neglected, blanks, without the cosubstrate *Li*H6TXN1, had to be measured and subtracted from each single curve for progression analysis.

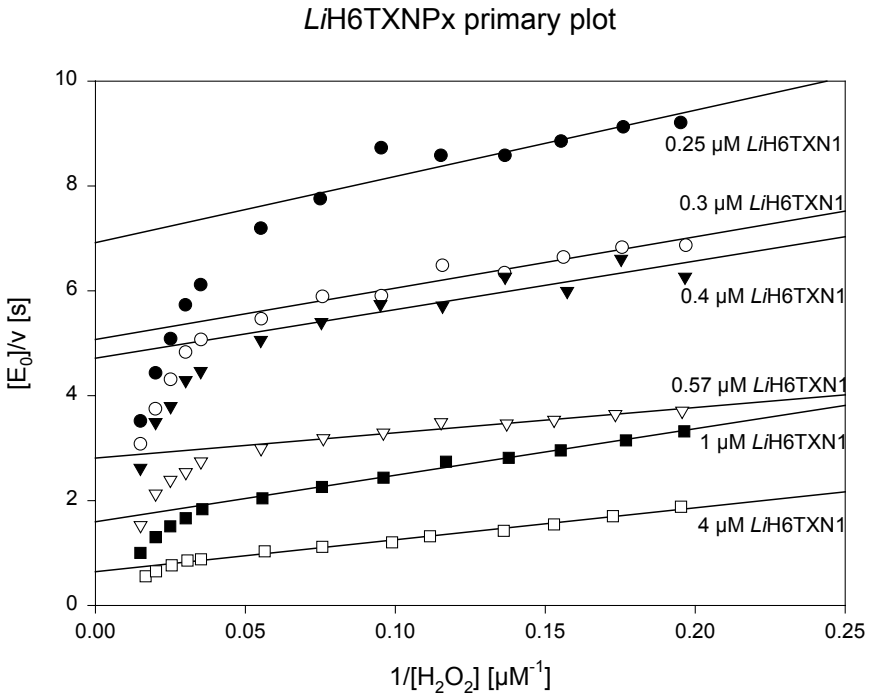

Figure 3.23: Steady-state kinetic analysis of *Li*H6TXNPx. Example of a double reciprocal primary plot showing dependency of enzyme-normalized initial velocities on H_2O_2 concentrations at 6 different concentrations of cosubstrate (*Li*H6TXN1) that were kept constant at regeneration.

The steady-state analysis of *Li*H6TXNPx yielded data that essentially complied with the data of other TXNPxs (see chapter 3.1.3). Enzyme-normalized double reciprocal primary Dalziel plots (i. e. $[E_0]/v$ versus $1/[H_2O_2]$) derived from single curve progression analysis at various fixed cosubstrate concentrations showed straight lines which deviate a little bit from parallelity.

Similar to the kinetic pattern of *Tb*H6TXNPx, the slopes of the primary plot are clearly biphasic, being steeper at high peroxide concentrations. Only the flatter parts of the curves are used for data processing, because of technical reasons. The secondary plot shows how the reciprocal apparent maximum velocities ($[E_0]/V_{max.\ app.}$) obtained as the ordinate intercepts of the primary plot depend on the reciprocal cosubstrate (*Li*H6TXN1) concentrations. It provides the limiting maximum velocity ($V_{max.}$ = ordinate intercept) and the limiting K_M value for the *Li*H6TXN1 (abscissa intercept). An attempt to calculate $\Phi_{1,2}$ from a total of 18 primary slopes did not yield a value that differed significantly from zero.

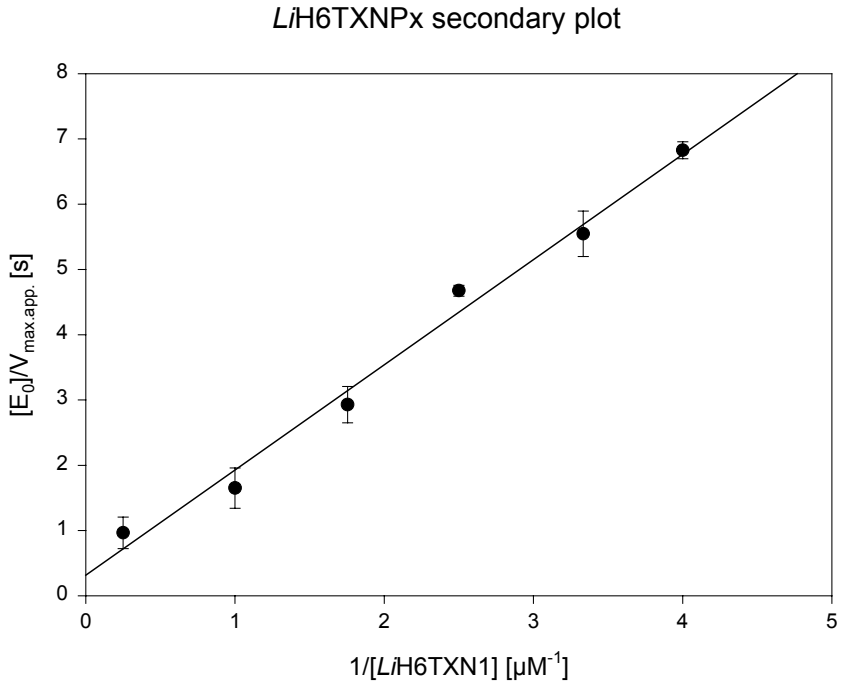

Figure 3.24: Secondary Dalziel plot for *Li*H6TXNPx demonstrating the reciprocal apparent maximum velocities for infinite hydrogen peroxide concentrations in relation to the reciprocal *Li*H6TXN concentrations.

The catalytic cycle thus represents an enzyme-substitution mechanism, which in the kinetic analysis is reflected in a ping-pong pattern as observed with

other peroxiredoxins (Nogoceke *et al.*, 1997; Montemartini *et al.*, 1999; Guerrero *et al.*, 2000a; Baker *et al.*, 2001; Flohé *et al.*, 2002a).

Φ_0 [s]	Φ_1 [s µM]	Φ_2 [s µM]	$K_{M\ HOOH}$ [µM]	$K_{M\ LiTXN1}$ [µM]	$V_{max.}$ [µM s^{-1}]	$k_{cat.}$ [s^{-1}]
0.32	7.99	1.61	25.19	5.08	1.58	3.15

Table 3.7: Kinetic constants for the *Li*H6TXNPx. Reaction with *Li*H6TXN1 and hydrogen peroxide, as analyzed according to Dalziel (1957).

Minor differences in the kinetic pattern that are observed between peroxiredoxins depend on the relation of rate constants for complex formation and reactions within complexes. Saturation kinetics may be observed, as reported here for *Li*H6TXNPx, *Tb*H6TXNPx and previously for *Ld*TXNPx (Flohé *et al.*, 2002a) and *Tc*TXNPx (Guerrero *et al.*, 2000a), or not, as reported for *Cf*TXNPx (Nogoceke *et al.*, 1997) (see Table 3.3).

Like tryparedoxins from *C. fasciculat*a (Gommel *et al.*, 1997; Montemartini *et al.*, 1998a; Guerrero *et al.*, 2000b) and *T. brucei brucei* (Lüdemann *et al.*, 1998), the tryparedoxin, a thioredoxin-related protein from *L. infantum* catalyzes the reduction of a peroxiredoxin-type peroxidase, *Li*H6TXNPx, at the expense of trypanothione. Kinetic characterization of the enzyme was initially performed as described by Gommel *et al.* (1997). The variation of the *Li*H6TXNPx concentration from 1.5 to 20 µM resulted in an inhibition of the peroxidase at concentrations higher than 3 µM. Therefore the assay mixture contained 300 µM NADPH, 1 U/ml trypanothione reductase, 0.56 µM *Li*H6TXN1, *Li*H6TXNPx in a range from 1.5 to 2.5 µM and trypanothione in concentrations from 10 to 300 µM. The reaction was started after 15 min of incubation with 70 µM H_2O_2. The kinetic analysis revealed a kinetic pattern which, as in the case of *Cf*TXNs, complies with the ping-pong mechanism and can be described by the simplified Dalziel equation:

$$\frac{[E_0]}{v} = \Phi_0 + \frac{\Phi_1}{[A]} + \frac{\Phi_2}{[B]}$$

Equation 3.2: Simplified Dalziel equation for a typical ping-pong or enzyme-substitution mechanism, wherein the term $\Phi_{1,2}$/[A] [B] is zero. [A] is the molarity of peroxiredoxin and [B] that of trypanothione.

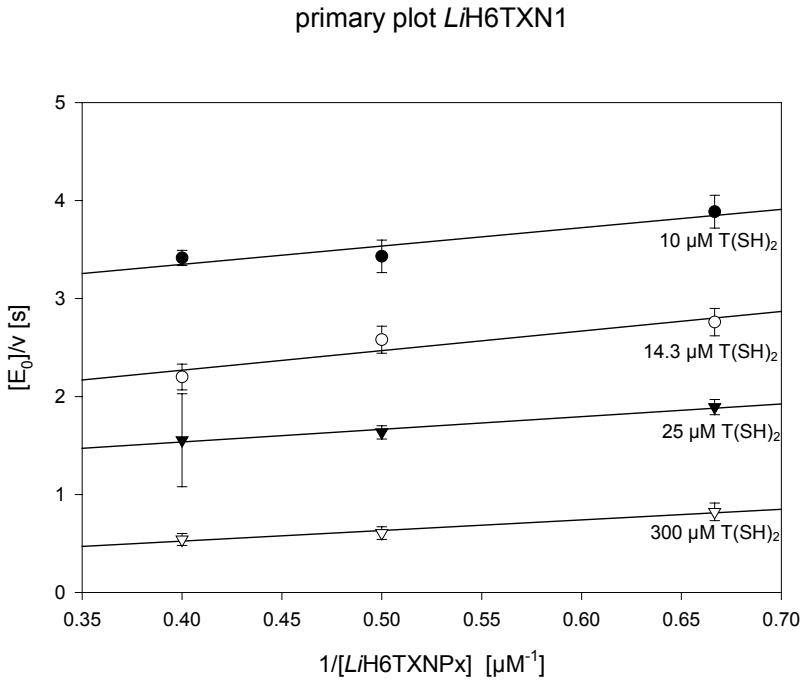

Figure 3.25: Enzyme-normalized double reciprocal primary plots ($[E_0]/v$ versus 1/[*Li*H6TXNPx]) derived from measurements at various fixed co-substrate [$T(SH)_2$] concentrations.

The primary Dalziel plot of *Li*H6TXN1 shows straight lines that do not deviate significantly from parallelity, which complies with the proposed ping-pong mechanism as reported for other TXNs (Gommel *et al.*, 1997; Montemartini *et al.*, 1998a; Guerrero *et al.*, 1999).

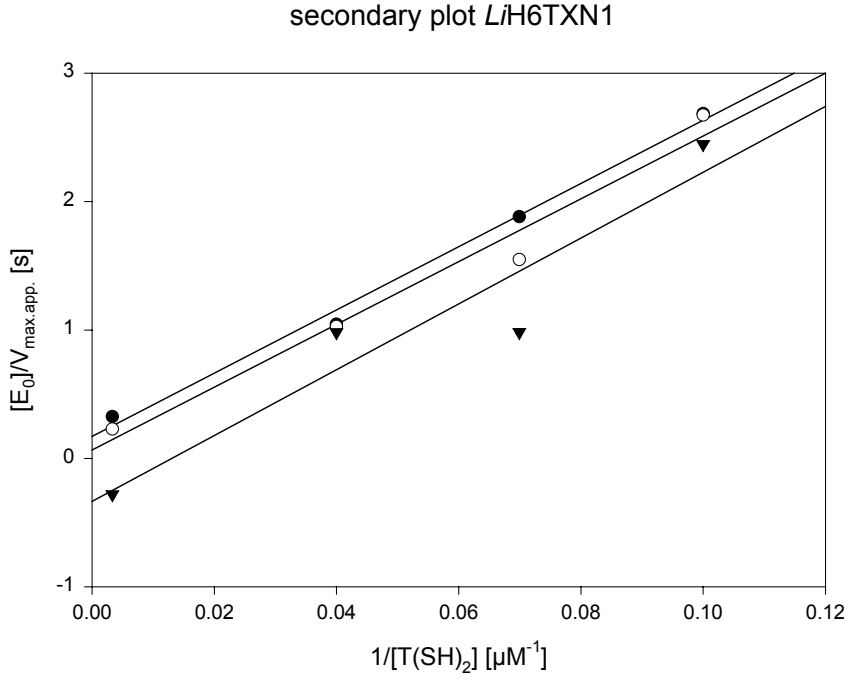

Figure 3.26: The secondary plot of *Li*H6TXN1. The apparent maximum velocities ($[E_0]/v_{max.app.}$) were plotted versus the reciprocal cosubstrate concentrations ($1/[T(SH)_2]$)

As demonstrated in Figure 3.26, a double reciprocal plot of the apparent $V_{max.}$ for infinite [*Li*H6TXNPx] against cosubstrate concentration shows three lines intersecting the ordinate at zero, within experimental errors. Ping-pong kinetics with infinite K_M and infinite $V_{max.}$ are thus observed, which are not unusual for oxidoreductases as previously reported for glutathione peroxidases (Flohé *et al.*, 1972; Ursini *et al.*, 1995) and *Cf*TXNPx (Nogoceke *et al.*, 1997).

Φ_0 [s]	Φ_1 [s µM]	Φ_2 [s µM]	$K_{M\ LiTXNPx}$ [µM]	$K_{M\ T(SH)2}$ [µM]	$V_{max.}$ [µM s^{-1}]	$k_{cat.}$ [s^{-1}]
~ 0	1.56 ± 0.61	24.91 ± 0.22	∞	∞	∞	∞

Table 3.8: Kinetic coefficients of *Li*TXN1. Reaction was performed with *Li*H6TXNPx, $T(SH)_2$ and analyzed according to Dalziel (1957).

The kinetic pattern, however, does not exclude the formation of specific enzyme-substrate complexes, but it predicts that the decay of any such complexes cannot be the rate-limiting step of the overall reaction. The constants k'_1 and k'_2 determine the apparent limiting rates for the net oxidation and reductive regeneration of *Li*TXN1 and are defined as the reciprocal values of the empirical Dalziel coefficients Φ_1 and Φ_2.

[++] Own contributions to this chapter: Complete kinetic analysis of *Li*H6TXNPx and *Li*H6TXN1.

3.2.6 Inhibitory activity of N^1, N^8-bis-(γ-Glu-Ala-Gly)-spermidine towards tryparedoxins[+++]

A pseudosubstrate of TXN was synthesized in which the redox active glutathione residues were replaced by ophthalmic acid (γ-glutamyl-alanyl-glycine). The use of the pseudosubstrate was expected to better disclose the molecular interactions than trypanothione itself, which, upon reaction, becomes a cyclic disulfide that does no longer interact with the enzyme.

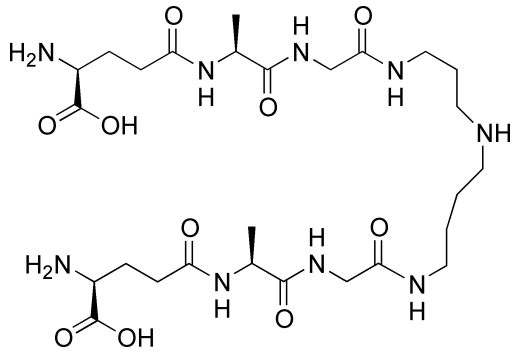

Figure 3.27: Structure of the Bis-(ophthamyl)-spermidine, a homologue of $T(SH)_2$ in which the both cysteines are replaced by alanines.

The redox inactive homologue of trypanothione weakly inhibited the two TXN isozymes of *C. fasciculata* and TXN of *T. brucei*. A slightly inhibition could be detected by adding 500 fold excess of pseudosubstrate over trypanothione to the reaction (see Figure 3.28).

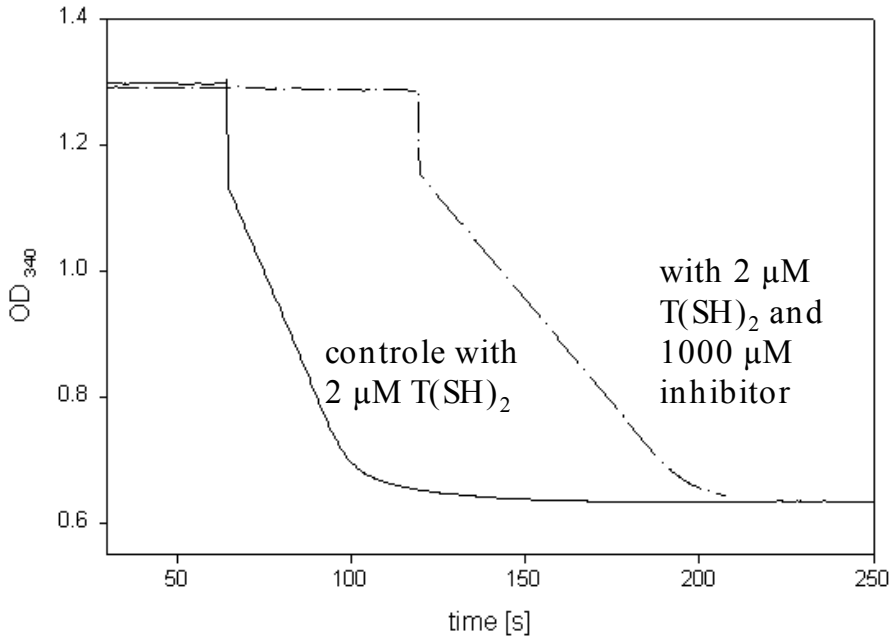

Figure 3.28: Inhibition of *Cf*TXN1 by bis-(ophthamyl)-spermidine. The weak inhibitor, in which the two cysteines were replaced by alanines, occupied the $T(SH)_2$ binding sites.

Inhibition constants, calculated on the basis of a competitive inhibition with trypanothione, were in the high micromolar range, as was to be expected from weak TXN/trypanothione interaction. The interactions primarily seem to depend on electrostatic attractions of the substrate´s carboxyl functions and arginine residues at the enzyme surface (Hofmann *et al.*, 2001) (see chapter 3.2.1).

$T(SH)_2$ [µM]		0.72	0.96	1.32	2.64	
	pseudosubstrate [µM]	Inhibition [%]				K_i [µM]
***Cf*TXN1**	400	33.8	27.4	25.0	16.2	524.9 ± 106.9
	800	54.3	45.7	47.1	35.0	
	1500	76.0	71.4	67.5	59.6	
***Cf*TXN2**	400	26.1	26.6	25.6	21.4	791.1 ± 192.0
	800	47.0	46.2	44.5	40.2	
	1500	71.4	72.0	68.1	65.1	
***Tb*TXN**	400	-	30.6	-	-	603.0 ± 97.0
	800	-	50.8	-	-	

Table 3.9: Inhibitory activity of the bis-(ophthamyl)-spermidine. The type of inhibition was characterized as competitive with the tryparedoxins of *Chrithidia fasciculata* (*Cf*TXN) the isoenzymes 1 and 2 and the tryparedoxin of *T. brucei* (*Tb*TXN). The weak inhibition is charaterized by the high K_i values.

[+++] Own contributions to this chapter: Determination of inhibition constants.

3.2.7 RNA interference constructs of *Tb*TXNPx and *Tb*TXN[#]

The discovery of double-stranded RNA interference (dsRNAi) in *Trypanosoma brucei* provided a convenient method to generate knockout phenotypes in this protozoan parasite (Ngo *et al.*, 1998). The presence of double-stranded RNA (dsRNA) in the cell dominantly silences gene expression in a sequence specific manner by causing the corresponding endogenous RNA to be degraded (Bosher and Labouesse, 2000). The technique of dsRNA interference was first described in the nematode *Caenorhabtidis elegans* (Fire *et al.*, 1998) and later observered in *Drosophila* (Kennerdell and Carthew, 1998; Misquitta and Paterson, 1999), hydra (Lohmann *et al.*, 1999), planaria (Sanchez Alvarado and Newmark, 1999), zebrafish (Wargelius *et al.*, 1999; Li *et al.*, 2000), mice (Wianny and Zernicka-Goetz, 2000), and trypanosomes

(Ngo *et al.*, 1998). As the double-stranded RNA interfere with the gene expression at the RNA level, it significantly reduces time and effort to generate knockout phenotypes.

A trypanosomal RNA interference plasmid, p2T7, was kindely provided from Dr. John E. Donelson (Dep. of Biochemistry, University of Iowa, IA, USA). The plasmid containes two tetracycline inducible T7 promoters in the opposite orientation. This promoter arrangement generates transcripts of both strands of DNA inserted between the promoters, which spontaneously form dsRNA in the cells. As a counterpart the plasmid needs a specialized host cell line called *T. brucei 13-90* in which the genes for the bacteriophage T7 RNA polymerase (T7RNP) and the bacterial tetracycline repressor protein (Tet^R) have been inserted into the genome via the plasmids pLew13 and pLew90 (Wirtz *et al.*, 1999). In this cell line the T7 RNA polymerase and the tetracycline repressor are expressed constitutively in a level that does not harm the cells and provide a thight regulation of the tetracycline operator. A third plasmid containing a sequence under the control of a tetracycline inducible T7 promoter can be transfected and modulated by the addition of tetracycline to the medium. The genes of *Tb*TXN and *Tb*TXNPx were cloned into the p2T7 vector by the *Hind*III/*BamH*I-*Bgl*II restriction sites and confirmed by PCR and DNA sequencing.

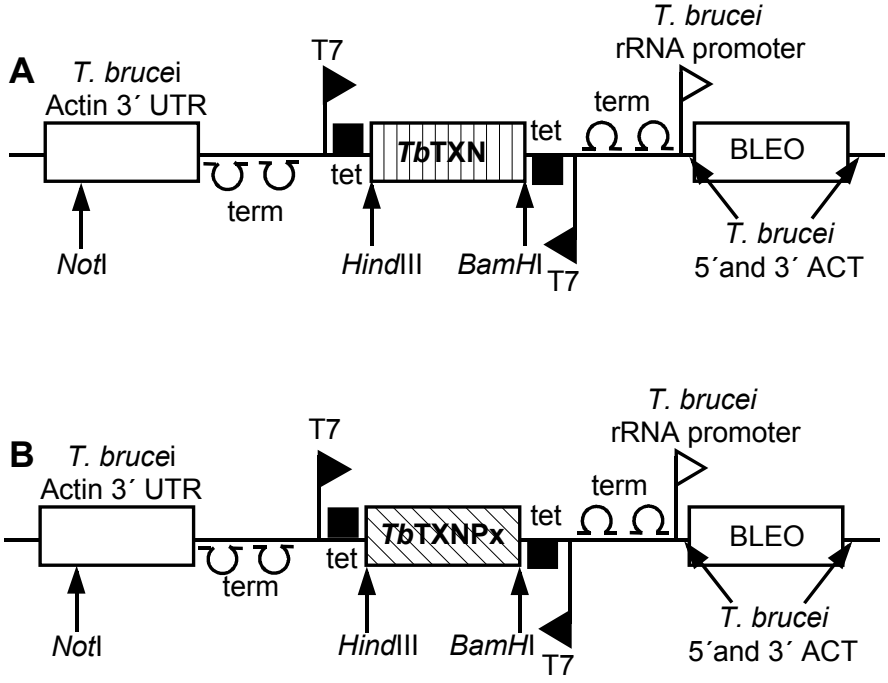

Figure 3.29: Schematic diagram of the plasmid p2T7 containing *Tb*TXN (A) or *Tb*TXNPx (B). Abbreviations are, T7, promoter for T7 polymerase; term, two adjacent termination

signals for the T7 RNA polymerase; tet, tetracycline operator; BLEO, phleomycin resistant gene; Actin 3´ UTR, Actin 3´ untranslated region.

As *Tb*TXN is a catalysator for the ribonucleotide reductase, a knockout of that gene would expect arrested cells that cannot proliferate anymore. The construct of p2T7 containing the whole gene sequence of *Tb*TXN were transfected to *T. brucei 13-90*. As a control of the ribonucleotide reductase function of *Tb*TXN, incorporation of ^{3}H-labled Thymidine to the DNA during proliferation was measured. Preliminary tests showed that the cell growth of the tetracycline induced cells is inhibited (not shown) and nearly no incorporation of ^{3}H-thymidine occured over 48 hours.

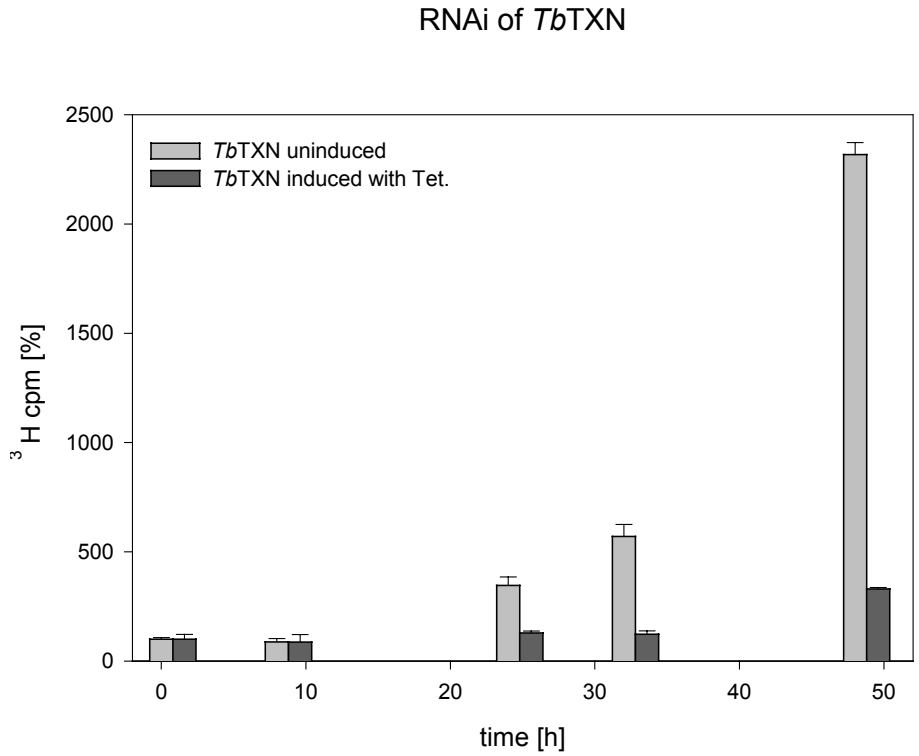

Figure 3.30: The incorporation of ^{3}H-marked thymidine to bloodstream trypanosomal strain *13-90*, transfected with p2T7 containing *Tb*TXN was calculated in percentage. The cells induced with 1 µg/ml tetracycline were compared with uninduced cells at 0, 8, 24, 32, and 48 hours after induction.

Western blot analysis confirmed that the observed phenotype is correlating to RNA interference of *Tb*TXN. Cell extracts correlating to 0, 8, 24, 32, and 48 hours after induction with 1 µg/ml tetracycline were separated on a 15 % SDS-PAGE and incubated with anti-*Cf*TXNPx and anti-*Cf*TXN1 rabbit serum. The protein bands of *Tb*TXNPx could be seen over 48 hours and abrogated after

72 hours. After 8 hours of induction no tryparedoxin of *T. brucei* could be detected by Western blot (see Figure 3.31).

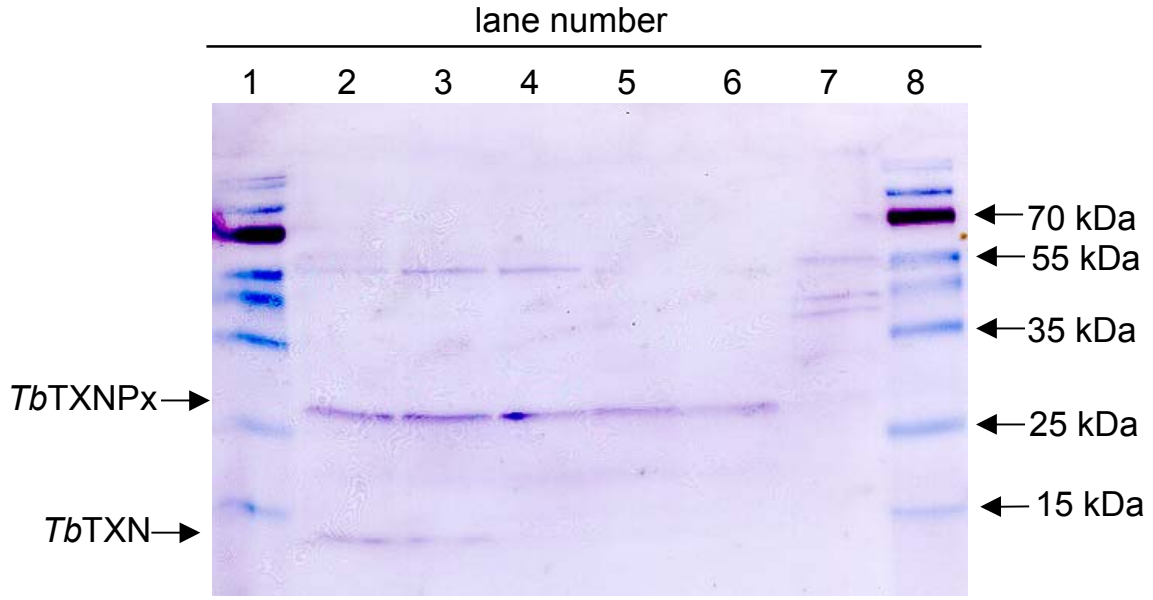

Figure 3.31: Western blot analysis of *T. brucei 13-90* transfected with p2T7 containing *Tb*TXN after induction with 1 µg/µl tetracycline. *Cf*TXNPx and *Cf*TXN1 antisera were used. lane 1 and 8: Prestained protein marker (MBI, Fermentas, St. Leon-Roth, Germany); lane 2: cell extract directly after induction with tetracycline; lane 3: 8 hours after induction; lane 4: 24 hours after induction; lane 5: 32 hours after induction; lane 6: 48 hours after induction; lane 7: 72 hours after induction.

These preliminary results have to be confirmed with further experiments and will be done by M. Comini.

[#] Own contributions to this chapter: Construction of vectors; preliminary experiments as described.

4 Discussion

4.1 Reconstitution of kinetoplast peroxidase systems

Reduction of hydroperoxides, as an essential part of the biological antioxidant defense is, by definition, catalyzed by peroxidases. In Kinetoplastida the low-efficiency peroxiredoxin-type peroxidases, tryparedoxin peroxidases, seem to be the major, if not the only, peroxide detoxifying enzymes, since they lack the more efficient mammalian peroxidases such as catalase and the selenium-containing glutathione peroxidases (Flohé *et al.*, 1999; Krauth-Siegel *et al.*, 2003). The first trypanosomatide peroxidase was purified from *Crithidia fasciculata* and shown to be active in a cascade composed of NADPH, trypanothione reductase, trypanothione, and tryparedoxin (Nogoceke *et al.*, 1997). In comparison to the classical glutathione peroxidases, the activities of tryparedoxin peroxidases are usually 2 – 3 orders of magnitude lower. This might be compensated by the extremely high cellular concentration, being 6 % of the total soluble protein of *C. fasciculata* (Nogoceke *et al.*, 1997). TXNPx is oxidized by hydroperoxides and reduced at the expense of tryparedoxin. TXNs are thioredoxin-related enzymes that are specifically reduced by trypanothione (Gommel *et al.*, 1997; Nogoceke *et al.*, 1997). They differ in their molecular weight of 16 kDa and in the active site motif CPPC from classical thioredoxins with CGPC, and glutaredoxins with CPYC. Trypanothione, a bis-(glutathionyl) derivative of spermidine (Fairlamb *et al.*, 1985), is synthesized from GSH, spermidine, and ATP (Henderson *et al.*, 1990; Koenig *et al.*, 1997; Oza *et al.*, 2002; Comini *et al.*, 2003) and regenerated of its oxidized cyclic disulfide by the flavoprotein, trypanothione reductase (Fairlamb and Cerami, 1992; Krauth-Siegel *et al.*, 2003). The NADPH supplying trypanothione reductase is homologous to glutathione reductase, lipoamide reductase, thioredoxin reductase and the bacterial AhpF (Williams, 1992; Flohé, 1998). Despite the use of phylogenetically related components, the hydroperoxide detoxification system of Kinetoplastida is the most complex cascade, comprising of three enzymes and one low molecular weight mediator.

The trypanothione-dependent peroxidase system that was reconstituted from heterologously expressed proteins, was here described in *T. brucei brucei*, the causative agent of Nagana disease. The results may be considered to be also representative for the homologous systems of *T. brucei rhodesiense* and *T.*

brucei gambiense, the causative agents of African Sleeping sickness in humans. The TXNPx sequence of *T. brucei brucei* elucidated here proved to be identical, for the primer independent amino acid residues, with that of *T. brucei rhodesiense* (el-Sayed *et al.*, 1995) and should be very similar to the second subspecies. A TXN has not yet been isolated from any of the African trypanosomatids pathogenic in humans, but the TXNs of different species are highly conserved and can substitute each other in TXNPx assays (Flohé *et al.*, 2002b). The trypanothione system may also play an important role in the virulence of the human pathogens, as it has been demonstrated for the TR synthesis in *T. brucei brucei* (Krieger *et al.*, 2000). Bloodstream cells were generated with only one TR gene under the control of a tetracycline inducible promoter. The TR synthesis could be shut down to 10 % of wild-type activity and the parasites became substantially more sensitive to H_2O_2 and resulted in an arrest of proliferation (Krieger *et al.*, 2000). Therefore *Tb*TXN and *Tb*TXNPx are valuable tools in the search for trypanocidal drugs.

A trypanothione-dependent hydroperoxide detoxification system was elucidated in *L. infantum* (by H. Castro and M. Santos, IBMC, Porto, Portugal), a human pathogen prevailing in the mediterranean countries. A cytosolic TXNPx gene was identified that is identical to a peroxiredoxin-type peroxidase of *L. chagasi* (Barr and Gedamu, 2001) and almost indistinguishable from those of other *Leishmania* species (Levick *et al.*, 1998; Flohé *et al.*, 2002a). Characterized by two active site VCP motifs, the peroxiredoxin-type peroxidase is homologous to the TXNPxs of other species of the order Kinetoplastida (Levick *et al.*, 1998; Tetaud *et al.*, 1998; Lopez *et al.*, 2000; Castro *et al.*, 2002b; Flohé *et al.*, 2002a). A gene coding for an active TXN with the characteristic WCPPCR motif was identified in *L. infantum*, and is yet the first tryparedoxin described in the species *Leishmania*. The cytosolic localization of the hydroperoxide detoxification system appears ideal to protect the parasites against oxidative attacks, as expected from the phagocytic attack of the host.

Since the trypanothione-dependent peroxidase system as detected in *C. fasciculata* (Nogoceke *et al.*, 1997) is cytosolic, the search for a complementing mitochondrial system, comprising the endogenously produced mitochondrial H_2O_2, appears rewarding. A second gene coding for a tryparedoxin peroxidase was isolated from *L. infantum* (Castro *et al.*, 2002a) that reminds of the mitochondrial peroxiredoxins of *T. cruzi* (Wilkinson *et al.*,

2000b) and *T. brucei* (Tetaud *et al.*, 2001). Immunohistochemistry showed that this protein was indeed localized in this organelle (Castro *et al.*, 2002b). The mitochondrial form of *Li*TXNPx (*Li*mTXNPx) differs from the typical cytosolic tryparedoxin peroxidases in possessing an N-terminal mitochondrial leader sequence and in the second active site motif, which is IPC instead of VCP. Despite these differences the *Li*mTXNPx (Castro *et al.*, 2002a) and the *Tb*mTXNPx (Tetaud *et al.*, 2001) were shown to be tryparedoxin peroxidases. Overexpression studies of the cytosolic form of *Li*TXNPx in *L. infantum* promastigots showed a marked resistance to exogenous H_2O_2. Overexpression of the mitochondrial TXNPx of *L. infantum* is less effective to the exogenous H_2O_2 that likely does not reach the mitochondrion (Castro *et al.*, 2002b). Therefore the two peroxidases seem to complement each other in the detoxification of host-derived exogenous hydroperoxides and endogenously produced mitochondrial H_2O_2. No mitochondrial tryparedoxin could yet be identified and the mechanism of how the tryparedoxin peroxidase is reduced in the mitochondrion remains elusive.

4.2 The growing complexity of kinetoplast peroxide metabolism

The ability to detoxify low hydrogen peroxide concentrations was first attributed to the spontaneous reduction by trypanothione (Penketh *et al.*, 1987; Carnieri *et al.*, 1993). Trypanothione is the main redox mediator in trypanosomatids that can be regenerated from its energetically preferred cyclic disulfide form (TS_2) to reduced $T(SH)_2$ by NADPH and trypanothione reductase. The expected “trypanothione peroxidase” could never be identified instead, the reaction turned out to be catalyzed by two distinct enzymes the tryparedoxin peroxidase and the tryparedoxin (Nogoceke *et al.*, 1997). This unique pathway of peroxide detoxification was first discovered in the insect pathogen *C. fasciculata* (Nogoceke *et al.*, 1997), but seems common to all pathogenic species of the order Kinetoplastida. TXNPx homologous enzymes have been characterized in *L. major* (Levick *et al.*, 1998), *T. cruzi* (Lopez *et al.*, 2000), *T. brucei* (Tetaud *et al.*, 2001), *L. infantum* (Castro *et al.*, 2002a), and *L. donovani* (Flohé *et al.*, 2002a). Tryparedoxins, so far, have been detected in *C. fasciculata* (Nogoceke *et al.*, 1997), *T. brucei* (Lüdemann *et al.*, 1998), *T. cruzi* (Lopez *et al.*, 2000; Wilkinson *et al.*, 2000b), and *L. infantum* (Castro *et al.* unpublished).

Over the past three years, the seemingly established trypanosomal hydroperoxide metabolism has been enriched by further complexities:

(i) A cytosolic localization of TXN and TXNPx of *C. fasciculata* has been reported (Steinert *et al.*, 1999) to compensate the exogenous oxidative attack of the host. The trypanothione reductase is also considered to be a primarily cytosolic protein (Smith *et al.*, 1991), although in *T. cruzi* also association with the mitochodrion and the kinetoplast was reported (Meziane-Cherif *et al.*, 1994). A complementary antioxidant defense system in the kinetoplastidal mitochondria comprising the endogenously produced H_2O_2 was expected. The discovery of mitochondrial isoenzymes of TXNPx in *T. cruzi* (Wilkinson *et al.*, 2000b), *T. brucei* (Tetaud *et al.*, 2001) and *L. infantum* (Castro *et al.*, 2002a) support the suggestion of an independent mitochondrial peroxide detoxification system in Kinetoplastida.

(ii) Two peroxiredoxins from *L. chagasi*, detoxifying hydrogen peroxide, hydroperoxides, and hydroxyl radicals, were isolated (Barr and Gedamu, 2001; Barr and Gedamu, 2003). Pxn1 from *L. chagasi* (*Lc*Pxn1) was even able to detoxify RNIs in addition to ROIs. Like the tryparedoxin peroxidases, the two peroxiredoxins seemed to be localized to the cytoplasm as it was confirmed by overexpression of the GFP/Pxn-fusion proteins in *L. chagasi* (Barr and Gedamu, 2001).

(iii) A second class of peroxidases, related to glutathione peroxidases, but containing cysteines instead of selenocysteines, were first studied in *T. cruzi* (Wilkinson *et al.*, 2000a). Two isoforms *Tc*GPxI, located to the cytoplasm and the glycosomes, and the *Tc*GPxII, restricted to the endoplasmic reticulum, could be characterized (Wilkinson *et al.*, 2002). With glutathione the peroxidases have marginal activity reducing linoleic acid hydroperoxide and phosphatidylcholine hydroperoxide but no hydrogen peroxide (Wilkinson *et al.*, 2000a). Recently *Tc*GPxI was shown to be reduced by a *T. cruzi* tryparedoxin resulting in an 8 – 15 fold increase of activity. Three different homologues of the GPxI gene were found in *T. brucei*, which are almost identical and differ only in their N- and C-terminal regions (Hillebrand *et al.*, 2003). Two peroxidases contain a C-terminal tripeptide ARI and occur in glycosomes and in the cytosol. The *T. brucei* GPxIII differs in possessing a C-terminal ARL motif. The activity of *Tb*GPxIII was studied with hydrogen peroxide, *t*-bOOH and cumene hydroperoxide, which are all substrates for the peroxidase. Regeneration of the reduced GPxIII by the trypanothione/tryparedoxin couple showed the highest reaction rates compared with that of glutathione (K_M values of about 30 mM) and thioredoxin (Hillebrand *et al.*, 2003).

(iv) A thioredoxin occurs in *T. brucei* (Reckenfelderbäumer *et al.*, 2000). It is reduced by human thioredoxin peroxidase. But no thioredoxin peroxidase in any organism of the order Kinetoplastida could be detected until now. Beside the lack of any functional thioredoxin reductase in the parasites, gene silencing, as it was performed by classical disruption of the gene sequence and by dsRNA interference showed that Trx is not essential (Schmidt *et al.*, 2002). The thioredoxin system has been shown to be of vital importance in mammals (Matsui *et al.*, 1996), as thioredoxins of mammals are involved in a variety of cellular processes: i. e. they deliver reducing equivalents for ribonucleotide reductase (RiboR) during DNA synthesis (Holmgren, 1985; Powis and Montfort, 2001). In trypanosomes this part seems to be undertaken by tryparedoxin and not by the conventional thioredoxin (Dormeyer *et al.*, 2001; Krauth-Siegel and Schmidt, 2002).

(v) A 3-mercaptopyruvate sulfurtransferase (MST) has been reported for *L. major* that is able to oxidize thioredoxin and to react with peroxides. Since 3-mercaptopyruvate is not a natural substrate, the physiological function of the sulfurtransferase remains uncertain (see Figure 4.1).

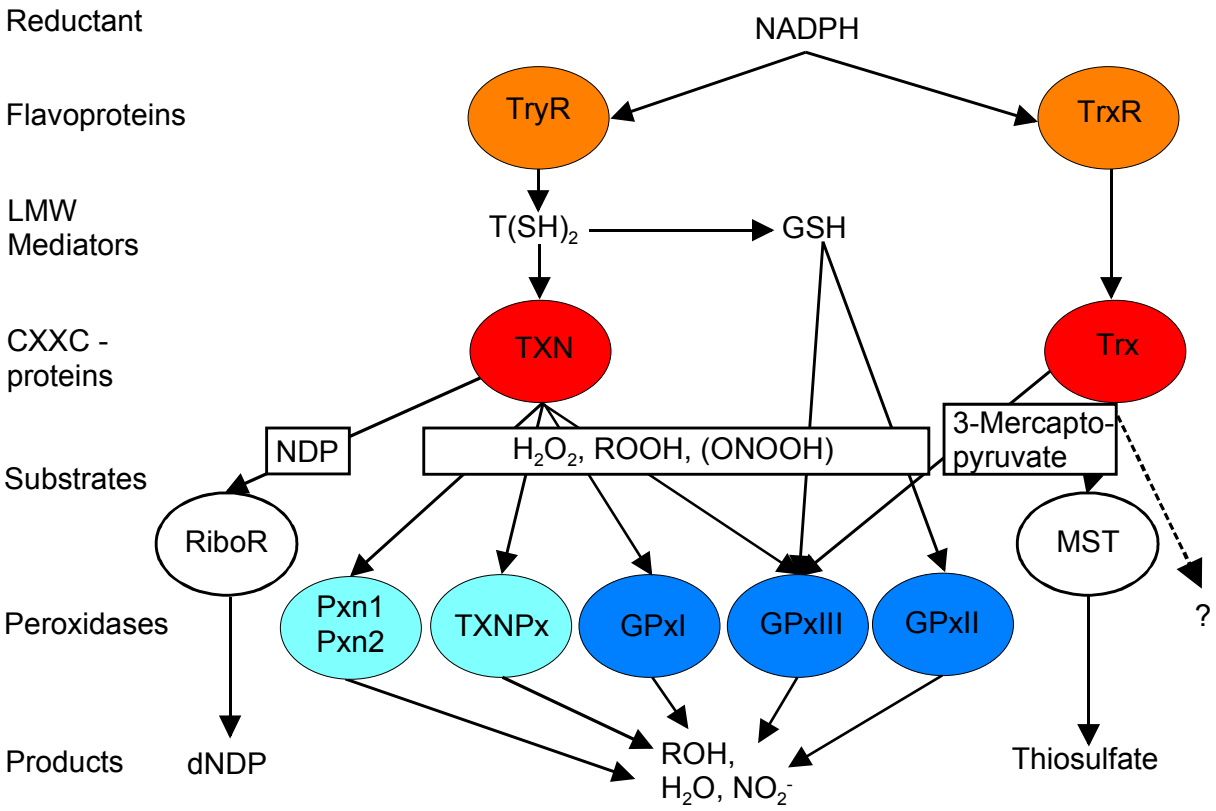

Figure 4.1: A broad spectrum of peroxidases are in charge of antioxidant defense in Kinetoplastida. Homologous proteins are shown in identically marked circles. TryR,

trypanothione reductase; TrxR, thioredoxin reductase; $T(SH)_2$, trypanothione; GSH, glutathione; TXN, tryparedoxin; Trx, thioredoxin; RiboR, ribonucleotide reductase; MST, 3-mercaptopyruvate sulfurtransferase; Pxn1 + Pxn2, peroxiredoxins; TXNPx, tryparedoxin peroxidase; GpxI – III, non-selenuim glutathione peroxidases.

Taken together the parasite seems to possess a variety of proteins that react with peroxides and further studies on their precise role have to be done. But since knockout studies on thioredoxin proved that this enzyme is not essential for the parasites (Schmidt *et al.*, 2002) and the glutathione-peroxidase related enzymes showed only very weak reaction rates with glutathione (Wilkinson *et al.*, 2000a; Wilkinson *et al.*, 2002; Hillebrand *et al.*, 2003) the detoxification of hydroperoxides has likely to be attributed to the trypanothione-dependent tryparedoxin pathway.

4.3 The catalytic cycle of TXNPx

4.3.1 The accepted view

Peroxiredoxins are proteins without any prosthetic group. The only redox-active residues are cysteines. The typical 2-Cys-peroxiredoxins are identified by the conservation of two redox-active cysteines as was demonstrated for tryparedoxin peroxidases. The oxidized proximal cysteine first reacts with the distal one. As it has become evident from structural data (Hirotsu *et al.*, 1999), the co-reacting distal cysteine stems from a second inverted subunit of the oligomeric enzyme (Equ. 1). The reaction center is build up between two subunits of the homooligomeric protein (Equ. 2). The intermolecular disulfide bridge is solved by the attack of a reducing dithiol, like tryparedoxin, and regeneration of the reduced ground state enzyme is achieved.

$$R_1\text{- Cys 52 -S}^- + H_2O_2 \overset{k'_1}{\leftrightarrows} \left[R_1\text{- Cys 52 -S}^- \bullet H_2O_2\right] \overset{k'_2}{\leftrightarrows} R_1\text{- Cys 52 - SOH} + OH^- \quad (1)$$

$$R_1\text{- Cys 52 - S} \overset{O}{\underset{\leftarrow}{\curvearrowright}} \overset{H}{\text{S-Cys 173'-}R_2} \xrightarrow{k_3} R_1\text{-Cys 52 - S - S - Cys 173'-}R_2 + OH^- \quad (2)$$

Equation 4.1: Oxidation of the conserved N-terminal cysteine residue (C52 in TXNPx) to a sulfenic acid derivative by hydrogen peroxide or an alkyl hydroperoxide (Equ. 1). This oxidative step is followed by the reaction of the sulfenic acid with the second conserved cysteine (C173) residue of a secondly inverted oriented subunit (C173´).

The catalytic cycle, as shown, is supported by experimental evidence. The predicted intermolecular disulfide bridge of the peroxidase, was clearly

detected in the structure of oxidized human thioredoxin peroxidase (TrxPx) (Hirotsu *et al.*, 1999). Covalently linked dimers of peroxiredoxins could also be detected by non-reducing SDS-PAGE (Chae *et al.*, 1994c; Ellis and Poole, 1997b). An exchange of the distal cysteine against a serine resulted in decreased specific activities when tested with the specific substrates, as shown for TrxPx of yeast (Chae *et al.*, 1993), for TXNPx of *Crithidia fasciculata* (Montemartini *et al.*, 1999), *Leishmania donovani* (Flohé *et al.*, 2002a) and *Trypanosoma brucei* (Budde *et al.*, 2003a), and for AhpC of *Salmonella typhimurium* (Ellis and Poole, 1997b). Interestingly, activity in the glutamine synthetase protection assay is retained in these mutants (Chae *et al.*, 1993; Flohé *et al.*, 2002a), because they are able to reduce H_2O_2 by the remaining solvent-exposed C52 using the thiol, DTT, as an unspecific reducing substrate (Netto and Stadtman, 1996).

4.3.2 The catalytic triad

Compared to the reaction rates of heme- or selenoprotein-catalyzed reduction (Flohé *et al.*, 1972; Günzler *et al.*, 1972; Flohé *et al.*, 1999; Krauth-Siegel *et al.*, 2003), the trypanosomatid system appears slow, but surprisingly fast in comparison with the glutathione peroxidase homologues whose active site selenocysteine has been replaced by a cysteine (Rocher *et al.*, 1992; Maiorino *et al.*, 1995). Those rate constants can only be achieved if the reacting thiol group is deprotonated by activation (Flohé *et al.*, 2002a; Flohé *et al.*, 2002b). Mutagenesis studies on *L. donovani*, based on the crystal structure of TXNPx of *C. fasciculata* (Alphey *et al.*, 2000), were performed to get a better insight of the catalytic mechanism (Flohé *et al.*, 2002a). Replacement of the C52 by serine abrogated the activity of *Ld*TXNPx completely and the mutein was also inactive in the glutamine synthetase protection assay (see chapter 3.2.2). These findings support the view that the C52 is the residue that is oxidized by the peroxide substrate. This conclusion is further confirmed by molecular models, as in the reduced state of *Ld*TXNPx the sulfur of C52 is the only solvent-exposed one. The residue Arg128 seems to be relevant for the activation of C52, as an exchange to an acidic residue in *Cf*TXNPx (Montemartini *et al.*, 1999) and *Ld*TXNPx (Flohé *et al.*, 2002a) led to a product with no measurable activity, without a hint of denaturation. A further candidate for interaction with C52 could be provided from the model of the reduced TXNPx. The T49 is in the ideal position for building a hydrogen bond to the sulfur. Therefore the threonine was replaced by a serine, as a control, and by

a valine, to get an inert variant. Surprisingly the *Ld*TXNPxT49S showed a higher activity than the wild-type, and the *Ld*TXNPxT49V variant showed the expected marginal activity (Flohé *et al.*, 2002a). This results provide a novel catalytic triad, in which the thiol function of a cysteine is fixed and polarized by hydrogen bonding with the hydroxyl group of a threonine and forced into dissociation by the positively charged guanidine group of an arginine. Due to the conservation of the activating residues the activation mechanism of C52 can be proposed for many other peroxiredoxins.

Molecular modeling and mutation studies proved that the C52 is the only solvent exposed sulfur in the reduced form of TXNPx and can be attacked by the peroxide. Inversely the C173´ becomes exposed to the surface upon oxidation and is the only one to be attacked by the high molecular weight reducing substrate, TXN. Marginal activity of the TXNPxC173S muteins, and abolished activity of the TXNPxC52S muteins of *C. fasciculata* (Montemartini *et al.*, 1999), *T. brucei* (Budde *et al.*, 2003a) and *L. donovani* (Flohé *et al.*, 2002a), support this suggestions. The insight into the activation mechanism improves the understanding how a plain protein can become a reasonably efficient peroxidase, but remain disappointing for the interpretation of hydroperoxide specificity and sensitivity as it could be observed for TXNPxs of *L. donovani* (Flohé *et al.*, 2002a), *L. infantum* (Castro *et al.*, 2002a), *L. major* (Levick *et al.*, 1998), and *T. brucei* (Budde *et al.*, 2003a). They accept naturally occuring lipid hydroperoxides with much lower rates and fast inactivation by these substrates can be observed, in contrast to the TXNPx of *C. fasciculata* (Nogoceke *et al.*, 1997), which accepts all oxidizing substrates with comparable rates. The solved crystal structures of peroxiredoxins (Hirotsu *et al.*, 1999; Alphey *et al.*, 2000; Schröder *et al.*, 2000; Wood *et al.*, 2002) and models thereof cannot explain the substrate specificities of TXNPxs, but the mechanism of inactivation is correlated to an overoxidation of the peroxidatic cysteine to sulfinic acid (-SO_2H) (Wood *et al.*, 2003a; Wood *et al.*, 2003b).

4.3.3 Contributions to TXN/TXNPx interactions

The peroxiredoxin of *T. brucei* proved to be a tryparedoxin peroxidase, as is underscored by its specificity for the homologous *Tb*TXN. Some activity could also be observed with thioredoxin as a reductant, but trypanothione or glutathione did not yield any measurable activity. As postulated by modeling, the thiol group of C40 in reduced *Tb*TXN is activated by a network of hydrogen bridges (Hofmann *et al.*, 2001). Thereby this solvent-exposed cysteine residue

is dissociated and can react with the C173´ of the oxidized TXNPx to form a covalent intermediate. In the next step a thiol disulfide exchange within the catalytic intermediate is generated. The essential reducing thiol is that of C43 of TXN which is shielded from the solvent but can attack C40 to form an intramolecular disulfide bridge (see Equation 4.2).

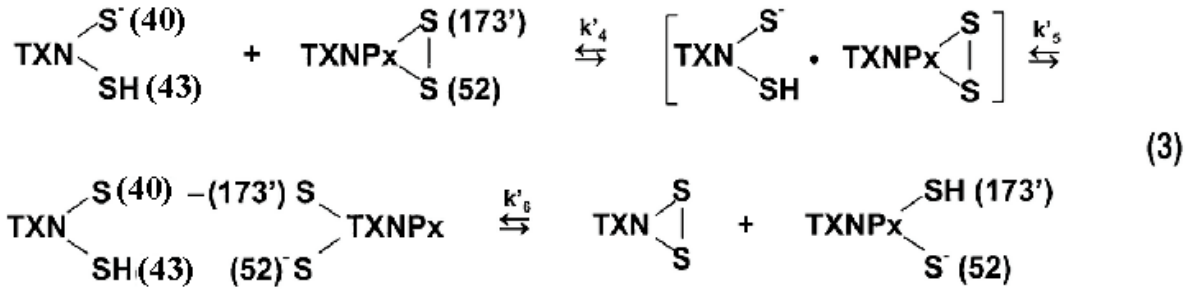

(3)

Equation 4.2: The sulfhydryl group of C40 in *Tb*TXN is shown to be dissociated to emphasize its presumed nucleophilic attack on the disulfide bridge of oxidized TXNPx. The intermediate state (TXN/TXNPx) is dissolved by building an internal disulfide bond between C40 and C43 of *Tb*TXN.

Exchange of the proximal cysteine C40 to serine abolished the activity completely, while a marginal activity could be detected if the same exchange has taken place at C43. The model of the catalytic intermediate between oxidized TXNPx and the reducing substrate TXN (see Equ. 3; see Figure 3.13) demonstrates sterically unhindered interaction. The reaction mechanism is supported by multiple electrostatic attractions between strictly conserved residues and, thus, common for all tryparedoxin peroxidases in Kinetoplastida (Levick *et al.*, 1998; Lopez *et al.*, 2000; Tetaud *et al.*, 2001; Castro *et al.*, 2002a; Flohé *et al.*, 2002a).

A model of the *Tb*TXNPx/*Tb*TXN interaction showed an acidic box on the surface of *Tb*TXN, comprising of E72, D76 and D79 residues, that could find its counterparts in the positive charges of R92, K93 and K94 of the peroxidase (see Figure 3.13). Additionally the R128 of *Tb*TXN is in the right position to form a salt bridge to E171 of *Tb*TXNPx. The validity of this assumption was checked by charge-inverting residues of *Tb*TXN. Reduced activity was observed with all muteins with the exception of *Tb*TXND79K. As the residues E72 and R128 have been shown to be also relevant to the TXN/trypanothione interaction in *C. fasciculata* (Hofmann *et al.*, 2001), mutations thereof would anyway impair the trypanothione-dependent hydroperoxide detoxification system.

NMR studies of the interaction of tryparedoxin with a redox-inactive homologue of trypanothione further confirmed the suggestions modeled, based on the crystal structures of *Cf*TXN (Hofmann *et al.*, 2001). The bis-(ophthamyl)-spermidine is a homologue of $T(SH)_2$ in which both cysteines are replaced by alanines. Activity assays showed weak inhibition by occupying $T(SH)_2$ binding sites. When the inhibitor is incubated with *Cf*TXN1 in the absence of $T(SH)_2$, characteristic shifts are seen in 2D-^{1}H,^{15}N-NMR spectra (NH resonance) pointing to residues involved in binding. Residues, implicated in $T(SH)_2$ binding as R128, Cys40, Ile109, Glu72 and Arg44, are evidently involved in inhibitor interaction (Krumme *et al.*, 2003). Replacing trypanothione by its redox-inactive homologue underscores the model of TXN/trypanothione interaction, as developed, based on crystallographic data.

The reaction mechanism of TXNPx with TXN was elucidated by molecular modeling, based on crystallographic studies (Alphey *et al.*, 2000; Hofmann *et al.*, 2001; Alphey *et al.*, 2003), supported by mutagenesis studies, as discussed above, but could never be supported by experimental data on the proposed catalytic intermediate between TXN and TXNPx, since it is processed too fast. Using a TXN mutein, in which the C43 was replaced by a serine, a dead-end intermediate could be achieved, as the second sulfur, for resolving the complex by building an intrasubunit disulfide bond in TXN, was missing. Cleavage of this material with trypsin and chymotrypsin followed by ESI-MS confirmed the presence of a peptide corresponding to the fragments of *Tb*TXN 36-44 linked to *Tb*TXNPx 169-177. ESI-MS/MS analysis of that peptide revealed that the fragment indeed correspond to the suggested disulfide bond between the C40 of TXN and the C173 of the peroxidase (Budde *et al.*, 2003b). According to the data, the reductive part of the catalytic cycle of *Tb*TXNPx indeed starts with an attack of the solvent-exposed C40 of *Tb*TXN on the distal conserved C173´ cysteine of the peroxidase. In conclusion, the hypothetical mechanism of TXN/TXNPx interaction was for the first time corroborated by direct physico-chemical analysis of a dead-end intermediate mimicking the postulated catalytic one. The understanding of the catalytic mechanism is demonstrating the TXN/TXNPx interaction, but cannot explain the specificity of tryparedoxin for tryparedoxin peroxidase. The specific affinity might be strengthened by the C-terminus of TXNPx, whose structure remains to be established. The tail is obviously swamping during catalysis and cannot be deduced from the structure of reduced *Cf*TXNPx (Alphey *et al.*, 2000) or the structure of another peroxiredoxin, HBP23 (Hirotsu *et al.*, 1999).

4.4 Kinetics and shapes

The kinetic analysis for *Tb*TXNPx, *Li*TXNPx and *Li*mTXNPx did not comply with a simple ping-pong mechanism, as is common for peroxidases, where the oxidation of the enzyme by the hydroperoxide substrate is followed by an independent reaction with the reductant (Dalziel, 1957; Ursini *et al.*, 1995; Flohé and Brigelius-Flohé, 2001; Hofmann *et al.*, 2002). Instead the kinetic pattern speaks in favor of a central complex mechanism, where both oxidant and reductant should be bound to the active site of the enzyme, before the reaction can proceed. This kinetic behavior appears incompatible with the reaction mechanism generally accepted for 2-Cys-Prx as reported for other peroxiredoxins (Nogoceke *et al.*, 1997; Hofmann *et al.*, 2002; Wood *et al.*, 2003b). The oxidation of these enzymes by the hydroperoxide is easily achieved without the aid of the cosubstrate and the reduction by the thiol cosubstrate does not depend on the presence of a hydroperoxide. Such reactions of independent enzymatic steps meets the definition of enzyme-substitution mechanism that should result in ping-pong kinetics, as it has been reported for peroxiredoxins (Nogoceke *et al.*, 1997; Montemartini *et al.*, 1999; Guerrero *et al.*, 2000a; Baker *et al.*, 2001; Wood *et al.*, 2003b). The kinetic pattern of *Tb*TXNPx and *Li*mTXNPx showed non-linear slopes in the double-reciprocal primary Dalziel plot, being clearly biphasic, as it could also be seen for the cytosolic *Li*TXNPx. They reflect lower than expected rates at high peroxide concentrations and low reductant levels. The coefficient $\Phi_{1,2}$, that is formally related to the formation of a ternary complex, deviates from zero.

As elucidated from X-ray analysis of peroxiredoxins (Alphey *et al.*, 2000; Harris *et al.*, 2001; Wood *et al.*, 2002), these enzymes build decameric structures consisting of five homodimers. The minimum functional unit is a dimer, utilizing a unique intermolecular redox-active disulfide center for the reduction of peroxides. Two oligomeric states are known for peroxiredoxins: The oxidized form of the human peroxiredoxin II crystallized as a dimer (Hirotsu *et al.*, 1999), the preferentially aggregation state of the reduced form is being unknown. This coincides with the oligomerization properties of AhpC from *Salmonella thyphimurium*. Analytical ultracentrifugation and dynamic light scattering showed that AhpC´s oligomeric state is redox-linked, with oxidation favoring the dimeric state and the decameric state favored upon reduction (Wood *et al.*, 2002). Similar dissociation of AhpC from *Mycobacterium tuberculosis* was observed by Jäger *et al.* (unpublished), with a higher activity in the decameric, reduced state. No “dimer to doughnut” transition could be

described for *Tb*TXNPx as the ring-shaped decamer (“doughnut”) is formed in the oxidized and reduced conformation of the enzyme. Instead of dissociation, a clear stabilization could be detected by oxidation, as high aggregated material could be detected by gel chromatography. In the reduced state the main part of *Tb*TXNPx elutes as decamers, which tend to destabilize, as pearl-like structures appeared, that are interpreted as smaller aggregates of dimers, (see Figure 3.17). Thus, the oligomerization of 2-Cys-peroxiredoxins seems to be redox-sensitive, but no general mechanism is presently discernible.

The deviations from linearity in the double-reciprocal plots and the changes of shape, dependent on the redox state of the peroxidase are incompatible with the simple rate equation for other peroxidases. The common rate equation of enzymatic reactions relies on the assumption of a simple interaction of substrates with the equivalent reaction centers and could lead to wrong mechanistic predictions for complex oligomeric enzymes such as the peroxiredoxins (Hofmann *et al.*, 2002; Wood *et al.*, 2003b). From the crystal structures of *Cf*TXNPx (Alphey *et al.*, 2000) and a mammalian thioredoxin peroxidase (Harris *et al.*, 2001) the 2-Cys-Prx were shown to build-up ring-like structures composed of five homodimers, each having two intersubunit reaction centers. These complex decameric structures appears to essentially influence the activity. Formally, the shape of curves, shown in Figure 3.6, complies with a negative cooperativity of the enzymatic reaction centers (Koshland, 1970). The cooperativity concept was originally described by Monod, Wyman and Changeux (Monod *et al.*, 1965). The content of the concept contains that the conformation of a particular subunit within an oligomeric protein may be changed due to binding of a ligand or a reaction that has taken place in another subunit. Such conformational changes may positively or negatively affect the affinities or reactivities. An enzyme, which shows cooperativity, needs four pre-requisites: (i) The protein has to be oligomeric; (ii) binding of, or reaction with, the substrate should be associated with conformational changes; (iii) the conformational change of the reaction center has to enforce a conformational change in the adjacent subunit; and (iv) the conformational change has to be functionally relevant. There are evidences that all these criteria are met by TXNPx:

1. The minimum theoretically catalytic entitles of TXNPxs are dimers, that built-up the active site by two inverted oriented subunits. Since the dimer of *Cf*TXNPx is devoid of activity and *Ld*TXNPx and *Li*mTXNPx lose activity

upon dilution, probably due to dissociation, a tendency of the dimers to form oligomers seems to have functional implications. The oligomer structures are formed by five dimers building a ring as evident from the X-ray structure of *Cf*TXNPx (Alphey *et al.*, 2000) and the electron micrographs of *Li*mTXNPx (Castro *et al.*, 2002a) and *Tb*TXNPx (Budde *et al.*, 2003a) and the proof of ten functional reaction centers (see Figure 3.16).

2. In reduced *Cf*TXNPx, the sulfurs of C52 and C173´, that have to react with each other, are up to 30 Å apart. The evidently necessary formation of a disulfide bond during catalysis is not possible without substantial rearrangement of the C-α backbone (see Figure 3.10) (Hofmann *et al.*, 2002). The tendency of oxidized decameric *Tb*TXNPx to depolymerize upon reduction with formation of lower MW open chain structures (see Figure 3.12) clearly shows that the redox-dependent conformational change is not restricted to the active site but also affects the dimer/dimer interface.

3. Conformational changes between subunits have, to our knowledge, never been directly demonstrated for any enzyme but, in the case of *Tb*TXNPx, it may be inferred from the kinetics that suggests cooperativity.

4. Molecular modeling of the reduced and oxidized state of TXNPx (Hofmann *et al.*, 2002) may be inferred with the functional relevance of conformational changes: In the reduced form the only solvent-exposed sulfur is that of the C52, while that of C173´ is shielded by an α-helix. In the oxidized form the sulfur of C173´ becomes accessible, whereas that of C52 is buried. The reactive thiol (C40) of the reducing substrate tryparedoxin reacts with the C173´ to form a covalent intermediate which became evident from ESI-MS analysis (see chapter 3.1.5.1).

To sum up, it can be said that the kinetic and morphological data suggest the concept of negative cooperativity to adequately explain the data. The negative cooperativity of *Tb*TXNPx seems strange as it implies that hydroperoxide detoxification is less efficient if the oxidant challenge is high. This particular feature may, however, explain the well documented sensitivity of trypanosomatids to hydroperoxide challenge (Flohé *et al.*, 1999). The effect of cooperativity is not only restricted to the *Tb*TXNPx, since cooperativtiy of a

glutathione-dependent peroxidase in *Haemophilus influenze* Rd (Pauwels *et al.*, 2003) is reported.

4.5 Clinical relevance

World-wide, 12 million people are infected by *Leishmania* species (WHO, 2003c), 18 million people by *T. cruzi* (WHO, 2003b) and the number of people affected by African trypanosomiasis are estimated to be between 300,000 to 500,000 (WHO, 2003a). The re-emergence of sleeping sickness presents a major public health problem, since it is one of the most important but equally most neglected tropical infection. The diagnosis of human African trypanosomiasis requires a high degree of training and expertise. Molecular or serological tools have not replaced the classical parasitological procedures until now. The treatment requires admission to hospital and is costly, potentially dangerous, and limited by the widespread appearance of drug resistance. The range of drugs used against sleeping sickness is limited to Suramine, Pentamidine, Melarsoprol, and Eflornithine. Medical teams in the field need better drugs and improved treatment schedules as they still face an unacceptably high treatment-related mortality as well as increasing resistance of the parasite. New drugs are therefore urgently needed (Stich *et al.*, 2002).

The antioxidant defense of trypanosomatids differ sufficiently from those of other eukaryotes. The pathogenic trypanosomatids do neither contain catalase or selenium-containing glutathione peroxidases (Fairlamb and Cerami, 1992). They are able to synthesize GSH, but transform most of it to a bis-(glutathionyl)-derivative of spermidine, called trypanothione, using two distinct enzymes, the glutathionyl-spermidine synthetase (GSS) and trypanothione synthetase (TS) (Henderson *et al.*, 1990; Koenig *et al.*, 1997; Oza *et al.*, 2002; Comini *et al.*, 2003). Unlike mammals, trypanosomatids are unable to reduce oxidized GSH at the expense of NADPH (Ouaissi *et al.*, 1995). Trypanothione was shown to be present in all trypanosomatids and is maintained in the reduced state by an NADPH-dependent disulfide reductase, trypanothione reductase, closely related in sequence and structure to the glutathione reductase but they both show exclusive specificity for their respective disulfide substrates (Sullivan and Walsh, 1991; Stoll *et al.*, 1997). Despite the use of phylogenetically related components, the trypanosomatid system is remarkable in being the most complex hydroperoxide detoxification system discovered so far. In contrast to the GSH-mediated system it requires three (trypanothione reductase, tryparedoxin, and tryparedoxin peroxidase)

enzymes to channel the reduction equivalents from NADPH to hydroperoxide. The thioredoxin-dependent system also requires three enzymes (thioredoxin reductase, thioredoxin, and thioredoxin peroxidase), but does not involve a low molecular weight mediator (Nogoceke *et al.*, 1997). The specificity of the hydroperoxide detoxification in trypanosomatids have made this aspect of their metabolism an attractive target for the development of new antitrypanosomal drugs.

The biological significance of that detoxification system has been corroborated by inverse genetics. In *L. donovani*, a downregulation of TR to about 15 % of the wild-type cells, was achieved by overexpression of a trans-dominant mutant homologue. The parasites were able to survive in resting, but not in cytokine-activated macrophages (Tovar *et al.*, 1998). Bloodstream cells of *T. brucei* were generated with only one functional TR gene under control of a tetracycline-dependent promoter. Trypanosomes with less than 10 % of wild-type activity showed arrest of proliferation, loss of virulence and increased H_2O_2 sensitivity (Krieger *et al.*, 2000). Knock-out approaches by RNAi of *Tb*TXNPx and *Tb*TXN showed that both enzymes are essential for the proliferation of the parasites. Trypanosomes, showing the knock-out phenotype of *Tb*TXNPx, had an increased sensitivity to H_2O_2 (Wilkinson *et al.*, 2003). TR, tryparedoxin and tryparedoxin peroxidase may thus be considered as validated molecular targets for the development of trypanocidal drugs, but it remains to be demonstrated if the enzymes involved in trypanothione synthesis, may be of equal vital importance to the parasite. Therefore RNA interference tests are planned.

The usefulness of molecular targets depends on a variety of parameters such as (i) status of validation (ii) dissimilarity of the parasitic targets from homologous host proteins (iii) accessibility (iv) ease and robustness of test (v) mechanistic and (vi) structural knowledge. While the primary goal of this work was to make available the *T. brucei* hydroperoxides detoxification system for test purposes, contributions to the other aspects of target validation/ characterization were also achieved: (i) a better understanding of the system´s kinetic peculiarities that is indispensable for the development of a reliable test routine; (ii) confirmation of basic catalytic mechanism and (iii) details of substrate/enzyme interactions that together with the knowledge of crystal structures from trypanothione reductase (Krauth-Siegel *et al.*, 1987; Hunter *et al.*, 1990; Kuriyan *et al.*, 1991), tryparedoxin (Hofmann *et al.*, 2001; Alphey *et*

al., 2003) and tryparedoxin peroxidase (Alphey *et al.*, 2000) developed, should facilitate the design of specific inhibitors that might provide novel trypanocidal drugs.

5 Summary

Two genera of protozoa belonging to the order Kinetoplastida, *Trypanosoma* and *Leishmania*, are pathogenic for mammals and cause widespread diseases of man and his livestock in developing countries. Their successful survival depends mainly on evading the hosts´ immune system by penetrating and multiplying within the cells. As intracellular pathogens they need a strategy to evade the immune response of the host, like the production of reactive oxygen intermediates (ROI). These protozoa have evolved a hydroperoxide detoxification system, comprising of trypanothione reductase, trypanothione, tryparedoxin and tryparedoxin peroxidase, which differ markedly from that of the mammalian host, since they lack catalase and selenium-containing glutathione peroxidases. During this work the trypanothione-dependent hydroperoxide system of *T. brucei brucei* was characterized and a better understanding of the enzyme/substrate interactions was achieved.

1. The trypanothione-dependent hydroperoxide detoxification system was reconstituted from heterologously expressed proteins in *T. brucei brucei*. *Tb*TXNPx efficiently reduces H_2O_2 and organic hydroperoxides including phosphatidylcholin hydroperoxide and is specifically reduced by *Tb*TXN, less efficiently by thioredoxin, but not by GSH or $T(SH)_2$.

2. The kinetic pattern in a steady-state-kinetic analysis of *Tb*TXNPx is expected as it is common for other peroxidases (Nogoceke *et al.*, 1997; Montemartini *et al.*, 1998a; Guerrero *et al.*, 2000a; Flohé *et al.*, 2002a). The kinetic behavior of *Tb*TXNPx deviates, as the slopes in the double-reciprocal primary Dalziel plot are not linear and clearly biphasic. This rather suggests cooperativity of the reaction centers, as is not uncommon for oligomeric proteins (Koshland, 1970; Pauwels *et al.*, 2003).

3. A kinetic characterization of *Li*TXNPx and *Li*TXN1 could be obtained that reflect a classical ping-pong pattern. The *Li*TXN1 is the first active tryparedoxin so far identified in a *Leishmania* species and, thus, corroborating the trypanothione-dependent hydroperoxide detoxification pathway in this species.

4. Different oligomeric states, depending on the redox status, are known for peroxiredoxins (Hirotsu *et al.*, 1999; Wood *et al.*, 2002). A stabilization of

the decameric form during oxidation of *Tb*TXNPx and a tendency to destabilize in the reduced form (pearl-like structures) could be detected by electron microscopy.

5. The reaction mechanism of the reductive part of the *Tb*TXNPx could be verified. A tryptic cleavage of an intermediate, consisting of *Tb*TXNC43S and *Tb*TXNPx, followed by ESI-MS/MS analysis, corroborated the hypothetical mechanism. The solvent exposed C40 of tryparedoxin attacks the C173´ of the peroxidase to be reduced.

6. A model of the decameric TXNPx structure showed that all ten possible reaction centers might be active. Reductively cleavage of the dead-end intermediate (*Tb*TXNPx/*Tb*TXNC43S) could confirm the predicted stoichiometry. Ten tryparedoxin molecules bind to the decameric tryparedoxin peroxidase.

7. *Ld*TXNPx (Flohé *et al.*, 2002a) consumed a broad range of hydroperoxides, but was inactivated by lipid hydroperoxides as could be observed for *Tb*TXNPx (Budde *et al.*, 2003a) and *Li*mTXNPx (Castro *et al.*, 2002a). Mutagenesis studies on *Ld*TXNPx confirmed the assumed reaction mechanism of TXNPx with hydroperoxides, but could not efficiently explain the substrate specificity.

8. A model for TXN/trypanothione interaction was created, based on the known X-ray structure of *Cf*TXN (Hofmann *et al.*, 2001), and confirmed by mutagenic studies. Based on that data a trypanothione homologue inhibitor was synthesized and showed to behave as a weak comparative inhibitor.

In this study more information about the size and shape of the native TXNPx, the reaction mechanism of the reduced TXNPx with oxidized TXN, the shape of the catalytic intermediate TXN/TXNPx, and the interaction of TXN with trypanothione were given. As the hydroperoxide detoxification mechanism in trypanosomatids proved to be significant for the parasites (Tovar *et al.*, 1998; Krieger *et al.*, 2000; Wilkinson *et al.*, 2003), all components of the systems appear as attractive targets to evolve new drugs, as urgently needed.

6 Literature

Alphey, M. S., Leonard, G. A., Gourley, D. G., Tetaud, E., Fairlamb, A. H., and Hunter, W. N. (1999a). The high resolution crystal structure of recombinant *Crithidia fasciculata* tryparedoxin-I. J. Biol. Chem. *274*, 25613-25622.

Alphey, M. S., Tetaud, E., Gourley, D. G., Fairlamb, A. H., and Hunter, W. N. (1999b). Crystallization of recombinant *Crithidia fasciculata* tryparedoxin. J. Struct. Biol. *126*, 76-79.

Alphey, M. S., Bond, C. S., Tetaud, E., Fairlamb, A. H., and Hunter, W. N. (2000). The structure of reduced tryparedoxin peroxidase reveals a decamer and insight into reactivity of 2Cys-peroxiredoxins. J. Mol. Biol. *300*, 903-916.

Alphey, M. S., Gabrielsen, M., Micossi, E., Leonard, G. A., McSweeney, S. M., Ravelli, R. B., Tetaud, E., Fairlamb, A. H., Bond, C. S., and Hunter, W. N. (2003). Tryparedoxins from *Crithidia fasciculata* and *Trypanosoma brucei*: photoreduction of the redox disulfide using synchrotron radiation and evidence for a conformational switch implicated in function. J. Biol. Chem. *21*, in press.

Aumann, K. D., Bedorf, N., Brigelius-Flohé, R., Schomburg, D., and Flohé, L. (1997). Glutathione peroxidase revisited-simulation of the catalytic cycle by computer-assisted molecular modeling. Biomed. Environ. Sci. *10*, 136-155.

Babior, B. M. (2000). Phagocytes and oxidative stress. Am. J. Med. *109*, 33-44.

Baker, L. M., Raudonikiene, A., Hoffman, P. S., and Poole, L. B. (2001). Essential thioredoxin-dependent peroxiredoxin system from *Helicobacter pylori*: genetic and kinetic characterization. J. Bacteriol. *183*, 1961-1973.

Barr, S. D., and Gedamu, L. (2001). Cloning and characterization of three differentially expressed peroxidoxin genes from *Leishmania chagasi*. Evidence for an enzymatic detoxification of hydroxyl radicals. J. Biol. Chem. *276*, 34279-34287.

Barr, S. D., and Gedamu, L. (2003). Role of peroxidoxins in *Leishmania chagasi* survival. Evidence of an enzymatic defense against nitrosative stress. J. Biol. Chem. *278*, 10816-10823.

Beckman, J. S., and Koppenol, W. H. (1996). Nitric oxide, superoxide and peroxynitrite: the good, the bad and the ugly. Am. J. Physiol. *271*, C1424-C1437.

Bosher, J. M., and Labouesse, M. (2000). RNA interference: genetic wand and genetic watchdog. Nat. Cell Biol. *2*, E31-E36.

Boveris, A., and Stoppani, A. O. (1977). Hydrogen peroxide generation in *Trypanosoma cruzi*. Experientia. *33*, 1306-1308.

Bradford, M. M. (1976). A rapid and sensitive method for the quantitation of microgram quantities of protein utilizing the principle of protein-dye binding. Anal. Biochem. *72*, 248-254.

Brigelius-Flohé, R., Maiorino, M., Ursini, F., and Flohé, L. (2002). Selenium: An Antioxidant? In Handbook of Antioxidants, E. Cadenas, and L. Packer, eds. (Basel, New York, Marcel Dekker), pp. 633-664.

Bryk, R., Griffin, P., and Nathan, C. (2000). Peroxynitrite reductase activity of bacterial peroxiredoxins. Nature. *407*, 211-215.

Budde, H., and Flohé, L. (2002). Enzymes of the thiol-dependent hydroperoxide metabolism in pathogens as potential drug targets. In Thiol metabolism and redox regulation of cellular functions, A. Pompella, G. Bánhegyi, and M. Wellman-Rousseau, eds. (Berlin, NATO Science Series), pp. 85-95.

Budde, H., Flohé, L., Hecht, H.-J., Hofmann, B., Stehr, M., Wissing, J., and Lünsdorf, H. (2003a). Kinetics and redox-sensitive oligomerization reveal negative subunit cooperativity in tryparedoxin peroxidase of *Trypanosoma brucei brucei*. Biol. Chem. *384*, 619-633.

Budde, H., Flohé, L., Hofmann, B., and Nimtz, M. (2003b). Verification of the interaction of a tryparedoxin peroxidase with tryparedoxin by ESI-MS/MS. Biol. Chem. *384*, 1305-1309.

Carnieri, E. G., Moreno, S. N., and Docampo, R. (1993). Trypanothione-dependent peroxide metabolism in *Trypanosoma cruzi* different stages. Mol. Biochem. Parasitol. *61*, 79-86.

Castro, H., Budde, H., Flohé, L., Hofmann, B., Lünsdorf, H., Wissing, J., and Tomás, A. M. (2002a). Specificity and kinetics of a mitochondrial peroxiredoxin of *Leishmania infantum*. Free Radic. Biol. Med. *33*, 1563-1574.

Castro, H., Sousa, C., Santos, M., Cordeiro-da-Silva, A., Flohé, L., and Tomás, A. M. (2002b). Complementary antioxidant defense by cytoplasmic and mitochondrial peroxiredoxins in *Leishmania infantum*. Free Radic. Biol. Med. *33*, 1552-1562.

CDC, (2003). http://www.cdc.gov/.

C. D. Foundation, (2003). http://www.cdfound.to.it/HTML/don2.htm.

Chae, H. Z., Kim, I. H., Kim, K., and Rhee, S. G. (1993). Cloning, sequencing, and mutation of thiol-specific antioxidant gene of *Saccharomyces cerevisiae*. J. Biol. Chem. *268*, 16815-16821.

Chae, H. Z., Chung, S. J., and Rhee, S. G. (1994a). Thioredoxin-dependent peroxide reductase from yeast. J. Biol. Chem. *269*, 27670-27678.

Chae, H. Z., Robison, K., Poole, L. B., Church, G., Storz, G., and Rhee, S. G. (1994b). Cloning and sequencing of thiol-specific antioxidant from mammalian brain: alkyl hydroperoxide reductase and thiol-specific antioxidant define a large family of antioxidant enzymes. Proc. Natl. Acad. Sci. U S A. *91*, 7017-7021.

Chae, H. Z., Uhm, T. B., and Rhee, S. G. (1994c). Dimerization of thiol-specific antioxidant and the essential role of cysteine 47. Proc. Natl. Acad. Sci. U S A. *91*, 7022-7026.

Chae, H. Z., Kang, S. W., and Rhee, S. G. (1999). Isoforms of mammalian peroxiredoxin that reduce peroxides in presence of thioredoxin. Methods Enzymol. *300*, 219-226.

Chauhan, R., and Mande, S. C. (2001). Characterization of the *Mycobacterium tuberculosis* H37Rv alkyl hydroperoxidase AhpC points to the importance of ionic interactions in oligomerization and activity. Biochem. J. *354*, 209-215.

Choi, H. J., Kang, S. W., Yang, C. H., Rhee, S. G., and Ryu, S. E. (1998). Crystal structure of a novel human peroxidase enzyme at 2.0 Å resolution. Nat. Struct. Biol. *5*, 400-406.

Chung, C. T., Niemela, S. L., and Miller, R. H. (1989). One-step preparation of competent *Escherichia coli*: transformation and storage of bacterial cells in the same solution. Proc. Natl. Acad. Sci. U S A. *86*, 2172-2175.

Comini, M., Menge, U., and Flohé, L. (2003). Biosynthesis of trypanothione in *Trypanosoma brucei brucei*. Biol. Chem. *384*, 653-656.

Dalziel, K. (1957). Initial steady state velocities in the evaluation of enzyme-coenzyme-substrate reaction mechanisms. Acta Chem. Scand. *11*, 1706-1723.

Denicola-Seoane, A., Rubbo, H., Prodanov, E., and Turrens, J. F. (1992). Succinate-dependent metabolism in *Trypanosoma cruzi* epimastigotes. Mol. Biochem. Parasitol. *54*, 43-50.

Deretic, V., Song, J., and Pagan-Ramos, E. (1997). Loss of oxyR in *Mycobacterium tuberculosis*. Trends Microbiol. *5*, 367-372.

Dormeyer, M., Reckenfelderbäumer, N., Lüdemann, H., and Krauth-Siegel, R. L. (2001). Trypanothione-dependent synthesis of deoxyribonucleotides by *Trypanosoma brucei* ribonucleotide reductase. J. Biol. Chem. *276*, 10602-10606.

Doublie, S., Tabor, S., Long, A. M., Richardson, C. C., and Ellenberger, T. (1998). Crystal structure of a bacteriophage T7 DNA replication complex at 2.2 Å resolution. Nature. *391*, 251-258.

Dumas, C., Ouellette, M., Tovar, J., Cunningham, M. L., Fairlamb, A. H., Tamar, S., Olivier, M., and Papadopoulou, B. (1997). Disruption of the trypanothione reductase gene of *Leishmania* decreases its ability to survive oxidative stress in macrophages. Embo J. *16*, 2590-2598.

Duszenko, M., Muhlstadt, K., and Broder, A. (1992). Cysteine is an essential growth factor for *Trypanosoma brucei* bloodstream forms. Mol. Biochem. Parasitol. *50*, 269-273.

Ellis, H. R., and Poole, L. B. (1997a). Novel application of 7-chloro-4-nitrobenzo-2-oxa-1,3-diazole to identify cysteine sulfenic acid in the AhpC component of alkyl hydroperoxide reductase. Biochemistry. *36*, 15013-15018.

Ellis, H. R., and Poole, L. B. (1997b). Roles for the two cysteine residues of AhpC in catalysis of peroxide reduction by alkyl hydroperoxide reductase from *Salmonella typhimurium*. Biochemistry. *36*, 13349-13356.

el-Sayed, N. M., Alarcon, C. M., Beck, J. C., Sheffield, V. C., and Donelson, J. E. (1995). cDNA expressed sequence tags of *Trypanosoma brucei rhodesiense* provide new insights into the biology of the parasite. Mol. Biochem. Parasitol. *73*, 75-90.

Epp, O., Ladenstein, R., and Wendel, A. (1983). The refined structure of the selenoenzyme glutathione peroxidase at 0.2- nm resolution. Eur. J. Biochem. *133*, 51-69.

Fairlamb, A. H., Blackburn, P., Ulrich, P., Chait, B. T., and Cerami, A. (1985). Trypanothione: a novel bis(glutathionyl)spermidine cofactor for glutathione reductase in trypanosomatids. Science. *227*, 1485-1487.

Fairlamb, A. H., and Cerami, A. (1985). Identification of a novel, thiol-containing co-factor essential for glutathione reductase enzyme activity in trypanosomatids. Mol. Biochem. Parasitol. *14*, 187-198.

Fairlamb, A. H., and Cerami, A. (1992). Metabolism and functions of trypanothione in the Kinetoplastida. Annu. Rev. Microbiol. *46*, 695-729.

Fire, A., Xu, S., Montgomery, M. K., Kostas, S. A., Driver, S. E., and Mello, C. C. (1998). Potent and specific genetic interference by double-stranded RNA in *Caenorhabditis elegans*. Nature. *391*, 806-811.

Flohé, L., Loschen, G., Günzler, W. A., and Eichele, E. (1972). Glutathione peroxidase, V. The kinetic mechanism. Hoppe Seylers Z. Physiol. Chem. *353*, 987-999.

Flohé, L. (1989). The selenoprotein glutathione peroxidase. In Glutathione: Chemical, biochemical and medical aspects-part A, D. Dolphin, R. Poulson, and O. Avramovic, eds. (New York, John Wiley & Sons, Inc), pp. 644-731.

Flohé, L. (1998). The Achilles' heel of trypanosomatids: trypanothione-mediated hydroperoxide metabolism. Biofactors. *8*, 87-91.

Flohé, L., Hecht, H.-J., and Steinert, P. (1999). Glutathione and trypanothione in parasitic hydroperoxide metabolism. Free Rad. Biol. Med. *27*, 966-984.

Flohé, L., and Brigelius-Flohé, R. (2001). Selenoproteins of the glutathione system. In Selenium. Its molecular biology and role in human health, D. L. Hatfield, ed. (Boston/Dordrecht/London, Kluwer Academic Publishers), pp. 157-178.

Flohé, L., Budde, H., Bruns, K., Castro, H., Clos, J., Hofmann, B., Kansal-Kalavar, S., Krumme, D., Menge, U., Plank-Schumacher, K., Sztajer, H., Wissing, J., Wylegalla, C., and Hecht, H.-J. (2002a). Tryparedoxin peroxidase of *Leishmania donovani*: molecular cloning, heterologous expression, specificity, and catalytic mechanism. Arch. Biochem. Biophys. *397*, 324-335.

Flohé, L., Steinert, P., Hecht, H.-J., and Hofmann, B. (2002b). Tryparedoxin and tryparedoxin peroxidase. In Methods in Enzymology, H. Sies, ed. (London, New York, Academic Press), pp. 244-258.

Fujii, J., and Ikeda, Y. (2002). Advances in our understanding of peroxiredoxin, a multifunctional, mammalian redox protein. Redox. Rep. *7*, 123-130.

Gabb, H. A., Jackson, R. M., and Sternberg, M. J. (1997). Modelling protein docking using shape complementarity, electrostatics and biochemical information. J. Mol. Biol. *272*, 106-120.

Gommel, D. U., Nogoceke, E., Morr, M., Kiess, M., Kalisz, H. M., and Flohé, L. (1997). Catalytic characteristics of tryparedoxin. Eur. J. Biochem. *248*, 913-918.

Guerrero, S. A., Flohé, L., Kalisz, H. M., Montemartini, M., Nogoceke, E., Hecht, H.-J., Steinert, P., and Singh, M. (1999). Sequence, heterologous expression and functional characterization of tryparedoxin1 from *Crithidia fasciculata*. Eur. J. Biochem. *259*, 789-794.

Guerrero, S. A., Lopez, J. A., Steinert, P., Montemartini, M., Kalisz, H. M., Colli, W., Singh, M., Alves, M. J., and Flohé, L. (2000a). His-tagged tryparedoxin peroxidase of *Trypanosoma cruzi* as a tool for drug screening. Appl. Microbiol. Biotechnol. *53*, 410-414.

Guerrero, S. A., Montemartini, M., Spallek, R., Hecht, H.-J., Steinert, P., Flohé, L., and Singh, M. (2000b). Cloning and expression of tryparedoxin I from *Crithidia fasciculata*. Biofactors. *11*, 67-69.

Guhl, F., Jaramillo, C., Vallejo, G. A., Yockteng, R., Cardenas-Arroyo, F., Fornaciari, G., Arriaza, B., and Aufderheide, A. C. (1999). Isolation of *Trypanosoma cruzi* DNA in 4,000-year-old mummified human tissue from northern Chile. Am. J. Phys. Anthropol. *108*, 401-407.

Günzler, W. A., Vergin, H., Müller, I., and Flohé, L. (1972). Glutathione peroxidase VI: the reaction of glutathione peroxidase with various hydroperoxides. Hoppe Seylers Z. Physiol. Chem. *353*, 1001-1004.

Hanahan, D. (1983). Studies on transformation of *Escherichia coli* with plasmids. J. Mol. Biol. *166*, 557-580.

Harris, J. R., Schröder, E., Isupov, M. N., Scheffler, D., Kristensen, P., Littlechild, J. A., Vagin, A. A., and Meissner, U. (2001). Comparison of the decameric structure of peroxiredoxin-II by transmission electron microscopy and X-ray crystallography. Biochim. Biophys. Acta. *1547*, 221-234.

Henderson, G. B., Yamaguchi, M., Novoa, L., Fairlamb, A. H., and Cerami, A. (1990). Biosynthesis of the trypanosomatid metabolite trypanothione: purification and characterization of trypanothione synthetase from *Crithidia fasciculata*. Biochemistry. *29*, 3924-3929.

Hillebrand, H., Schmidt, A., and Krauth-Siegel, R. L. (2003). A second class of peroxidases linked to the trypanothione metabolism. J. Biol. Chem. *278*, 6809-6815.

Hirotsu, S., Abe, Y., Okada, K., Nagahara, N., Hori, H., Nishino, T., and Hakoshima, T. (1999). Crystal structure of a multifunctional 2-Cys peroxiredoxin heme-binding protein 23 kDa/proliferation-associated gene product. Proc. Natl. Acad. Sci. U S A. *96*, 12333-12338.

Hofmann, B., Budde, H., Bruns, K., Guerrero, S. A., Kalisz, H. M., Menge, U., Montemartini, M., Nogoceke, E., Steinert, P., Wissing, J. B., Flohé, L., and Hecht, H.-J. (2001). Structures of tryparedoxins revealing interaction with trypanothione. Biol. Chem. *382*, 459-471.

Hofmann, B., Hecht, H.-J., and Flohé, L. (2002). Peroxiredoxins. Biol. Chem. *383*, 347-364.

Holmgren, A. (1985). Thioredoxin. Annu. Rev. Biochem. *54*, 237-271.

Hunter, W. N., Smith, K., Derewenda, Z., Harrop, S. J., Habash, J., Islam, M. S., Helliwell, J. R., and Fairlamb, A. H. (1990). Initiating a crystallographic study of trypanothione reductase. J. Mol. Biol. *216*, 235-237.

Jones, T. A., Zou, J. Y., Cowan, S. W., and Kjeldgaard (1991). Improved methods for binding protein models in electron density maps and the location of errors in these models. Acta Crystallogr. A. *47*, 110-119.

Karplus, P. A., and Schulz, G. E. (1989). Substrate binding and catalysis by glutathione reductase as derived from refined enzyme: substrate crystal structures at 2 Å resolution. J. Mol. Biol. *210*, 163-180.

Kato, H., Asanoi, M., Nakazawa, T., and Maruyama, K. (1985). Cylinder protein isolated from rat liver mitochondria. Zool. Sci. *2*, 485-490.

Kennerdell, J. R., and Carthew, R. W. (1998). Use of dsRNA-mediated genetic interference to demonstrate that frizzled and frizzled 2 act in the wingless pathway. Cell. *95*, 1017-1026.

Kim, K., Kim, I. H., Lee, K. Y., Rhee, S. G., and Stadtman, E. R. (1988). The isolation and purification of a specific "protector" protein which inhibits enzyme inactivation by a thiol/Fe(III)/O2 mixed-function oxidation system. J. Biol. Chem. *263*, 4704-4711.

Koenig, K., Menge, U., Kiess, M., Wray, V., and Flohé, L. (1997). Convenient isolation and kinetic mechanism of glutathionylspermidine synthetase from *Crithidia fasciculata*. J. Biol. Chem. *272*, 11908-11915.

Koshland, D. E., Jr. (1970). The molecular basis for enzyme regulation. In The enzymes, structures and control, P. D. Boyer, ed. (New York, London, Academic press), pp. 341-396.

Krauth-Siegel, R. L., Enders, B., Henderson, G. B., Fairlamb, A. H., and Schirmer, R. H. (1987). Trypanothione reductase from *Trypanosoma cruzi*. Purification and characterization of the crystalline enzyme. Eur. J. Biochem. *164*, 123-128.

Krauth-Siegel, R. L., and Schmidt, H. (2002). Trypanothione and tryparedoxin in ribonucleotide reduction. Methods Enzymol. *347*, 259-266.

Krauth-Siegel, R. L., Meiering, S. K., and Schmidt, H. (2003). The parasite specific trypanothione metabolism of trypanosomes and leishmania. Biol. Chem. *384*, 539-549.

Krieger, S., Schwarz, W., Ariyanayagam, M. R., Fairlamb, A. H., Krauth-Siegel, R. L., and Clayton, C. (2000). Trypanosomes lacking trypanothione reductase are avirulent and show increased sensitivity to oxidative stress. Mol. Microbiol. *35*, 542-552.

Kuriyan, J., Kong, X. P., Krishna, T. S., Sweet, R. M., Murgolo, N. J., Field, H., Cerami, A., and Henderson, G. B. (1991). X-ray structure of trypanothione reductase from *Crithidia fasciculata* at 2.4-Å resolution. Proc. Natl. Acad. Sci. U S A. *88*, 8764-8768.

Laemmli, U. K. (1970). Cleavage of structural proteins during assembly of the head bacteriophage T4. Nature. *227*, 680-685.

Levick, M. P., Tetaud, E., Fairlamb, A. H., and Blackwell, J. M. (1998). Identification and characterisation of a functional peroxidoxin from *Leishmania major*. Mol. Biochem. Parasitol. *96*, 125-137.

Li, Y. X., Farrell, M. J., Liu, R., Mohanty, N., and Kirby, M. L. (2000). Double-stranded RNA injection produces null phenotypes in zebrafish. Dev. Biol. *217*, 394-405.

Lohmann, J. U., Endl, I., and Bosch, T. C. (1999). Silencing of developmental genes in Hydra. Dev. Biol. *214*, 211-214.

Lopez, J. A., Nogoceke, E., Montemartini, M., Kalisz, H. M., Flohé, L., Carvalho, T. U., de Souza, W., Colli, W., and Alves, M. J. (1997). Trypanothione-dependent peroxidase activity in *Trypanosoma cruzi*. Mem. Inst. Oswaldo Cruz. *92*, 149.

Lopez, J. A., Carvalho, T. U., de Souza, W., Flohé, L., Guerrero, S. A., Montemartini, M., Kalisz, H. M., Nogoceke, E., Singh, M., Alves, M. J., and Colli, W. (2000). Evidence for a trypanothione-dependent peroxidase system in *Trypanosoma cruzi*. Free Rad. Biol. Med. *28*, 767-772.

Lucius, R., and Loos-Frank, B. (1997). Parasitologie (Heidelberg; Berlin, Spektrum Akademischer Verlag GmbH).

Lüdemann, H., Dormeyer, M., Sticherling, C., Stallmann, D., Follmann, H., and Krauth-Siegel, R. L. (1998). *Trypanosoma brucei* tryparedoxin, a thioredoxin-like protein in African trypanosomes. FEBS Lett. *431*, 381-385.

Ludtke, S. J., Baldwin, P. R., and Chiu, W. (1999). EMAN: semiautomated software for high-resolution single-particle reconstructions. J. Struct. Biol. *128*, 82-97.

Maiorino, M., Aumann, K. D., Brigelius-Flohé, R., Doria, D., van den Heuvel, J., McCarthy, J., Roveri, A., Ursini, F., and Flohé, L. (1995). Probing the presumed catalytic triad of selenium-containing peroxidases by mutational analysis of phospholipid hydroperoxide glutathione peroxidase (PHGPx). Biol. Chem. Hoppe Seyler. *376*, 651-660.

Manavalan, P., and Johnson, W. C., Jr. (1987). Variable selection method improves the prediction of protein secondary structure from circular dichroism spectra. Anal. Biochem. *167*, 76-85.

Manca, C., Paul, S., Barry, C. E., 3rd, Freedman, V. H., and Kaplan, G. (1999). *Mycobacterium tuberculosis* catalase and peroxidase activities and resistance to oxidative killing in human monocytes in vitro. Infect. Immun. *67*, 74-79.

Matsui, M., Oshima, M., Oshima, H., Takaku, K., Maruyama, T., Yodoi, J., and Taketo, M. M. (1996). Early embryonic lethality caused by targeted disruption of the mouse thioredoxin gene. Dev. Biol. *178*, 179-185.

Meziane-Cherif, D., Aumercier, M., Kora, I., Sergheraert, C., Tartar, A., Dubremetz, J. F., and Ouaissi, M. A. (1994). *Trypanosoma cruzi*: immunolocalization of trypanothione reductase. Exp. Parasitol. *79*, 536-541.

Misquitta, L., and Paterson, B. M. (1999). Targeted disruption of gene function in Drosophila by RNA interference (RNA-i): a role for nautilus in embryonic somatic muscle formation. Proc. Natl. Acad. Sci. U S A. *96*, 1451-1456.

Monod, J., Wyman, J., and Changeux, J. P. (1965). On the nature of allosteric transitions:a plausible model. J. Mol. Biol. *12*, 88-118.

Montemartini, M., Kalisz, H. M., Kiess, M., Nogoceke, E., Singh, M., Steinert, P., and Flohé, L. (1998a). Sequence, heterologous expression and functional characterization of a novel tryparedoxin from *Crithidia fasciculata*. Biol. Chem. *379*, 1137-1142.

Montemartini, M., Nogoceke, E., Singh, M., Steinert, P., Flohé, L., and Kalisz, H. M. (1998b). Sequence analysis of the tryparedoxin peroxidase gene from *Crithidia fasciculata* and its functional expression in *Escherichia coli*. J. Biol. Chem. *273*, 4864-4871.

Montemartini, M., Kalisz, H. M., Hecht, H.-J., Steinert, P., and Flohé, L. (1999). Activation of active-site cysteine residues in the peroxiredoxin-type tryparedoxin peroxidase of *Crithidia fasciculata*. Eur. J. Biochem. *264*, 516-524.

Montrichard, F., Le Guen, F., Laval-Martin, D. L., and Davioud-Charvet, E. (1999). Evidence for the co-existence of glutathione reductase and trypanothione reductase in the non-trypanosomatid Euglenozoa: *Euglena gracilis Z*. FEBS Lett. *442*, 29-33.

Murad, F. (1994). Regulation of cytosolic guanylyl cyclase by nitric oxide: the NO-cyclic GMP signal transduction system. Adv. Pharmacol. *26*, 19-33.

Netto, L. E., and Stadtman, E. R. (1996). The iron-catalyzed oxidation of dithiothreitol is a biphasic process: hydrogen peroxide is involved in the initiation of a free radical chain of reactions. Arch. Biochem. Biophys. *333*, 233-242.

Ngo, H., Tschudi, C., Gull, K., and Ullu, E. (1998). Double-stranded RNA induces mRNA degradation in *Trypanosoma brucei*. Proc. Natl. Acad. Sci. U S A. *95*, 14687-14692.

Nogoceke, E., Gommel, D. U., Kiess, M., Kalisz, H. M., and Flohé, L. (1997). A unique cascade of oxidoreductases catalyses trypanothione-mediated peroxide metabolism in *Crithidia fasciculata*. Biol. Chem. *378*, 827-836.

Ouaissi, M. A., Dubremetz, J. F., Schoneck, R., Fernandez-Gomez, R., Gomez-Corvera, R., Billaut-Mulot, O., Taibi, A., Loyens, M., Tartar, A., and

Sergheraert, C. (1995). *Trypanosoma cruzi*: a 52-kDa protein sharing sequence homology with glutathione S-transferase is localized in parasite organelles morphologically resembling reservosomes. Exp. Parasitol. *81*, 453-461.

Oza, S. L., Tetaud, E., Ariyanayagam, M. R., Warnon, S. S., and Fairlamb, A. H. (2002). A single enzyme catalyses formation of trypanothione from glutathione and spermidine in *Trypanosoma cruzi*. J. Biol. Chem. *277*, 35853-35861.

Pauwels, F., Vergauwen, B., Vanrobaeys, F., Devreese, B., and Van Beeumen, J. J. (2003). Purification and characterization of a chimeric enzyme from *Haemophilus influenzae Rd* that exhibits glutathione-dependent peroxidase activity. J. Biol. Chem. *278*, 16658-16666.

Penketh, P. G., Kennedy, W. P., Patton, C. L., and Sartorelli, A. C. (1987). Trypanosomatid hydrogen peroxide [corrected] metabolism. FEBS Lett. *221*, 427-431.

Poole, L. B., and Ellis, H. R. (1996). Flavin-dependent alkyl hydroperoxide reductase from *Salmonella typhimurium*. 1. Purification and enzymatic activities of overexpressed AhpF and AhpC proteins. Biochemistry. *35*, 56-64.

Powis, G., and Montfort, W. R. (2001). Properties and biological activities of thioredoxins. Annu. Rev. Biophys. Biomol. Struct. *30*, 421-455.

Prata, A. (2001). Clinical and epidemiological aspects of Chagas disease. Lancet Infect. Dis. *1*, 92-100.

Qin, J., Clore, G. M., Kennedy, W. M., Huth, J. R., and Gronenborn, A. M. (1995). Solution structure of human thioredoxin in a mixed disulfide intermediate complex with its target peptide from the transcription factor NF kappa B. Structure. *3*, 289-297.

Reckenfelderbäumer, N., Lüdemann, H., Schmidt, H., Steverding, D., and Krauth-Siegel, R. L. (2000). Identification and functional characterization of thioredoxin from *Trypanosoma brucei brucei*. J. Biol. Chem. *275*, 7547-7552.

Rocher, C., Lalanne, J. L., and Chaudiere, J. (1992). Purification and properties of a recombinant sulfur analog of murine selenium-glutathione peroxidase. Eur. J. Biochem. *205*, 955-960.

Sali, A., and Blundell, T. L. (1993). Comparative protein modelling by satisfaction of spatial restraints. J. Mol. Biol. *234*, 779-815.

Sambrook, J., Russell, D. W., and Sambrook, J. (2001). Molecular Cloning: A laboratory manual (3-Volume Set), 3 rd edn (Rockville, MD, USA, Cold Spring Harbor Laboratory Press).

Sanchez Alvarado, A., and Newmark, P. A. (1999). Double-stranded RNA specifically disrupts gene expression during planarian regeneration. Proc. Natl. Acad. Sci. U S A. *96*, 5049-5054.

Schmidt, A., Clayton, C. E., and Krauth-Siegel, R. L. (2002). Silencing of the thioredoxin gene in *Trypanosoma brucei brucei*. Mol. Biochem. Parasitol. *125*, 207-210.

Schonbaum, G. R., and Chance, B. (1976). Catalase. In The Enzymes, P. D. Boyer, ed. (New York, San Francisco, London, Academic Press), pp. 363-408.

Schröder, E., Littlechild, J. A., Lebedev, A. A., Errington, N., Vagin, A. A., and Isupov, M. N. (2000). Crystal structure of decameric 2-Cys peroxiredoxin from human erythrocytes at 1.7 Å resolution. Structure Fold. Des. *8*, 605-615.

Sherman, D. R., Mdluli, K., Hickey, M. J., Arain, T. M., Morris, S. L., Barry, C. E., 3rd, and Stover, C. K. (1996). Compensatory ahpC gene expression in isoniazid-resistant *Mycobacterium tuberculosis*. Science. *272*, 1641-1643.

Smith, K., Opperdoes, F. R., and Fairlamb, A. H. (1991). Subcellular distribution of trypanothione reductase in bloodstream and procyclic forms of *Trypanosoma brucei*. Mol. Biochem. Parasitol. *48*, 109-112.

Smith, K., Nadeau, K., Bradley, M., Walsh, C., and Fairlamb, A. H. (1992). Purification of glutathionylspermidine and trypanothione synthetases from *Crithidia fasciculata*. Protein Sci. *1*, 874-883.

Steenkamp D. J. (2002). Trypanosomal antioxidants and emerging aspects of redox regulation in the trypanosomatids. Antioxid. Redox Signal. *4*, 105-121

Steinert, P., Dittmar, K., Kalisz, H. M., Montemartini, M., Nogoceke, E., Rohde, M., Singh, M., and Flohé, L. (1999). Cytoplasmic localization of the trypanothione peroxidase system in *Crithidia fasciculata*. Free Rad. Biol. Med. *26*, 844-849.

Steinert, P., Plank-Schumacher, K., Montemartini, M., Hecht, H.-J., and Flohé, L. (2000). Permutation of the active site motif of tryparedoxin 2. Biol. Chem. *381*, 211-219.

Stich, A., Abel, P. M., and Krishna, S. (2002). Human African trypanosomiasis. Bmj. *325*, 203-206.

Stoll, V. S., Simpson, S. J., Krauth-Siegel, R. L., Walsh, C. T., and Pai, E. F. (1997). Glutathione reductase turned into trypanothione reductase: structural analysis of an engineered change in substrate specificity. Biochemistry. *36*, 6437-6447.

Sullivan, F. X., and Walsh, C. T. (1991). Cloning, sequencing, overproduction and purification of trypanothione reductase from *Trypanosoma cruzi*. Mol. Biochem. Parasitol. *44*, 145-147.

Tetaud, E., Giroud, C., Prescott, A. R., Parkin, D. W., Baltz, D., Biteau, N., Baltz, T., and Fairlamb, A. H. (2001). Molecular characterisation of mitochondrial and cytosolic trypanothione-dependent tryparedoxin peroxidases in *Trypanosoma brucei*. Mol. Biochem. Parasitol. *116*, 171-183.

Tetaud, E., Manai, F., Barrett, M. P., Nadeau, K., Walsh, C. T., and Fairlamb, A. H. (1998). Cloning and characterization of the two enzymes responsible for trypanothione biosynthesis in *Crithidia fasciculata*. J. Biol. Chem. *273*, 19383-19390.

Thompson, J. D., Gibson, T. J., Plewniak, F., Jeanmougin, F., and Higgins, D. G. (1997). The CLUSTAL_X windows interface: flexible strategies for multiple sequence alignment aided by quality analysis tools. Nucleic Acids. Res. *25*, 4876-4882.

Tovar, J., Cunningham, M. L., Smith, A. C., Croft, S. L., and Fairlamb, A. H. (1998). Downregulation of *Leishmania donovani* trypanothione reductase by heterologous expression of a transdominant mutant homologue: effect on parasite intracellular survival. Proc. Natl. Acad. Sci. U S A. *95*, 5311-5316.

Turrens, J. F., and Cazzulo, J. J. (1987). Inhibition of growth and respiration of *Leishmania mexicana* by the antitumor agent Ionidamine. Comp. Biochem. Physiol. C. *88*, 193-196.

Ursini, F., Maiorino, M., Brigelius-Flohé, R., Aumann, K. D., Roveri, A., Schomburg, D., and Flohé, L. (1995). Diversity of glutathione peroxidases. Methods Enzymol. *252*, 38-53.

Ursini, F., Maiorino, M., and Gregolin, C. (1985). The selenoenzyme phospholipid hydroperoxide glutathione peroxidase. Biochim. Biophys. Acta. *839*, 62-70.

Valentine, R. C., Shapiro, B. M., and Stadtman, E. R. (1968). Regulation of glutamine synthetase. XII. Electron microscopy of the enzyme from *Escherichia coli*. Biochemistry. *7*, 2143-2152.

Vickermann, K. (1976). The diversity of the kinetoplastid flagellates. In Biology of the Kinetoplastida, W. H. R. Lumsden, and D. A. Evans, eds. (London/New York/San Francisco, Academic Press), pp. 1-34.

Wargelius, A., Ellingsen, S., and Fjose, A. (1999). Double-stranded RNA induces specific developmental defects in zebrafish embryos. Biochem. Biophys. Res. Commun. *263*, 156-161.

Weinberg, J. B., Misukonis, M. A., Shami, P. J., Mason, S. N., Sauls, D. L., Dittman, W. A., Wood, E. R., Smith, G. K., McDonald, B., Bachus, K. E., and *et al.* (1995). Human mononuclear phagocyte inducible nitric oxide synthase (iNOS): analysis of iNOS mRNA, iNOS protein, biopterin, and nitric oxide production by blood monocytes and peritoneal macrophages. Blood. *86*, 1184-1195.

WHO (2002). http://www.who.int/tdr.
Strategic Direction for Research: Chagas disease.

WHO (2003a).
http://www.mdtravelhealth.com/infectious/who_trypanyogeo_5.html.

WHO (2003b). http://www.who.int/ctd/chagas/geo.htm.

WHO (2003c). http://www.who.int/emc/diseases/leish/leisgeo1.html.

WHO (2003d). http://www.who.int/tdr/.

Wianny, F., and Zernicka-Goetz, M. (2000). Specific interference with gene function by double-stranded RNA in early mouse development. Nat. Cell Biol. *2*, 70-75.

Wilkinson, S. R., Meyer, D. J., and Kelly, J. M. (2000a). Biochemical characterization of a trypanosome enzyme with glutathione- dependent peroxidase activity. Biochem. J. *352*, 755-761.

Wilkinson, S. R., Temperton, N. J., Mondragon, A., and Kelly, J. M. (2000b). Distinct mitochondrial and cytosolic enzymes mediate trypanothione-dependent peroxide metabolism in *Trypanosoma cruzi*. J. Biol. Chem. *275*, 8220-8225.

Wilkinson, S., Meyer, D. J., Taylor, M. C., Bromley, E. V., Miles, M. A., and Kelly, J. M. (2002). The *Trypanosoma cruzi* enzyme TcGPxI is a glycosomal peroxidase and can be linked to trypanothione reduction by glutathione or tryparedoxin. J. Biol. Chem. *277*, 17062-17071.

Wilkinson, S., Horn, D., Radhika Prathalingam, S., and Kelly, J. M. (2003). RNAi identifies two hydroperoxide metabolizing enzymes that are essential to the bloodstream form of the African trypanosome. J. Biol. Chem. in press.

Williams, C. H. J. (1992). Lipoamide dehydrogenase,glutathione reductase, thioredoxin reductase, and mercuric ion reductase-a family of flavoenzyme transhydrogenases. In Chemistry and biochemistry of flavoenzymes, F. Müller, ed. (Boac Raton, FL, CRC Press), pp. 121-211.

Wirtz, E., Leal, S., Ochatt, C., and Cross, G. A. (1999). A tightly regulated inducible expression system for conditional gene knock-outs and dominant-negative genetics in *Trypanosoma brucei*. Mol. Biochem. Parasitol. *99*, 89-101.

Wood, Z. A., Poole, L. B., Hantgan, R. R., and Karplus, P. A. (2002). Dimers to doughnuts: redox-sensitive oligomerization of 2-cysteine peroxiredoxins. Biochemistry. *41*, 5493-5504.

Wood, Z. A., Poole, L. B., and Karplus, P. A. (2003a). Peroxiredoxin evolution and the regulation of hydrogen peroxide signaling. Science. *300*, 650-653.

Wood, Z. A., Schröder, E., Harris, J. R., and Poole, L. B. (2003b). Structure, mechanism and regulation of peroxiredoxins. Trends Biochem. Sci. *28*, 32-40.

7 Appendix

7.1 Abbreviations

ε	extinction coefficient
∞	infinite
Φ_0	reciprocal value of the velocity at infinite substrate concentrations
Φ_1	reciprocal value of the reaction velocity k'_1 for the substrate A
$\Phi_{1,2}$	kinetic coefficient characterizing a central complex mechanism
$\Phi_{1app.}$	interpolated Φ_1 values
Φ_2	reciprocal value of the reaction velocity k'_2 for the substrate B
[A] or [B]	substrate concentration
$[E_0]$	total enzyme concentration
Å	Ångström
AhpC	alkyl hydroperoxide reductase subunit C
AhpF	alkyl hydroperoxide reductase subunit F
APS	ammoniumperoxodisulfate
ATP	adenosine triphosphate
BC	before Christ
bp	base pair

BSA	bovine serum albumine
CD	circular dichroism
Cf	*Crithidia fasciculata*
COOH	cumene hydroperoxide
C-terminal	carboxy-terminal
Da	Dalton
dest.	destilled
DNA	deoxyribonucleic acid
dNDP	deoxyribonucleotide diphosphate
dNTP	deoxyribonucleoside triphosphate
DSMO	dimethyl sulfoxide
dsRNAi	double strain RNA interference
DTT	dithiothreitol
EDTA	ethylene-diamine-tetraacetic acid
EFTEM	energy-filtered transmission electron microscope
EGTA	ethyleneglycoltetraacetic acid
EM or e. m.	electron microscopy
Equ.	equation
ESI	electrospray ionization mass spectrometry
E_x	extinction at x nm wavelength

FPLC	high performance liquid chromatography for fast protein purification
g	gravitation
GBF	German Research Centre for Biotechnology
GFP	green flourescence protein
GPx	glutathione peroxidase
GR	glutathione reductase
Grx	glutaredoxin
GSH	glutathione
Gsp	glutathionyl-spermidine
GspS	glutathionyl spermidine synthetase
HBP	heme-binding protein
HEPES	4-(2-hydroxyethyl)-1-piperazineethanesulfonic acid
i. e.	*it est*
IgG	immune globuline G
IMAC	immobilized-metal affinity chromatography
IPTG	isopropyl-β-D-thiogalactopyranoside
k'_1	reaction velocity of an enzyme reacting with substrate A

k'_2	reaction velocity of an enzyme reacting with substrate B
$k_{cat.}$	reaction velocity at infinite substrate concentrations
$K_{M\,x}$	Michaelis Menten constant for the substrate x
LB	Luria Bertani
Lc	*Leishmania chagasi*
Ld	*Leishmania donovani*
Li	*Leishmania infantum*
Lm	*Leishmania major*
LOOH	13-hydroperoxy octodecadienoic acid hydroperoxide
MALDI-TOF	matrix-assisted laser desorption and ionization time-of-flight
MEM	minimum essential medium
MS	mass spectrometry
MS/MS	tandem mass spectrometry
MST	3-mercaptopyruvate sulfurtransferase
MW	molecular weight
NADPH	nicotinamide adenine dinucleotide phosphate
NDP	nucleotide diphosphate
Ni-NTA	nickle-nitrilotriacetic acid
N-terminal	amino-terminal

OD_x	optical density at x nm wavelength
PAGE	polyacrylamide gel electrophoresis
PC	procyclic
PCOOH	soybean lipoxygenase-peroxidized phosphatidyl cholin hydroperoxide
PCR	polymerase chain reaction
PEG	polyethylenglycol
Prx	peroxiredoxin
PVDF	polyvinylidendifluoride
RiboR	ribonucleotide reductase
RNA	ribonucleic acid
RNI	reactive nitrogen intermediates
ROI	reactive oxygen intermediates
rpm	rounds per minute
RT	room temperature
SDS	sodium dodecyl sulfate
spec. act.	specific activity
$T(SH)_2$	trypanothione
Taq	*Thermophilus aquaticus*

Tb	*Trypanosoma brucei brucei*
TBE	tris-borate EDTA
t-bOOH	tertiary-butyl hydroperoxide
TBS	Tris buffered saline
Tc	*Trypanosoma cruzi*
TE	Tris-EDTA
TEMED	N,N,N´,N´-tetramethylethylethylenediamine
TR or TryR	trypanothione reductase
Trx	thioredoxin
TrxPx	thioredoxin peroxidase
TrxR	thioredoxin reductase
TryS	trypanothione synthetase
TSS	Transformation and storage solution
TXN	tryparedoxin
TXNPx	tryparedoxin peroxidase
UV	ultraviolet
v	initial velocity
v/v	volume per volume
$v_{app.}$	interpolated apparent velocities
$V_{max.\ app.}$	apparent maximum velocities
$V_{max.}$	interpolated maximum velocity of an enzyme

VSG variant surface glycoprotein

w/v weight per volume

WHO World Health Organization

7.2 Abbreviations of nucleotides and amino acids

Base	Abbreviation
Adenosine	A
Cytidine	C
Guanosine	G
Thymidine	T

Amino acid	Three letter code	One letter code
Alanine	Ala	A
Arginine	Arg	R
Asparagine	Asn	N
Aspartatic acid	Asp	D
Cysteine	Cys	C
Glutamic acid	Glu	E
Glycine	Gly	G
Histidine	His	H
Isoleucine	Ile	I
Leucin	Leu	L
Lysine	Lys	K
Methionine	Met	M
Phenylalanine	Phe	F
Proline	Pro	P
Serine	Ser	S
Threonine	Thr	T
Tryptophan	Trp	W
Tyrosine	Tyr	Y
Valine	Val	V

7.3 List of Primers

Name of the primer	Sequence of the primer
*Tb*TXN Forward	5′ GCC GCG ***CAT ATG*** TCT GGC CTC GCC AAG TAT CTT 3′
*Tb*TXN Reverse	5′ GCC GCG ***CTC GAG*** GTT GGG CCA CGG AAA GTT GGC 3′
*Tb*H6TXN Reverse	5′ CGG CGC ***CTC GAG*** **TCA** GTT GGG CCA CGG AAA GTT 3′
*Tb*TXNPx Forward	5′ GCC GCG ***CAT ATG*** TCC TGC GGT GAT GCG AAA CTC 3′
*Tb*TXNPx Reverse	5′ GCC GCG ***CTC GAG*** **TTA** GTT CAT GCT GCT GAA GTA 3′
*Tb*TXNC43S Forward	5′ TCC TGG TGC CCC CCA *TCC* CGG GT 3′
*Tb*TXNC43S Reverse	5′ ACC CCG *GGA* TGG GGG GCA CCA GGA 3′
*Tb*TXNC40A Forward	5′ GCC TCC TGG *TCC* CCC CCA TGC CGG 3′
*Tb*TXNC40A Reverse	5′ CCG GCA TGG GGG *GGA* CCA GGA GGC 3′
*Tb*TXNE72R Forward	5′ CC TGG GAT *CGC* AAC GAG AGC G 3′
*Tb*TXNE72R Reverse	5′ C GCT CTC GTT *GCG* ATC CCA GG 3′
*Tb*TXND76K Forward	5′ C GAG AGC *AAA* TTC CAT GAT TA 3′

Name of the primer	Sequence of the primer
*Tb*TXND76K Reverse	5′ GTA ATC ATG GAA *TTT* GCT CTC G 3′
*Tb*TXND79K Forward	5′ C GAC TTC CAT *AAA* TAC TAC GGC 3′
*Tb*TXND79K Reverse	5′ GCC GTA GTA *TTT* ATG GAA GTC G 3′
*Tb*TXND76/79K Forward	5′ GAG AGC *AAA* TTC CAT *AAA* TAC TAC G 3′
*Tb*TXND76/97K Reverse	5′ C GTA GTA *TTT* ATG GAA *TTT* GCT CTC 3′
*Tb*TXNR128D Forward	5′ C ACT CAG GCC *GAT* ACC CGT GTC 3′
*Tb*TXNR128D Reverse	5′ GAC ACG GTT *ATC* GGC CTG AGT 3′
*Tb*TXNPxC52S Forward	5′ C ACG TTT GTG *TCC* CCC CAC TGA 3′
*Tb*TXNPxC52S Reverse	5′ TC AGT GGG *GGA* CAC AAA CGT G 3′
*Tb*TXNPxC173S Forward	5′ GGT GAG GTG *TCC* CCC GCT AAC 3′
*Tb*TXNPxC173S Reverse	5′ GTT AGC GGG *GGA* CAC CTC ACC 3′
*Cf*TXN2E73R Forward	5′ G GAT *CGG* TCA GCA GAG GAC TTT AAG G 3′
*Cf*TXN2E73R Reverse	5′ C CTC TGC TGA *CCG* ATC CCA GGA GAT GAG CAT CAC C 3′

Name of the primer	Sequence of the primer
*Cf*TXN2R129D Forward	5′ GGC GGA CAC *GAT* GGT GGT GAA GG 3′
*Cf*TXN2R129D Reverse	5′ CC ACC *ATC* GTG TCC GCC TGC GTT GTG ATG ATG TT 3′
*Ld*TXNPxC173S Forward	5′ G AAG CAC GGC GAG GTG *TCC* CCC GCG AAC TCG GAG 3′
*Ld*TXNPxC173S Forward	5′CTT CCA GTT CGC GGG *GGA* CAC CTC GCC GTG CTT C 3′

Table 7.1: List of primers used in this thesis. Restriction sites are shown in bold and italics; Stop codons are marked in bold; Mutated amino acids are highlighted in italic.

Danksagung

Die vorliegende Arbeit wurde unter Anleitung von Herrn Prof. Dr. Dr. h.c. Leopold Flohé in der Abteilung Physiologische Chemie der Technischen Universität Braunschweig an der Gesellschaft für Biotechnologische Forschung mbH (GBF) in Braunschweig angefertigt.

Herrn Prof. Dr. Dr. h.c. Leopold Flohé möchte ich für die Überlassung des interessanten Themas, seine Unterstützung bei der Durchführung dieser Arbeit sowie alle seine Anregungen geistiger und kulinarischer Art danken.

Herrn Prof. Dr. Jürgen Bode danke ich für die bereitwillige Übernahme des Korreferates.

Mein besonderer Dank gilt meine Kollegen Timo Jäger und Marcelo Comini für ihre ausgesprochene Hilfsbereitschaft. Das unkomplizierte und meist sehr fröhliche Laborklima, sowie für das gemeinschaftliche Grillen und Baden, das zum guten Gelingen dieser Arbeit beigetragen hat.

An dieser Stelle sei auch allen Mitglieder der Arbeitsgruppe TU-AG für ihre freundliche Aufnahme und Unterstützung gedankt. Besonderer Dank gilt hierbei Frau Karin Plank-Schumacher für Ihre tatkräftige Unterstützung bei der Proteinaufreinigung und DNA-Sequenzierung, Frau Claudia Wylegalla für DNA-Sequenzierungen und Herrn Dr. Matthias Stehr für die Herstellung einiger Mutanten. Herrn Dr. Josef Wissing für die Hilfestellung beim tryptischen Verdau von Proteinen und deren Auswertungen.

Besonderer Dank gilt Frau Dr. Birgit Hofmann und Herrn Dr. Hans-Jürgen Hecht für die Herstellung von Proteinmodellen, Messungen am MALDI und am ESI, sowie den sehr aufwendigen Auswertungen, und auch für die stete Diskussionsbereitschaft und den vielen Anregungen. Weiterhin bedanken möchte ich mich bei Herrn Dr. Heinrich Lünsdorf für die Erstellung der elektronenmikroskopischen Bildern. Herrn Dr. J. J. van den Heuvel danke ich für die gute Unterstützung meiner Klonierungsversuche. Für die ESI Messungen möchte ich Dr. Manfred Nimtz und Fraun Andrea Ambrahamik danken und für die vielen Proteinsequenzierungen Frau Rita Getzlaff.

Für die Hilfestellungen bei der Transfection von Trypanosomen möchte ich der Arbeitsgruppe von Prof. Dr. Michael Boshart, Biologie 1, Bereich Genetik, der Ludwig-Maximilians-Universität in München danken. Für die Überlassung des

Vektors p2T7 sei Dr. John E. Donelson, Dep. of Biochemistry, University Iowa, USA, und der Zelllinie *T. brucei 13-90* sei Dr. George Cross, Rockefeller University, New York, USA Dank.

Meinen Lieblingskollegen Frau Tanja Behn, Frau Ute Widow, Frau Martina Bittner, Herrn Dr. Ulrich Menge, Frau Dr. Mariella Bollati, Herrn Roland Schucht, Comander Dr. Ralf Spallek, Admiral Dr. Carsten Hornig und Herrn Dr. Sergio Guerrero, der leider viel zu früh nach Argentinien zurückgezogen ist, danke ich für die kreative Zusammenarbeit auch über die Arbeitsgruppengrenzen hinweg. Die hervorragende Zusammenarbeit mit Frau Helena Castro aus Porto hat viel zum Gelingen dieser Arbeit beigetragen.

Für die nötige moralische Unterstützung und viel mehr für seine Computer-Kentnnissen möchte ich meinem Mann Rüdiger danken. Wie auch meinen Eltern, ohne die das alles nicht möglich gewesen wäre.

Die Arbeit wurde finanziell von der Deutschen Forschungsgemeinschaft (Grant Fl 61/8-4), in der Endphase von der GBF unterstützt.